GKSS
FORSCHUNGSZENTRUM
in der HELMHOLTZ-GEMEINSCHAFT

Spatial Scale Separation in Regional Climate Modelling

(Vom Fachbereich Geowissenschaften der Universität Hamburg als Dissertation angenommene Arbeit)

Authoress:
F. Feser

GKSS 2005/9

ISSN 0344-9629

GKSS 2005/9

Spatial Scale Separation in Regional Climate Modelling

(Vom Fachbereich Geowissenschaften der Universität Hamburg
als Dissertation angenommene Arbeit)

Authoress:

F. Feser

(Institute for Coastal Research)

GKSS-Forschungszentrum Geesthacht GmbH • Geesthacht • 2005

Die Berichte der GKSS werden kostenlos abgegeben.
The delivery of the GKSS reports is free of charge.

Anforderungen/Requests:

GKSS-Forschungszentrum Geesthacht GmbH
Bibliothek/Library
Postfach 11 60
D-21494 Geesthacht
Germany
Fax.: (49) 04152/871717

ISSN 0344-9629

GKSS-Forschungszentrum Geesthacht GmbH · Telefon (04152)87-0
Max-Planck-Straße 1 · D-21502 Geesthacht / Postfach 11 60 · D-21494 Geesthacht

GKSS 2005/9

Spatial Scale Separation in Regional Climate Modelling

(Vom Fachbereich Geowissenschaften der Universität Hamburg als Dissertation angenommene Arbeit)

Frauke Feser

112 pages, 33 figures, and 6 tables

Abstract

In this thesis the concept of scale separation is introduced as a tool for first improving regional climate model simulations and, secondly, to explicitly detect and describe the added value obtained by regional modelling. The basic idea behind this is that global and regional climate models have their best performance at different spatial scales.

Therefore the regional model should not alter the global model's results at large scales. The for this purpose designed concept of nudging of large scales controls the large scales withing the regional model domain and keeps them close to the global forcing model whereby the regional scales are left unchanged. For ensemble simulations nudging of large scales strongly reduces the divergence of the different simulations compared to the standard approach ensemble that occasionally shows large differences for the individual realisations. For climate hindcasts this method leads to results which are on average closer to observed states than the standard approach.

Also the analysis of the regional climate model simulation can be improved by separating the results into different spatial domains. This was done by developing and applying digital filters that perform the scale separation effectively without great computational effort. The separation of the results into different spatial scales simplifies model validation and process studies. The search for 'added value' can be conducted on the spatial scales the regional climate model was designed for giving clearer results than by analysing unfiltered meteorological fields. To examine the skill of the different simulations pattern correlation coefficients were calculated between the global reanalyses, the regional climate model simulation and, as a reference, of an operational regional weather analysis. The regional climate model simulation driven with largescale constraints achieved a high increase in similarity to the operational analyses for medium-scale 2 meter temperature anomaly fields compared to the global model or the regional model run without nudging of large scales.

Räumliche Skalentrennung in der regionalen Klimamodellierung

Zusammenfassung

In dieser Dissertation wird das Konzept der Skalenseparation einerseits als Werkzeug für die Verbesserung regionaler Klimamodelle und andererseits für die Beschreibung und den Nachweis des

"added values" der regionalen Klimamodellierung vorgestellt. Die grundlegende Idee hierfür ist, dass globale und regionale Klimamodelle ihre jeweils beste Leistung auf unterschiedlichen räumlichen Skalen zeigen.

Aus diesem Grund sollte das regionale Modell die Ergebnisse des globalen Modells auf der großen Skala unverändert belassen. Das aus diesem Grund entwickelte Konzept des "Nudgen der großen Skalen" steuert die großen Skalen innerhalb des regionalen Modellgebietes und sorgt dafür, dass sie nahe an den Ergebnissen des Globalmodells bleiben, während die regionalen Skalen davon unbeeinflusst sind. Das Nudgen der großen Skalen reduziert die Divergenz einzelner Ensemble-Simulationen erheblich im Vergleich zum Ensemble des Standardansatzes, das teilweise große Unterschiede zwischen den einzelnen Realisierungen zeigt. Für klimatische Nachhersagen ('hindcasts') führt diese Methode zu Ergebnissen, die im Durchschnitt näher an beobachteten Zuständen sind als der Standardansatz.

Auch die Analyse der regionalen Klimasimulation kann durch die Trennung der Ergebnisse in verschiedene räumliche Bereiche verbessert werden. Dies wurde durch die Anwendung eigens hierfür entwickelter digitaler Filter erreicht, die die Skalenseparation effektiv und ohne großen rechentechnischen Aufwand durchführt. Die Trennung der Ergebnisse in verschiedene räumliche Skalen vereinfacht die Modellevaluierung sowie Prozessstudien. Die Suche nach einem "added value" kann auf den räumlichen Skalen durchgeführt werden, für die das regionale Klimamodell enwickelt wurde und so klarere Ergebnisse liefern als für ungefilterte meteorologische Felder. Um die Güte der verschiedenen Simulationen zu untersuchen, wurden Musterkorrelationskoeffizienten zwischen der globalen Reanalyse, den regionalen Klimasimulationen sowie als Referenz einer operationellen regionalen Analyse berechnet. Die regionale Klimamodellsimulation mit großskaligem nudging im Modellinneren erzielte im Vergleich sowohl zum Globalmodell als auch zum regionalen Modellauf ohne nudging der großen Skalen für die mittelskalige 2-Meter-Temperatur einen großen Zugewinn an Ähnlichkeit zu den operationellen Analysen.

Manuscript received / Manuskripteingang in TDB: 9. November 2005

Contents

List of Papers

The thesis is based on the following journal papers:

Hans von Storch, Heike Langenberg, and Frauke Feser: A Spectral Nudging Technique for Dynamical Downscaling Purposes.
Monthly Weather Review, Vol. 128, No. 10, pp. 3664-3673, 2000.

Ralf Weisse and Frauke Feser: Evaluation of a method to reduce uncertainty in wind hindcasts performed with regional atmosphere models.
Coastal Engineering, Volume 48, No. 4, pp. 211-225, 2003.

Frauke Feser and Hans von Storch: A spatial two-dimensional discrete filter for limited area model evaluation purposes.
Monthly Weather Review, Vol. 133, No. 6, pp. 1774-1786, 2005.

Frauke Feser: Enhanced detectability of added value in limited area model results separated into different spatial scales.
Submitted to *Monthly Weather Review*, 2005.

Chapter 1

Introduction

Regional atmospheric models have matured in the past few years and they are currently utilised in a broad spectrum of applications. These range from process studies, reconstructions of recent climate and of paleo climates, simulation of pathways and depositions of anthropogenic matter, construction of plausible scenarios of future climate change to regional weather analysis and forecast. Regional climate models (RCMs)[1] are often used to gain information on a regional scale that global models[2] could only give at a much coarser resolution. The large number of regional modelling studies that have been conducted have resulted in mainly four different study types:

- Climate scenarios (e.g. Christensen and Christensen (2003), de Elía et al. (2005), Dorn et al. (2003), Jones et al. (1995), Jones et al. (1997), Plummer et al. (2005), and Räisänen et al. (2004)) refer to a plausible future climate that has been constructed for explicit use in investigating the potential consequences of anthropogenic climate change. Such climate scenarios should represent future conditions that account for both human-induced climate change and natural climate variability (Giorgi et al. (2001)). RCMs are forced with, e.g., global warming simulations to compute climate scenarios and those often serve as input to impact models.

[1] Local climate is influenced by regional features such as the local orography, land-sea-contrast, and small-scale atmospheric features (e.g. convection), which are not well represented in global climate models because of their coarse resolution. Models of higher resolution cannot practically be used for global simulation of long periods of time due to limited computer resources. To overcome this, regional climate models are constructed for limited areas with a higher resolution (typically 10 to 50 km). They are driven with boundary conditions provided by global climate models.

[2] Coupled atmosphere-ocean general circulation models consist of a three-dimensional representation of the atmosphere, coupled with ocean general circulation models, with models of land-surface processes, and with sea-ice models. A general circulation model operates at a coarser level of detail than a model used for numerical weather prediction because it has to produce projections for decades or centuries rather than short-term forecasts.

- Reconstructions (e.g. Feser et al. (2001), Meinke et al. (2004), and Müller (2004)) are usually driven by global modelled data for the preceding decades taking into account all available observations. These so-called reanalyses[3] are used to provide boundary conditions for the regional model. Hereby the global model fields are quite accurate on the large scale and should not be altered by the regional model other than on the regional scale. The regional model is used to refine the coarse-resolution reanalysis both spatially and temporally to be analysed in detail or to be used as driving fields in further simulation studies, e.g. storm surge, wave or current modelling.

- Process studies (e.g. Jacob and Podzun (1997), Rinke and Dethloff (2000), and Weisse et al. (2000)) provide understanding of certain meteorological processes by means of regional modelling. Also, the model sensitivity to changed boundary conditions or parameterisations can be tested using ensemble studies[4]. Process studies may also be useful to improve the regional model's quality.

- Regional Forecasts (e.g. Johnsen and Rockel (2001)) are computed using short-term regional weather forecast models driven by global analyses with assimilated observed atmospheric states. Usually ensemble studies are calculated by slightly disturbing the driving model data to create a number of possible future atmospheric states on the regional scale. For regional forecasts the model is supposed to produce high-resolution forecast with some reliance on the large-scale global forecast. However, the regional model may, in this case, be used to slightly improve also the large-scale field, because the large-scale field may contain errors (Kanamaru and Kanamitsu (2005)).

Reviews on regional climate modelling can be found in, among others, McGregor (1997), Giorgi and Mearns (1999), and Wang et al. (2004).

A multi-decadal hindcast (reconstruction of weather) for western Europe (Feser et al. (2001)) showed that for certain weather conditions large deviations between the driving global reanalyses and the regional model may occur. These deviations are of course wanted, but only at the regional scale that can be reliably simulated by the regional model, not at the large scale that should be well-resolved by the forcing global reanalyses. A more detailed analysis showed that these differences happened mainly

[3]Reanalyses represent global model simulations containing assimilated observation data like buoys, rawinsondes, land surface, satellite or ship and airplane measurements. The data sets are usually available for the last 50 years. They provide comprehensive information of the atmospheric state as a gridded, temporally evenly spaced data set.

[4]Ensemble studies represent a number of almost similar simulations, differing only slightly in their initial conditions. These differences may be e.g. a different starting time or slightly changed model parameters. In reality these slightly changed initial conditions may represent errors in the observations or insufficient knowledge of physical processes. The resulting ensemble simulations give a measure for the internal model variability.

at the large scales. These scales are the ones that can be successfully resolved by the global reanalyses and therefore should remain unchanged in the regional simulation. To prevent the regional model from deviating from the driving data for large weather systems the nudging of large scales was developed (von Storch et al. (2000)). This method adds nudging terms to the regional model solution which nudge the atmospheric fields towards the direction of the global driving fields, but only at the large spatial scales. Thereby the nudging coefficients were applied only for the horizontal wind components for selected low wave numbers and above 850 hPa, with increasing strength for higher model levels. The spectral nudging technique combines the work of Kida et al. (1991) and the approach of Waldron et al. (1996), and further refines them and applies this technique to an atmospheric climate simulation.

Applications of spectral nudging lead to encouraging results, also for ensemble studies (Weisse and Feser (2003)). Several almost similar simulations with and without nudging of large scales were calculated, differing only in their starting date. For these ensemble studies it often poses a problem that ensemble hindcasts can show high variability between the individual ensemble members. For regional hindcasts, only the single solution closest to the observations is wanted. However, the chance to pick the simulation closest to observations is reduced by large ensemble variability. These ensemble deviations were greatly reduced using spectral nudging, leading, on average, to smaller errors in comparison with observations.

The scale separation used for the nudging of large scales lead to the idea of analysing limited-area model results separated into different spatial scales. The scale separation was expected to lead to advanced model validation, enhanced detection of added value of regional modelling as well as to more detailed process studies. This required that an appropriate tool be developed for the scale separation. Fourier filters proved not to be appropriate because of their erroneous description of spatial trends as being composed of waves. The most cost-effective way for the filtering process of large data sets in terms of computing time was to design an isotropic, discrete filter (Feser and von Storch (2005)). The filtered fields now provided for a new way of data analysis. Given an appropriate reference field on the same model grid, direct comparisons between the simulated data and observation fields are made possible. The regional model can be examined according to the spatial scale it was designed for and not only in total, giving more accurate results for the model's downscaling ability. An added value was detected especially for more regional-scale variables such as near-surface temperature (Feser (2005)). Furthermore, for spatially smooth quantities, such as mean sea level pressure, a gain of additional information on the smaller scales could be extracted for the simulation using spectral nudging. This filtering technique, in combination with the analysis of model results on different spatial scales, presents a new approach to detect added value in limited-area model simulations.

This work is organised as follows:
The concept of scale separation is briefly presented in Section 1.1. A short overview of the sponge zone and dynamical downscaling is given in 1.2. The nudging of large scales is described in Section 1.3 and a short introduction to the description of added value in regional modelling is given in Section 1.4. Since spectral nudging has been introduced in 2000, a number of tests and applications have been published. Those, of which the author of this thesis has made contributions, are briefly summarised in Section 1.5. A short conclusion and overview is given in Section 1.6. Chapters 2-5 are the four papers constituting this thesis. The summary and conclusions are given in Chapter 6.

1.1. The concept of scale separation

Global and regional climate models have their individual best simulation performance at different spatial scales. Global model results perform best for large spatial scales, a distance of five to six grid boxes and more are often considered to be trustworthy. This lies in the range of about 800 km and larger, depending on the global model's resolution. The regional model should not modify these scales that can be well resolved by the global model. Laprise (2003) introduced a technique to identify the resolved scales and the non-linear interactions between these scales in nested limited-area models by adopting a spectral perspective.

Figure 1.1 shows model variance as a function of spatial scale. For both the global model (blue solid framed rectangles) and the regional model (red dashed framed rectangles) there is a well-resolved and an insufficiently-resolved spatial domain. For the regional model these areas are shifted towards smaller spatial scales. The blue-striped overlapping area between the global model's well-resolved domain and the regional model's well-resolved domain should be similar. The global model's results are regarded as trustworthy in this area and should not be modified. The white overlapping area between the insufficiently-resolved global model's scales and the still well-resolved regional model's scales is the part where value added by the regional model should be expected.

In the multi-decadal hindcast by Feser et al. (2001) it was found that regional model results differed for large-scale weather phenomena for certain periods and that a special large-scale control was needed. To assure that large-scale weather phenomena in the model's interior do not largely deviate from the global model's results the spectral nudging technique was developed. By introducing this large-scale control in the model's interior, RCMs can stably be integrated over many decades and provide information on spatial and temporal scales not sufficiently resolved by present day global climate models and weather analyses. The nudging of large scales will be explained in more detail in Section 1.3 and in Chapter 2; a spectral nudging application is presented

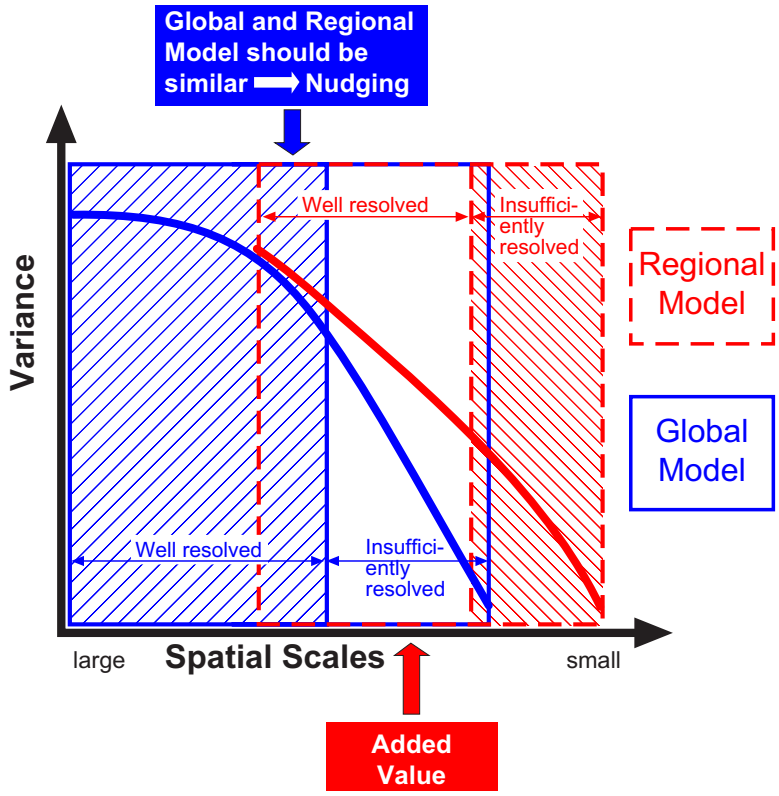

Figure 1.1: Model variance plotted as a function of spatial scales. Frames show spatial scales which are well or insufficiently resolved in the global (blue solid framed rectangles) and in the regional climate model (red dashed framed rectangles).

in Chapter 3.

By looking into the scale separation technique needed for the nudging of large scales, the idea of analysing climate model results separated according to their spatial scales developed. For this purpose several filters were developed that would cost-effectively perform the scale-separation for the long-term data sets. The filter construction is briefly sketched in Section 1.4 and described in more detail in Chapter 4. Chapter 5 shows the filter application and the resulting enhanced detection of limited-area model's added value.

1.2. Sponge zone and dynamical downscaling

The main goal in downscaling is to obtain regional weather phenomena that are influenced by the local orography, land-sea-contrast, and small-scale atmospheric features

(e.g. convection). The dynamical downscaling is supposed to retain all the large-scale information which can be resolved well by the global model or reanalyses. It should also add regional information that the coarse-resolution global model could not generate. For this purpose limited-area models require meteorological information at their boundaries from either a global climate model or reanalysis data. But, regional models have to deal with the mathematically not well-posed problem of lateral boundary conditions. That is, there is in general no well-defined solution fitting all prescribed boundary conditions in the model interior. There may be several or even none solutions fitting both the model equations and the boundary conditions, therefore in general no unique solution can be specified as demanded in mathematical terms. The inconsistencies between the model solution and the global forcing field along the boundaries produce noise and often instabilities. This problem was efficiently rectified by the inclusion of a sponge zone (Davies (1976)). This broadened buffer zone features exponentially decreasing weights ensuring the consistency of the interior flow with the boundary conditions at the outflow boundaries.

Castro et al. (2005) examined to what degree boundary conditions steer processes in the limited-area model interior. They found that for sufficiently large model domains the surface boundary forcing appeared to be the dominant factor in generating variability for small-scale features and it exerted greater control on the RCM solution as the influence of lateral boundary conditions diminished. Their results also showed that the influence of the surface boundary forcing was highly dependent on the model experimental design, such as domain size, nudging options, specification of the surface boundary itself, and model parameterisation schemes.

An efficient way to test the downscaling ability of nested RCMs is the Big-Brother Experiment (BBE) conducted by Denis et al. (2002). A high-resolution reference climate was computed and then degraded by low-pass filtering to use this filtered data to drive a limited-area model. The limited-area model results were then compared to the high-resolution reference data. Differences can thus be attributed to errors associated with the nesting and downscaling technique. Denis et al. (2003) examined the sensitivity of nested RCMs to the resolution of the lateral boundary conditions using the BBE. They found that satisfactory results were achieved for spatial resolutions degraded up to a factor of 12. For the lateral boundary conditions update interval it was shown that 12 hours were the upper limit but 6 hour update intervals gave significantly better results. Only recently, Herceg et al. (2005) applied the BBE to the NCEP Regional Spectral Model for a tropical region. They found that the results of the Big Brother were well reproduced by the Little Brother for most variables. Only precipitation posed a problem, but this was concluded to be rather a model-specific convection scheme deficiency and can not be blamed on the nesting strategy which the BBE was originally designed to test. de Elía and Laprise (2002) analysed the ability of a limited-area model to regenerate the removed small scales filtered out in an BBE. Their results show that the small-scale regional model was capable of recreating the right amount of

small-scale variability but differences with the reference run grew with time. The best BBE results can be achieved for model set-ups with high exchange rates between the lateral boundaries and the model interior. For model domains located in areas with, or weather conditions leading to, low exchange rates, the BBE may be less successful.

If the regional model is driven only by boundary conditions without controlling large-scale weather phenomena in the model interior some problems with large-scale features may occur, especially for blocking weather situations. Thereby the domain size is an important factor. Large model areas are more affected by large-scale deviations between the global and regional model. But also the exchange rate between the lateral boundaries and the inner model domain has an immediate effect on the large-scale constraint the driving global model exerts on the limited-area model. Rinke and Dethloff (2000) showed that in the circumpolar Arctic domain the lateral boundary control is weaker compared to that in model areas of similar domain size in mid-latitude areas. They also showed that RCMs may develop systematic errors in the simulation of the large-scale flow if the boundary forcing is weak. Spectral nudging is one way to minimise such deviations between regional and global model on the large scale.

1.3. Nudging of large scales

Kida et al. (1991) presented a new concept of a spectral boundary to join global and regional climate model. In this technique large-scale fields of a limited-area model are replaced with the corresponding large-scale fields supplied externally from the global climate model at a selected regular time interval. It was then further developed by Waldron et al. (1996) to a method that allows imposition of the large-scale fields throughout the limited-area model domain. von Storch et al. (2000) used and further refined the technique to nudge the long waves in the regional domain to those of the driving global reanalyses in a multi-decadal climate hindcast study. Horizontal wind components were nudged to match the driving reanalyses. Thereby the nudging coefficients were applied exclusively for low wave numbers and above 850 hPa, with increasing strength for higher model levels. The method was also implemented into a RCM to study the East Asian summer monsoon (Kang et al. (2005)). They found that the nudging led to improved model performance not only in simulating the mean features but also in capturing individual precipitation events. Recently, a new approach to nudge the large scales of the driving global model to a regional spectrally represented model was presented by Kanamaru and Kanamitsu (2005).

The application of a spectral nudging technique forces the model to approximate the large scales to the global model data for the whole integration area while the small scales develop freely according to the regional model. Large-scale control of regional climate modelling overcomes the fundamental problem of dealing with an ill-posed

boundary value problem, but its usefulness depends on the specific application. For reconstructions, so-called hindcasts, only one solution should be gained and spectral nudging is very helpful in this case. For a scenario simulation this is more complicated as global scenarios contain significant errors and the regional model may not be able to rely totally on the lateral forcing. But the one-way nesting prohibits the mutual interactions between global and regional model which makes it difficult to expect that the regional model could improve the accuracy of the large-scale portion of the global warming simulation within the regional domain (Kanamaru and Kanamitsu (2005)). For process studies, nudging of large scales may not always be favourable because the simulation for certain experiments should be as free as possible to respond to variations in internal parameters. For regional weather forecasts spectral nudging might be a promising approach to reduce regional model's ensemble deviations caused by large-scale deviations between regional and global model, but so far, to the author's knowledge, this has not been tested.

1.4. Detection of added value in regional modelling

The added value of regional models has not been well described so far. To learn more about the skill and added value given by RCMs a new way of analysing simulation data was developed. By using spatial filters, model data is separated into wave number ranges that should give the best improvement by either the global or the limited-area model. Also e.g. model variability, process studies, or model validation can be looked upon for a certain spatial scale range. Spatial filters were rarely used for the evaluation of RCM output so far, in particular not in the context of regional climate simulations with a RCM. In limited-area model forecasting and evaluation, one approach was to expand a limited field in a 2-d Fourier series and to rebuild a filtered field by recombining only Fourier components with relevant scales (Errico (1985), Stamus et al. (1992)). Bettge and Baumhefner (1980) introduced digital filters using classical ideas proposed by Shuman (1957) and Shapiro (1970). For the spatial scale separation used in this thesis several discrete, isotropic spatial filters were developed that perform the filter computations in a cost-effective and especially for the limited-area model designed manner (Feser and von Storch (2005)).

Employing appropriate spatial filters, the scale-dependent skill of a state-of-the-art RCM was examined by comparing its skill with that of the global reanalyses driving the RCM. Pattern correlation coefficients were calculated to measure the skill between spatially filtered global reanalyses or RCM simulations (with and without nudging of large scales) and a reference operational regional weather analysis. It is demonstrated that RCMs are indeed returning significant added value. For the medium scales the RCM improves the spatially smooth variable air pressure if the RCM is driven with large-scale constraints, but not for the large scales. For the regionally more struc-

tured quantity near-surface temperature the added value of the regional model using nudging of large scales is more obvious. An increase of the mean pattern correlation coefficient of up to 30% was described for the simulation of medium-scale 2m temperature anomaly fields. The filtering technique and its application are explained in more detail in Chapters 4 and 5.

After the introduction of spectral nudging in 2000, and the availability of a 40-year high-resolution reconstruction of western European weather which was obtained by downscaling NCEP reanalyses with spectral nudging (Feser et al. (2001)), the technique has been examined in a series of papers. It was found that the method's ability to enforce the right large-scale state also improved the performance of the regional model on the medium spatial scales. Also, the 40-year simulation was used to in a number of applications, specifically with respect to marine wind issues. The author of this thesis contributed to several of these. Therefore they are listed, together with their abstracts, in the following.

1.5. Applications of Spatial Scale Separation

The following articles give examples for the application of spatial scale separations in regional climate modelling. The author of this thesis has contributed to two spectral nudging validation studies, dealing with the simulation of cloudiness and with wind variability on time scales of a few hours. In both cases the method worked properly.

The skill of spectral nudging is demonstrated in this work on cloud parameterisation in the regional model SN-REMO:

A Validation of the Cloud Parameterization in the Regional Model SN-REMO

I. Meinke, H. von Storch, and F. Feser
Institute for Coastal Research, GKSS Research Centre
21502 Geesthacht, Germany
Published in:
J. Geophys. Res., Vol. 109, D13205, doi:10.1029/2004JD004520, 2004.

Abstract : The cloud parameterization in the regional atmospheric model SN-REMO (Spectrally Nudged Regional Model) was validated using satellite data from the ISCCP (International Satellite Cloud Climatology Project). There is an overall good agreement between the cloudiness of SN-REMO and ISCCP in terms of temporal and spatial means. However, with further investigation a deficiency was localized regarding the simulation of cloud amount: Too many clouds are simulated. This overestimation occurs especially during the night. It is connected with a poor simulation of the

cloud diurnal cycle. Clouds at low-level emissivity heights (1000 - 475 hPa) are causing this overestimation. The magnitude of the overall overestimation is also affected by the underestimation of simulated cloud amount at high-level emissivity heights ($<$ 475 hPa) and its diurnal variation. The overestimation of the simulated cloud amount is caused by subgrid-scale cloudiness. As the simulation of subgrid-scale clouds in the regional model SN-REMO is described by a relative humidity parameterization, these deficiencies are connected with this parameterization.

Another example for the skill of nudging of large scales is given in the work on aliasing in power spectra. It shows high similarity for near-surface wind spectra of NCEP and REMO if sampled at the same time intervals:

Aliasing in Power Spectra: Comment on 'Improved global maps and 54-year history of wind-work on ocean inertial motions' by M. H. Alford

F. Feser, H. von Storch, R. Weisse, and E. Zorita
Institute for Coastal Research, GKSS Research Centre
21502 Geesthacht, Germany
Published in:
Geophys. Res. Lett., Vol. 30, No. 22, p. 2165, 2003.

Abstract : In his paper 'Improved global maps and 54-year history of wind-work on ocean inertial motions' (GRL Vol. 30, No. 8, 6-1 - 6-4, 2003), the author is using near surface (10 meter) winds from a number of different sources as input for subsequent analyses. One of the sources is the gridded multi-decadal reconstruction prepared by Feser et al. (2001) with the help of the regional atmospheric model REMO. Other sources used are the NCEP reanalyses. Analyzing both types of data Alford (2003) comes to the conclusion that "The NCEP and the REMO winds are highly coherent at all frequencies over the entire domain. However, the spectra of the REMO winds at f are lower than the NCEP winds by a constant factor. To account for this attenuation, the REMO winds are multiplied by 1.32." We tried to reconstruct the spectra that led Alford (2003) to the conclusion that REMO winds have too little variance at high-frequencies. If the hourly REMO time-series is sampled at 6-hour intervals, the resemblance with NCEP in the high-frequency range is obvious. This suggests that the hourly sampled REMO winds do not underestimate spectral densities but that the 6-hourly sampled data suffer from an aliasing effect.

Other papers relevant in this context are García-Sotillo (2003), Kanamaru and Kanamitsu (2005), Meinke et al. (2005), and Miguez-Macho et al. (2004).

Spectral nudging and the hourly data set of the 40-year hindcast by Feser et al. (2001) has been used in a number of studies, such as changing storm counts in European seas and long-range transports of pollutants.

An application study of the multi-decadal data set computed with nudging of large scales is given in the following work on Northeast Atlantic and North Sea Storminess:

Northeast Atlantic and North Sea Storminess as Simulated by a Regional Climate Model during 1958-2001 and Comparison with Observations.

R. Weisse, H. von Storch, and F. Feser
Institute for Coastal Research, GKSS Research Centre
21502 Geesthacht, Germany
Published in:
J. Climate, Vol. 18, No. 3, pp. 465-479, 2005.

Abstract : An analysis of the storm climate of the Northeast Atlantic and the North Sea as simulated by a regional climate model for the past 44 years is presented. The model simulates the period 1958-2001 driven by the National Center for Environmental Prediction's (NCEP's) weather re-analysis. Comparison with observations shows that the model is capable of reproducing impact related storm indices such as the number of severe and moderate storms per year or the total number of storms and upper intra-annual percentiles of near-surface wind speed. The indices describe both, the year-to-year variability of the frequency as well as changes in the average intensity of storm events. Analysis of these indices reveals that the average number of storms per year has increased near the exit of the North Atlantic Storm track and over the Southern North Sea since the beginning of the simulation period (1958), but the increase has attenuated later over the North Sea and the average number of storms per year is decreasing over the Northeast Atlantic since about 1990-1995. The frequency of the most severe storms follows a similar pattern over the Northeast North Atlantic while there occurred too few severe storms in other areas of the model domain preventing a statistical analysis for these areas.

Another application study used the multi-decadal atmospheric data set computed with spectral nudging to reconstruct airborne pathways and depositions of gasoline lead in Europe:

Four Decades of Gasoline Lead Emissions and Control Policies in Europe: A Retrospective Assessment

H. v. Storch, M. Costa-Cabral, C. Hagner, F. Feser, J. Pacyna, E. Pacyna, and S. Kolb
Published in:
Science of the Total Environment (STOTEN), Vol. 311, pp. 151-176, 2003.

Abstract : Over decades, large amounts of the neurotoxin lead were released into the European environment, mostly from gasoline lead additives. Emissions were growing unabatedly until the 1970s, when a series of regulations on the allowable gasoline lead content were adopted. As a result, in the 1990s most gasoline contained only small amounts of lead. We have examined this case of environmental pollution and regulation, and performed a retrospective assessment of the extent of regional-scale lead pollution and the effects of gasoline lead regulations in Europe. With the help of a regional climate model, NCEP re-analyses, spatially disaggregated lead emissions from road traffic and point sources and various local data, the airborne pathways and depositions of gasoline lead in Europe since 1958 were reconstructed. It turns out that this approach is successful in describing the time-variable, spatially disaggregated deposition of gasoline lead. Additional data from analyses of concentrations in biota, including plant leaves, mussels and human blood, allows an assessment about the impact of the lead phase-out on the quality of the environment. Demonstrating the success of the lead policies, concentrations in leaves and human blood have steadily declined since the early 1980s. At the same time, the economic repercussions that had been feared did not emerge. Instead, the affected mineral oil and car manufacturing industries in Germany (our case-study) were able to deal with the effort without incurring significant extra costs. We suggest that our method of quantitatively reconstructing and anticipating fluxes and depositions of substances can be applied to other relevant substances as well, such as, for example, Persistent Organic Pollutants, radioactive substances or pollens.

Other publications which have used the long-term data set are Friedhoff (2005) and Koch and Feser (2005); another application study using spectral nudging was published by Kang et al. (2005).

1.6. Conclusion and Overview

In this introductory Chapter, the key aspects of dynamical downscaling with regional climate models have been briefly introduced and discussed. While the idea of regional atmospheric modelling is not new (see e.g. the review on regional modelling by Giorgi and Mearns (1999)) it soon became clear that extended integrations were

associated with methodical problems. The reason for this is that the solution in the model's interior is not well-defined by the boundary values. A first, and most significant break-through was the invention of the sponge zone (Davies (1976)). In this work a second important modification, the so-called spectral nudging (von Storch et al. (2000)), was added. In the following Chapters it is demonstrated in detail how spectral nudging works (Chapter 2), how it suppresses the tendency of RCM's to intermittently generate solutions in the model's interior decoupled from the global forcing (Chapter 3)(Weisse and Feser (2003)), and how the added value of regional modelling can be detected using an appropriate spatial filter (Chapter 4)(Feser and von Storch (2005)). An added value is described in Chapter 5 for two important variables, namely sea level pressure and near-surface temperature (Feser (2005)). Finally, the summary and conclusions are given in Chapter 6.

Bibliography

Bettge, T. W. and D. P. Baumhefner, 1980: A Method to Decompose the Spatial Characteristics of Meteorological Variables within a Limited Domain. *Mon. Wea. Rev.*, **108**, 843–854.

Castro, C. L., R. Pielke, and G. Leoncini, 2005: Dynamical downscaling: Assessment of value retained and added using the Regional Atmospheric Modeling System (RAMS). *J. Geophys. Res.*, **110**, art. No. D05108.

Christensen, J. and O. Christensen, 2003: Severe summertime flooding in Europe. *Nature*, **421**, 805–806.

Davies, H. C., 1976: A lateral boundary formulation for multi-level prediction models. *Quart. J. Roy. Meteor. Soc.*, **102**, 405–418.

de Elía, R., D. Caya, H. Côté, A. Frigon, S. Biner, M. Giguère, D. Paquin, R. Harvey, and D. Plummer, 2005: Uncertainty study of an ensemble of CRCM regional climate simulations over North America. Submitted to *J. Climate*.

de Elía, R. and R. Laprise, 2002: Forecasting Skill Limits of Nested, Limited-Area Models: A Perfect-Model Approach. *Mon. Wea. Rev.*, **130**, 2006–2023.

Denis, B., R. Laprise, and D. Caya, 2003: Sensitivity of a regional climate model to the resolution of the lateral boundary conditions. *Clim. Dyn.*, **20**, 107–126, DOI 10.1007/s00382-002-0264-6.

Denis, B., R. Laprise, D. Caya, and J. Côté, 2002: Downscaling ability of one-way nested regional climate models: The Big brother experiment. *Clim. Dyn.*, **18**, 627–646.

Dorn, W., K. Dethloff, A. Rinke, and E. Roeckner, 2003: Competition of NAO regime changes and increasing greenhouse gases and aerosols with respect to Arctic climate projections. *Clim. Dyn.*, **21**, 447–458, DOI 10.1007/s00382-003-0344-2.

Errico, R., 1985: Spectra Computed from a Limited Area Grid. *Mon. Wea. Rev.*, **113**, 1554–1562.

Feser, F., 2005: Enhanced detectability of added value in limited area model results separated into different spatial scales. Submitted to *Mon. Wea. Rev.*.

Feser, F. and H. von Storch, 2005: A spatial two-dimensional discrete filter for limited area model evaluation purposes. *Mon. Wea. Rev.*, **133**, 1774–1786.

Feser, F., R. Weisse, and H. von Storch, 2001: Multi-decadal Atmospheric Modeling for Europe Yields Multi-purpose Data. *EOS Transactions*, **82**, 305,310.

Friedhoff, B., 2005: *Entwicklung und Implementierung von Rechenverfahren zur Bewertung von RoRo-Schiffen unter Berücksichtigung von Fahrprofilen sowie Einflüsse von Wind und Seegang hinsichtlich ihrer Fahrplantreue*. Master's thesis, Universität Duisburg-Essen, Institut für Schiffstechnik und Transportsysteme.

García-Sotillo, M., 2003: *Reanálisis atmosférico pluridecenal de alta resolución en la cuenca Mediterránea*. Ph.D. thesis, Universidad Complutense de Madrid, Facultad de Ciencias Físicas, [Available from Universidad Complutense de Madrid, F.C Físicas, Ciudad Universitaria, 28040 MADRID.].

Giorgi, F., B. Hewitson, J. Christensen, M. Hulme, H. von Storch, P. Whetton, R. Jones, L. Mearns, and C. Fu: 2001, *Climate Change 2001. The Scientific Basis*, Cambridge University Press, chapter Regional climate information - evaluation and projections. 583–638.

Giorgi, F. and L. O. Mearns, 1999: Introduction to special section: Regional climate modeling revisited. *J. Geophys. Res.*, **104**, 6335–6352.

Herceg, D., A. H. Sobel, L. Sun, and S. E. Zebiak, 2005: The Big Brother Experiment with the NCEP Regional Spectral Model. Submitted to *Clim. Dyn.*

Jacob, D. and R. Podzun, 1997: Sensitivity Studies with the Regional Climate Model REMO. *Meteorol. Atmos. Phys.*, **63**, 119–129.

Johnsen, K. P. and B. Rockel, 2001: Validation of a regional weather forecast model with gps data. *Physics and Chemistry of the Earth Part B-Hydrology Oceans and Atmosphere*, **26**, 415–419.

Jones, R. G., J. M. Murphy, and M. Noguer, 1995: Simulation of climate change over Europe using a nested regional-climate model. I: Assessment of control climate, including sensitivity to location of lateral boundaries. *Quart. J. Roy. Meteor. Soc.*, **121**, 1413–1449.

Jones, R. G., J. M. Murphy, M. Noguer, and A. B. Keen, 1997: Simulation of climate change over Europe using a nested regional-climate model. II: Comparison of driving and regional model responses to a doubling of carbon dioxide. *Quart. J. Roy. Meteor. Soc.*, **123**, 265–292.

Kanamaru, H. and M. Kanamitsu, 2005: Scale Selective Bias Correction in a Downscaling of Global Analysis using a Regional Model. *submitted to Mon. Wea. Rev.*.

Kang, H. S., D. H. Cha, and D. K. Lee, 2005: Evaluation of the mesoscale model/land surface model (MM5/LSM) coupled model for East Asian summer monsoon simulations. *J. Geophys. Res.*, **110 (D10)**, d10105.

Kida, H., T. Koide, H. Sasaki, and M. Chiba, 1991: A New Approach for Coupling a Limited Area Model to a GCM for Regional Climate Simulations. *J. Meteor. Soc. Japan*, **69**, 723–728.

Koch, W. and F. Feser, 2005: Relationship between SAR-Derived Wind Vectors and Wind at ten meters Height Represented by a Mesoscale Model. Submitted to *Mon. Wea. Rev.*

Laprise, R., 2003: Resolved scales and nonlinear interactions in limited-area models. *J. Atmos. Sci.*, **60**, 768–779.

McGregor, J. L., 1997: Regional Climate Modelling. *Meteorol. Atmos. Phys.*, **63**, 105–117.

Meinke, I., B. Geyer, F. Feser, and H. von Storch, 2005: The Impact of Spectral Nudging on Cloud Simulation with a Regional Atmospheric Model. Submitted to *J. of Atmos. and Ocean. Tech.*

Meinke, I., H. von Storch, and F. Feser, 2004: A Validation of the Cloud Parameterization in the Regional Model SN-REMO. *J. Geophys. Res.*, **109**, d13205, doi:10.1029/2004JD004520.

Miguez-Macho, G., G. L. Stenchikov, and A. Robock, 2004: Spectral nudging to eliminate the effects of domain position and geometry in regional climate model simulations. *J. Geophys. Res.*, **109**, D13104, 10.1029/2003JD004495.

Müller, B., 2004: Eine regionale Klimasimulation für Europa zur Zeit des späten Maunder-Minimums (1675-1705). *GKSS-Report*, ISSN 0344-9629.

Plummer, D. A., D. Caya, A. Frigon, H. Côté, M. Giguère, D. Paquin, S. Biner, R. Harvey, and R. de Elía, 2005: Climate and Climate Change over North America as Simulated by the Canadian Regional Climate Model. Submitted to *J. Climate*.

Räisänen, J., U. Hansson, A. Ullerstig, R. Döscher, L. P. Graham, C. Jones, H. E. M. Meier, P. Samuelsson, and U. Willén, 2004: European climate in the late twenty-first century: regional simulations with two driving global models and two forcing scenarios. *Clim. Dyn.*, **22**, 13–31, dOI 10.1007/s00382-003-0365-x.

Rinke, A. and K. Dethloff, 2000: On the sensitivity of a regional Arctic climate model to initial and boundary conditions. *Clim. Res.*, **14**, 101–113.

Shapiro, R., 1970: Smoothing, Filtering, and Boundary Effects. *Reviews of Geophysics and Space Physics*, **8**, 359–387.

Shuman, F. G., 1957: Numerical methods in weather prediction: II. Smoothing and filtering. *Mon. Wea. Rev.*, **85**, 357–361.

Stamus, P., F. Carr, and D. Baumhefner, 1992: Application of a Scale-Separation Verification Technique to Regional Forecast Models. *Mon. Wea. Rev.*, **120**, 149–163.

von Storch, H., H. Langenberg, and F. Feser, 2000: A Spectral Nudging Technique for Dynamical Downscaling Purposes. *Mon. Wea. Rev.*, **128**, 3664–3673.

Waldron, K. M., J. Paegle, and J. D. Horel, 1996: Sensitivity of a Spectrally Filtered and Nudged Limited-Area Model to Outer Model Options. *Mon. Wea. Rev.*, **124**, 529–547.

Wang, Y., L. R. Leung, J. L. McGregor, D.-K. Lee, W.-C. Wang, Y. Ding, and F. Kimura, 2004: Regional Climate Modeling: Progress, Challenges, and Prospects. *J. Meteor. Soc. Japan*, **82**, 1599–1628.

Weisse, R. and F. Feser, 2003: Evaluation of a method to reduce uncertainty in wind hindcasts performed with regional atmosphere models. *Coastal Engineering*, **48**, 211–225.

Weisse, R., H. Heyen, and H. von Storch, 2000: Sensitivity of a regional atmospheric model to a sea state dependent roughness and the need of ensemble calculations. *Mon. Wea. Rev.*, **128**, 3631–3642.

Chapter 2

A spectral nudging technique for dynamical downscaling purposes

Hans von Storch, Heike Langenberg and Frauke Feser

Institute for Coastal Research, GKSS Research Centre
PO Box, 21502 Geesthacht, Germany

Published in:
Monthly Weather Review, Vol. 128, No. 10, pp. 3664-3673, 2000.

Abstract

The "spectral nudging" method imposes time variable large-scale atmospheric states on a regional atmospheric model. It is based on the idea that regional-scale climate statistics are conditioned by the interplay between continental-scale atmospheric conditions and such regional features as marginal seas and mountain ranges. Following this "downscaling" idea, the regional model is forced to satisfy not only boundary conditions, possibly in a boundary sponge region, but also large-scale flow conditions inside the integration area.

In the present paper we examine the performance of spectral nudging in an extended climate simulation. We demonstrate its success in keeping the simulated state close to the driving state at larger scales, while generating smaller-scale features. We also show that the standard boundary forcing technique in current use allows the regional model to develop internal states conflicting with the large-scale state. It is concluded that spectral nudging may be seen as a suboptimal and indirect data assimilation technique.

2.1. Background

The state of the atmosphere can not be observed in its entirety. Only samples of mostly point observations irregularly distributed in space are available. They are used by operational weather centers to construct, or "analyze", a continuous distribution of atmospheric variables. Such "analyses" are our best guess of the atmospheric state and deviate from the true, unknown state to some extent. Likely, the large scales are best described, simply because they are better sampled. On the other hand, the details on scales of a few tens of kilometers and less, are insufficiently sampled and subject to significant uncertainty.

In old days, the analyses were prepared by hand. The major breakthrough was the systematic interpretation of observational data aided by quasi-realistic dynamical models. However, the only features which can be well reproduced by these objective analyses with quasi-realistic models are those that are well resolved by the model. For example, while the effect of the Baltic Sea may to some extent be captured, the imprint of Jutland, separating the Baltic Sea from the North Sea, may not. Thus, the lacking detail in analyses remains at present a major problem in weather analyses.

While in former days the purpose of weather, or synoptic, analyses was for preparing short-term weather forecasts, these analyses have in recent years attained a different role, namely to provide a data base for climatic and other environmental studies (von Storch et al. (2000)). For fulfilling this purpose, it is no longer sufficient to have the best analysis at a given day. It is also necessary that the quality of the analyses is homogeneous, so that improvements of the analysis process do not introduce artificial signals in the climate data set. For meeting these requirements, weather services have prepared so-called global re-analyses, i.e., they have analyzed weather observations of the past decades with the same analysis scheme (Kalnay et al. (1996)).

We suggest the "spectral nudging" technique (Waldron et al. (1996)) for using these global re-analyses to derive smaller-scale analyses. This technique is based on the view that small scale details are the result of an interplay between larger-scale atmospheric flow and smaller-scale geographic features such as topography, land-sea distribution or land-use (von Storch (1999)). To describe this small-scale response, a regional climate model is forced with large-scale weather analyses. Differently from the conventional approach, the forcing is not only stipulated at the lateral boundaries but also in the interior. This interior forcing is maintained by adding nudging terms in the spectral domain, with maximum efficiency for large scales and no effect for small scales. Also, the nudging is confined to higher altitudes, so that the atmospheric state at lower levels is free to adjust to surface geographical properties. Waldron et al. (1996) named the technique "spectral nudging". As far as we know this technique has not been used in regional climate simulations, but it shares similarities with methods to force area averages upon the interior solution as proposed by Kida et al. (1991), Sasaki et al. (1995) and by McGregor et al. (1998), or the technique to insert the large scale state

(Juang and Kanamitsu (1994); Juang et al. (1997); Cocke and LaRow (2000)) in the spirit of ”anomaly models” (Navarra et al. (1988)). A conceptually similar technique has been used to impose a prescribed tropospheric state on a upper atmosphere model (Kouker et al. (1999)).

For purposes of weather analysis, our proposed technique is suboptimal. Ideally, inside the model area one would directly assimilate local observational data, which had little impact on the coarse-grid global re-analyses and, accordingly, were not fully exploited. However, such a scheme is technically very demanding and often not feasible. The proposed technique may be considered a “poor woman’s data assimilation technique”.

The same technique may be used to derive regional scale climate change scenarios from global climate models (”downscaling”; von Storch (1995)). The basic idea of downscaling is to transfer onto smaller scales that large-scale information which has been simulated reliably in climate change scenarios. This is done with the help of statistical models or dynamical regional climate models. The latter technique, named “dynamical downscaling” uses output from global climate models to force regional atmospheric (e.g., Giorgi (1990), Podzun et al. (1995), Jacob and Podzun (1997), Kidson et al. (1998), Rinke and Dethloff (2000)) or regional oceanic models (Kauker (1998)). In nearly all studies performed to date, the forcing is administered exclusively at the lateral boundaries. The technique of statistical dynamical downscaling developed by Fuentes and Heimann (1996) and Frey-Buness et al. (1995) is related to our approach, as they consider the response of a regional climate model to prescribed conditions such as the geostrophic wind.

In our view, the conventional practise of using forcing exclusively along the lateral boundaries stems from the classic view of regional weather modeling as being a boundary problem rather than a downscaling problem. Problems like data assimilation and downscaling were not considered in classical numerical mathematics. The inclusion of the “sponge zone” (Davies (1976)) was already a violation of the “pure” mathematical concept. In this paper we demonstrate that the boundary value format is conceptually inappropriate for the problem at hand.

The present paper is organized as follows. A brief introduction of the regional atmospheric model is given in Section 2.2. The spectral nudging technique is described in Section 2.3, and the results are presented and discussed in Section 2.4. The discussion makes use of measures, which quantify the degree of similarity or dissimilarity on different spatial scales. Sensitivity experiments dealing with the strength of the coupling are considered. Conclusions are summarized in Section 2.5.

2.2. REMO model

We use the regional climate model REMO (REgional MOdel) as described by Jacob and Podzun (1997). REMO is a grid point model featuring the discretized primitive equations in a terrain-following hybrid coordinates system. Details are given by Jacob and Podzun (1997) and Jacob et al. (1995). The finite differencing scheme is energy preserving. The prognostic variables are surface air pressure, horizontal wind components, temperature, specific humidity and cloud water. A soil model is added to account for soil temperature and water content.

The integration area shown in Figure 2.1 has a horizontal spherical resolution of 0.5^o with a pole at $170^oW, 35^oN$, resulting in 91 $\times$ 81 grid points. Because of the spherical resolution, the straight grid lines shown in the map are only approximate. A time step of 5 minutes is adopted.

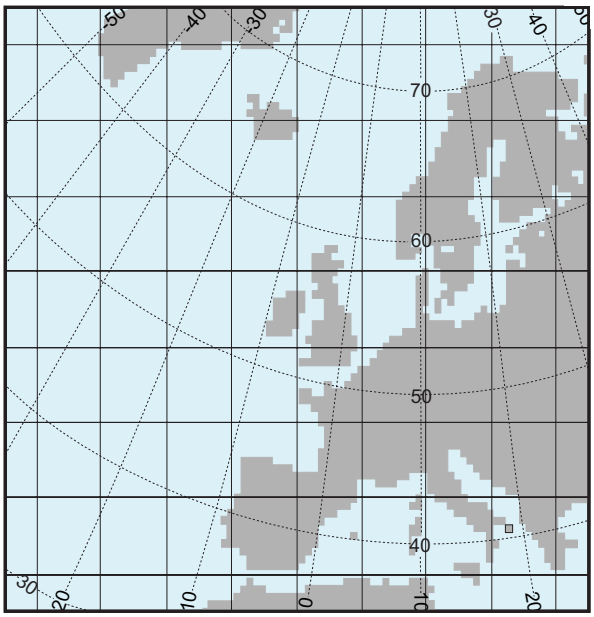

Figure 2.1: The model area and the REMO grid. Solid lines demarcate 100 (10 $\times$ 10) grid boxes. Because of the spherical resolution, the straight lines are only approximations.

REMO is forced with NCEP (National Centers for Environmental Prediction) reanalyses (Kalnay et al. (1996)) over the three month period of January to March 1993. These observed states are updated every six hours. In between, values are derived through linear interpolation. The horizontal resolution of the analyses is approximately 2^o longitudinally and latitudinally (Figure 2.2). Since REMO operates with a rotated spherical grid, its coverage with NCEP grid-boxes is inhomogeneous. In the north-south direction, there are 21 NCEP boxes, and in the east-west direction, 27 boxes

along the southern margin and 48 along the northern margin. That is, the REMO model offers a resolution enhanced by factor of 1:16, on average. Maximum improvement of resolution is achieved in the southern part of the integration area.

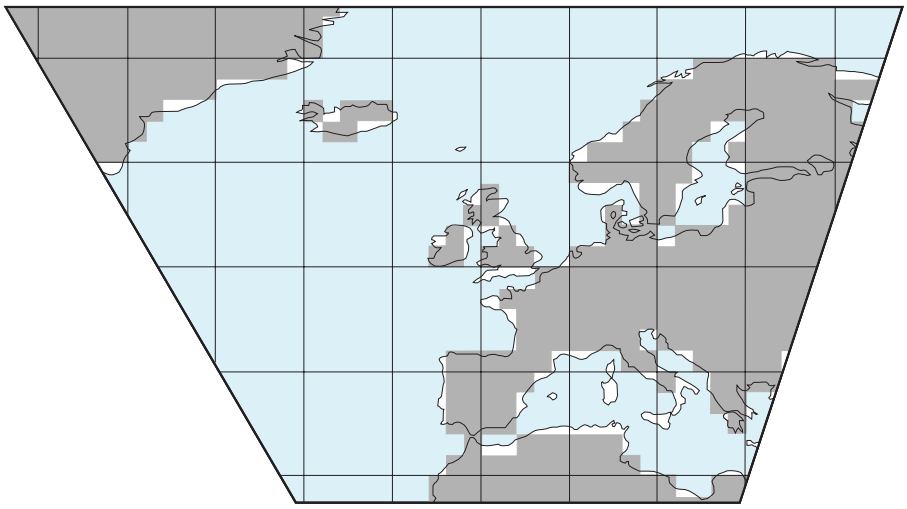

Figure 2.2: The REMO model domain and the NCEP grid. The lines demarcate every fifth grid box.

2.3. Spectral Nudging

As outlined in the Introduction, we have used two different approaches to force the regional model to follow the steering provided by the analyses. In the "standard" approach in current use, the steering takes place exclusively along the lateral boundaries in the spirit of a classical boundary value problem. In the "spectral nudging" approach, the atmospheric state inside the integration area is also forced to accept the analyses for large-scales whereas smaller scales are left to be determined by the regional model.

In the standard setup (Jacob and Podzun (1997)), the observed state is forced upon the model in a lateral boundary zone covering 8 grid points using Davies (1976) classical "sponge" technique: The "interior" solution of the model, denoted Ψ, is brought closer to, or "nudged" to the observed state, denoted Ψ^*, by adding an adjustment or restoring term $\gamma \cdot (\Psi^* - \Psi)$, where the "nudging coefficient" γ takes largest values at the lateral boundary and decreases towards the interior of the integration domain. When $\Psi > \Psi^*$, the restoring terms cause a decrease in Ψ, and when $\Psi < \Psi^*$ an increasing tendency of Ψ is induced. The nudging coefficient has units of 1/sec. This standard approach is commonly used in regional weather forecasting and regional climate simulations. The "sponge" zone has been introduced to avoid reflection of traveling features at the boundaries. Inconsistencies stemming from internally generated features travel-

ing towards the lateral boundaries and conflicting there with the prescribed conditions are dampened out in this manner.

In the "spectral nudging" approach, the lateral "sponge forcing" is kept and an additional steering is introduced as described next.

Consider the expansion of a suitable REMO variable:

$$\Psi(\lambda,\phi,t) = \sum_{j=-J_m,k=-K_m}^{J_m,K_m} \alpha_{j,k}^{m}(t) e^{ij\lambda/L_\lambda} e^{ik\phi/L_\phi} \tag{2.1}$$

with zonal coordinates λ, zonal wave-numbers j and zonal extension of the area L_λ. Meridional coordinates are denoted by ϕ, meridional wave-numbers by k, and the meridional extension by L_ϕ. t represents time. For REMO, the number of zonal and meridional wave-numbers is J_m and K_m. A similar expansion is done for the analyses, which are given on a coarser grid. The coefficients of this expansion are labeled $\alpha_{j,k}^{a}$, and the number of Fourier coefficients is $J_a < J_m$ and $K_a < K_m$. The confidence we have in the realism of the different scales of the re-analysis depends on the wavenumbers j and k and is denoted by $\eta_{j,k}$.

The model is then allowed to deviate from the state given by the re-analysis conditional upon this confidence. This is achieved by adding "nudging terms" in the spectral domain in both directions

$$\sum_{j=-J_a,k=-K_a}^{J_a,K_a} \eta_{j,k}(\alpha_{j,k}^{a}(t) - \alpha_{j,k}^{m}(t)) e^{ij\lambda/L_\lambda} e^{ik\phi/L_\phi} \tag{2.2}$$

In the following, we will use the nudging terms dependent on height. That is, our confidence in the reanalysis increases with height. On the other hand, we leave the regional model more room for its own dynamics at the lower levels where we expect regional geographical features are becoming more important. The better the confidence, the larger the $\eta_{j,k}$-values and the more efficient the nudging term.

In this study, we have applied nudging to the zonal and meridional wind components. Following Giorgi et al. (1993) we use a height dependence nudging coefficient. Specifically, we use the prescription of the German Weather Service version of REMO, which uses a pointwise nudging in case of excessively high wind speeds for preventing numerical instability

$$\eta^0(p) = \begin{cases} \alpha \left(1 - \frac{p}{850hPa}\right)^2 & \text{for} \quad p < 850hPa \\ 0 & \text{for} \quad p > 850hPa \end{cases} \tag{2.3}$$

with p denoting pressure (Doms et al. (1995)). In our base simulation with spectral nudging we used the ad-hoc value $\alpha = 0.05$, resulting in a vertical profile as shown in Figure 2.3. This choice amounts to an e-folding decay time of an introduced disturbance of about 20 days at 850 hPa, 10 hours at 500 hPa and about 2 hours at 100 hPa. (The e-folding time is given by $\Delta t/\eta$ with $\Delta t = 300\ sec.$)

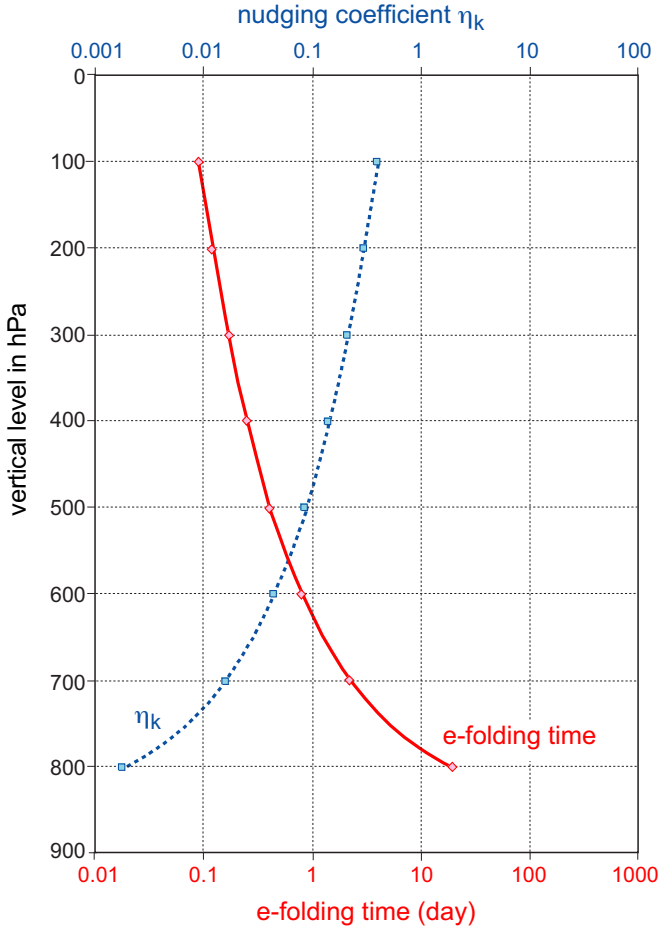

Figure 2.3: Vertical distribution of the spectral nudging term η^0 (blue dashed curve) and corresponding e-folding time in days (red solid curve).

We have set $\eta_{j,k} = \eta^0$ for $j = 0 \ldots 3$ in the north-south direction, $k = 0 \ldots 5$ in the east-west direction and $\eta_{j,k} = 0$ otherwise. That is, wavelengths of about 15^o and larger are considered to be reliably analysed by NCEP, corresponding to 6 and more NCEP grid points. More elaborate specifications could certainly have been used. However, some sensitivity experiments indicated that the effect would be somewhat marginal (see below).

2.4. Results

We demonstrate in Section 2.4a that spectral nudging successfully prevents the regional model from deviating from the given large-scale state. We also show that significant deviations take place when the standard approach is used. In Section 2.4b, a comparison with station data reveals that the spectral control is limited to the largest

scales, so that the representation of the local time series is indeed improved compared to the NCEP reanalyses and the REMO standard run. In Section 2.4c, a number of sensitivity experiments is presented and discussed.

a. Efficiency of Large-Scale Control

We divide the spectral domain into several intervals. We assume that both the regional and global model have two spectral domains: a large-scale domain, $\mathcal{L}$ and a small-scale domain, $\mathcal{S}$. The model has different skills in the domains $\mathcal{L}$ and $\mathcal{S}$ to realistically analyze or simulate the real state. Only the results in $\mathcal{L}$ are considered reliable. So far there is no objective way to identify the interval $\mathcal{L}$, but it is often believed that the largest wave-number in $\mathcal{L}$ is several mesh-sizes of the model's grid. Since the global model and the regional model have different grids, their "reliable" domains, $\mathcal{L}_g$ and $\mathcal{L}_r$, are different (Figure 2.4). In $\mathcal{L}_g \bigcap \mathcal{L}_r$ the results of the regional model should not deviate from the global analyses, as the results of $\mathcal{L}_g$ are considered skillful. Therefore, for these scales, large values of η_k are adopted. However, in the domain $\mathcal{S}_g \bigcap \mathcal{L}_r$ significant modifications are expected and wanted, because the regional model has the role of adding detail in these spatial scales. Accordingly, the nudging term η_k is set to zero for these scales.

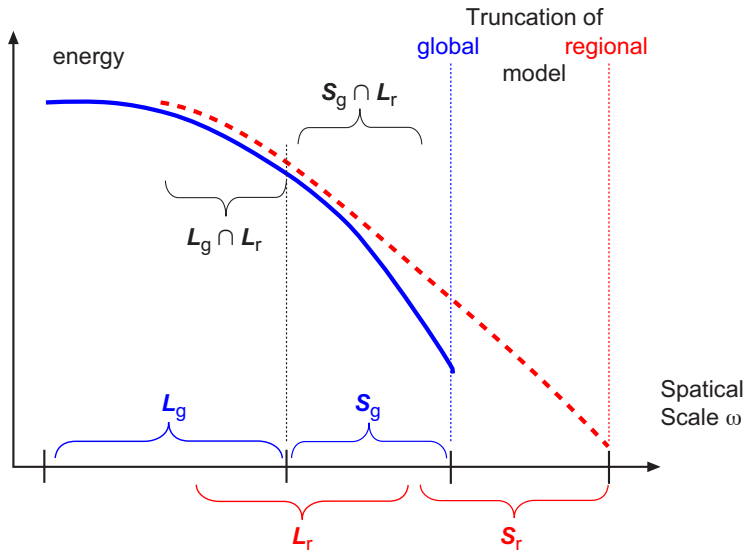

Figure 2.4: Sketch of spatial ranges $\mathcal{L}$ and $\mathcal{S}$ of global analyses and regional model.

We measure the similarity of input NCEP fields and output REMO fields at time t by the proportion of spatial variability of the output described by the input:

$$\mathcal{P}(t) = 1 - \frac{< (\Psi(t) - \Psi^*(t))^2 >}{< \Psi(t)^2 >} \tag{2.4}$$

where $\Psi(t)$ is the output REMO field at time t, Ψ^* the input NCEP field, and $< \cdot >$ a spatial average. When this averaging is done for scales $\omega \in \mathcal{L}_g \bigcap \mathcal{L}_r$, we denote the similarity measure as $\mathcal{P}_g$. This number should be close to one, as we do not want to modify the scales reliably described by the NCEP analysis. However, for the spectral domain $\mathcal{S}_g \bigcap \mathcal{L}_r$, we do not request the REMO field to be similar to the input fields, so that the measure of similarity $\mathcal{P}_r$ may be much smaller than 1.

In the present analysis, the set $\mathcal{L}_g \bigcap \mathcal{L}_r$ is set to comprise zonal wavenumbers up to $k \leq 5$ and meridional wavenumbers $j \leq 3$, so that for all $(j,k) \in \mathcal{L}_g \bigcap \mathcal{L}_r$ $\eta_{j,k} = \eta^0$. The domain $\mathcal{S}_g \bigcap \mathcal{L}_r$ contains $5 < k \leq 13$ and $3 < j \leq 10$ so that $\eta_{j,k}$ is zero for these scales . Note that the exact definition of these sets is inconsequential for the performance of the nudging technique as the numbers $\mathcal{P}_g$ and $\mathcal{P}_r$ are diagnostics; in fact also the diagnostic results are rather insensitive to the details of this choice.

The time series of the similarity measures, $\mathcal{P}_g$ and $\mathcal{P}_r$, calculated for both the standard run and the spectral nudging run, have been calculated for relative humidity and temperature as well as for the zonal and meridional wind components at 850 and 500 hPa. As the nudging is applied to velocity only, the effect is strongest in these variables, whereas the difference is significant but somewhat less dramatic in terms of temperature or humidity (not shown). For the sake of brevity results are shown only for the meridional wind at 500 hPa in Figure 2.5: In the spectral nudging run $\mathcal{P}_g$ hardly deviates from the ideal value of 1 whereas in the boundary forcing values of less than 1, sometimes as low as 0.6 are obtained (Figure 2.5). $\mathcal{P}_r$ values between 20% and 40% indicate that REMO considerably modifies the scales that had been insufficiently resolved by NCEP. $\mathcal{P}_r$ is mostly somewhat smaller for the standard boundary forcing run, i.e., controlling the large-scale features in $\mathcal{L}_g r$ has some effect on $\mathcal{S}_g \bigcap \mathcal{L}_r$ as well.

The other relevant measure is the variance for the different spectral domains: The variances in $\mathcal{S}_g \bigcap \mathcal{L}_r$ are similar in both regional simulations. This is exemplified by Table 1 listing averaged variances for the different spatial scales for the zonal and meridional wind components at 850 hPa. The variance in the large-scale domain of the NCEP analyses ($\mathcal{L}_g$) is about reproduced by both REMO runs, while the variances in the spatial domain well resolved by REMO but less well by NCEP ($\mathcal{S}_g \bigcap \mathcal{L}_r$) is markedly larger in both regional models than in the global analyses. In fact, the simulation with nudging is attaining even larger variances that the standard run.

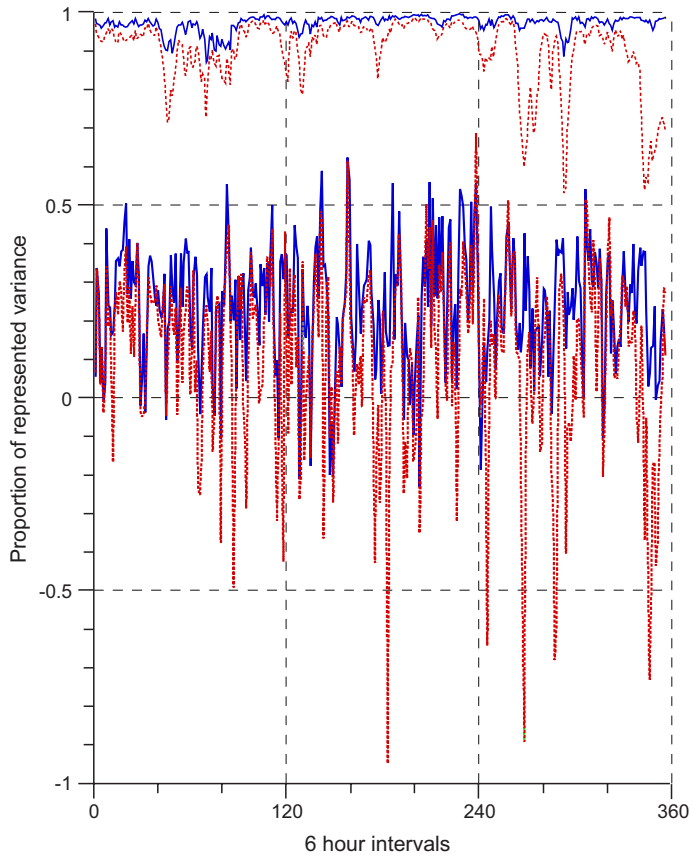

Figure 2.5: Measures of similarity $\mathcal{P}_g(t)$ (upper curves) and $\mathcal{P}_r(t)$ (lower curves) for the meridional wind at 500 hPa for the boundary forcing (red lines) and the spectral nudging (blue lines) simulation.

Table 1: Averaged variances for the different spatial scales for zonal and meridional wind components at 850 hPa.

scale/variable	units $m^2 s^{-2}$	NCEP analyses	REMO standard	REMO nudging
zonal wind				
$\mathcal{L}_g$	10^{-2}	1.6	1.2	1.6
$\mathcal{S}_g \bigcap \mathcal{L}_r$	10^{-6}	3.7	7.7	8.1
meridional wind				
$\mathcal{L}_g$	10^{-2}	1.4	1.3	1.5
$\mathcal{S}_g \bigcap \mathcal{L}_r$	10^{-6}	2.1	6.5	8.5

Thus, the desired double effect – a greater similarity in the spectral range $\mathcal{L}_g \bigcap \mathcal{L}_r$ without a restriction of the variability on the smaller scales – is achieved in the spectral nudging run.

With the standard boundary forcing, episodes emerge with patterns quite dissimilar to the driving NCEP analysis. An example is the episode of 9-12 March, which is marked by low $\mathcal{P}_g$-similarity for the zonal wind (Figure 2.5). In this situation (Figure 2.6), a persistent high pressure system is placed in the center of the integration area, blocking the eastward propagation of synoptic disturbances. For example, the low pressure center initially located over Iceland moves northeast-ward and the trough west of Ireland moves towards the British Isles and is dissipated there. In the standard run, this trough is not dissipated as quickly and causes the central European high to be distorted. In the spectral nudging run, on the other hand, the overall evolution is similar to that of the NCEP re-analyses, but the details deviate to some extent.

The different evolutions are revealed by the different mean sea-level air pressure distributions of the boundary forcing run and the NCEP analyses and of the spectral nudging run and NCEP analysis (Figure 2.7). Clearly, the pressure field in the boundary forcing run deviates on large scales from NCEP. This is particularly striking on 12 March 1993, when over most of the Atlantic negative pressure deviations prevail. In the spectral nudging run, on the other hand, the differences arise at a smaller spatial scale. Also the magnitude of the differences in the boundary forcing run, reaching values of 15 hPa and higher in all maps of 9-12 March, is considerably larger than in the spectral nudging run, where only a few isolated maxima of about 10 hPa occur. Also in other variables, large deviations emerge (not shown). In terms of 850 hPa temperature, for instance, large-scale differences up to 10K develop between the NCEP reanalyses and the standard run, whereas in the spectal nudging the differences are of much smaller spatial scale with maximum values of 4K. Similarly, in 500hPa geopotential height, differences of up to 300 m appear in the standard run compared to 50 m in the spectral nudging run.

A comparison with the manually drawn regional analyses of the Berliner Wetterkarte confirms that the regional model with boundary forcing only run has gone astray (Figure 2.8). Some details, like the deepening of the small cut-off low over Northern Norway, on 11 March with a core air pressure of 1000 hPa in NCEP but 995 hPa in the spectral nudging run is confirmed by the Berliner Wetterkarte. Also the formation of two separate cyclones over the Atlantic on 12 March is a feature missing in the NCEP re-analyses but identified by the Berlin meteorologists.

We suggest that the 9-12 March evolution in the standard run takes place because the interior dynamics is not capturing the blocking situation prevailing in the large scale state. Since this blocking is hardly encoded in the boundary conditions, the "outer" state given by NCEP and the "inner" state given by the standard REMO run become inconsistent. The spectral nudging technique, however, is efficient enough to

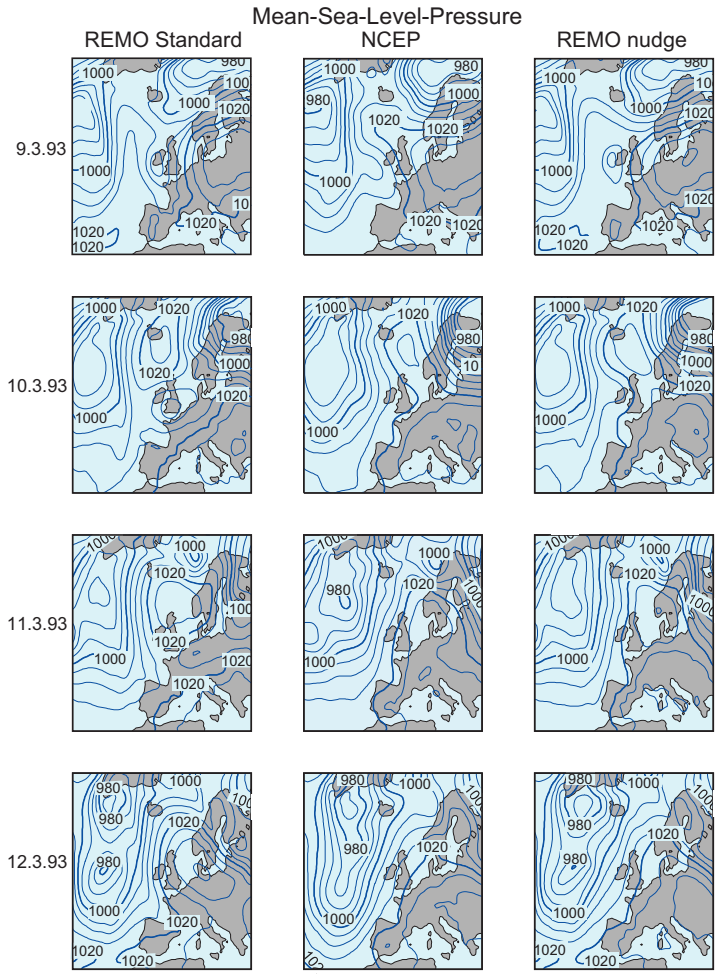

Figure 2.6: An episode with large differences between the standard run and the spectral nudging run: 9-12 March 1993. Mean sea-level air pressure distribution. Left column: boundary forcing run; middle: NCEP analyses (input); right: spectral nudging. Spacing: 5 hPa.

keep the "inner" solution on the right trajectory.

Closer inspection of Figure 2.7 reveals another positive feature of both REMO simulations, namely the small scale features related to fronts which are absent in the NCEP analyses but present in the Wetterkarten of Figure 2.8. Thus, the spectral nudging does not hamper the emergence of small-scale features.

An intercomparison in the frequency domain reveals that nudging dampens the regional model's tendency to develop its own low frequency dynamics. Figure 2.9 shows auto-spectra and squared coherence spectra for mean sea-level air pressure at the station of de Bilt, The Netherlands, for the driving NCEP analysis (blue line) and for the two REMO simulations (red and green lines). For time periods longer than about

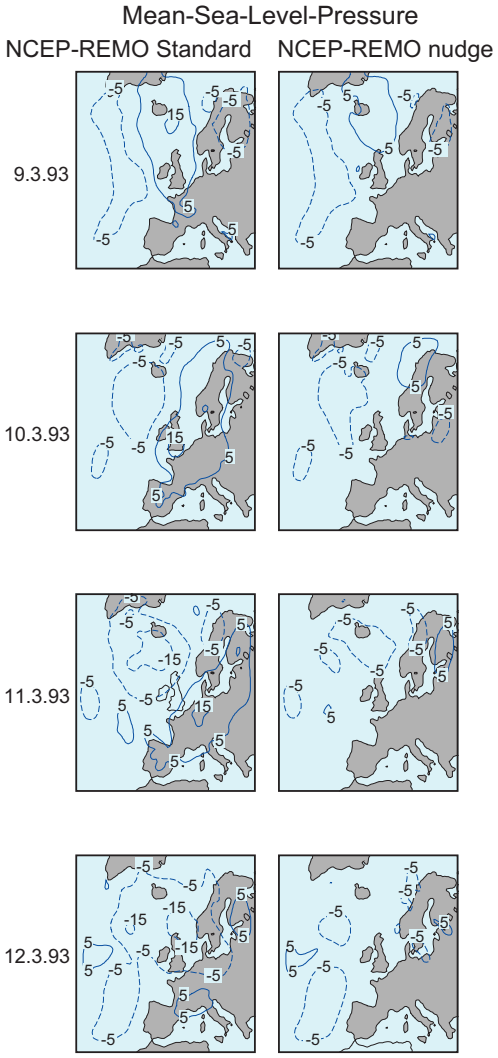

Figure 2.7: Mean sea-level air pressure differences NCEP minus boundary forcing run (left) and minus spectral nudging run (right). Spacing 10 hPa.

3 days, the REMO standard run generates additional low frequency variance, which is suppressed by the nudging. At higher frequencies, both REMO simulations are rather similar. These findings are supported by the squared coherence spectra between the NCEP analyses and the REMO-simulations; for time periods of 72 hours and more, a much higher coherence is obtained for the spectral nudging run than for the standard boundary control run, whereas for shorter time scales, the coherence drops down and the regional model develops its own dynamics.

We made an additional simulation with summer conditions and found similar results, including episodes when the model with standard forcing develops a meteorologically plausible but actually not observed state.

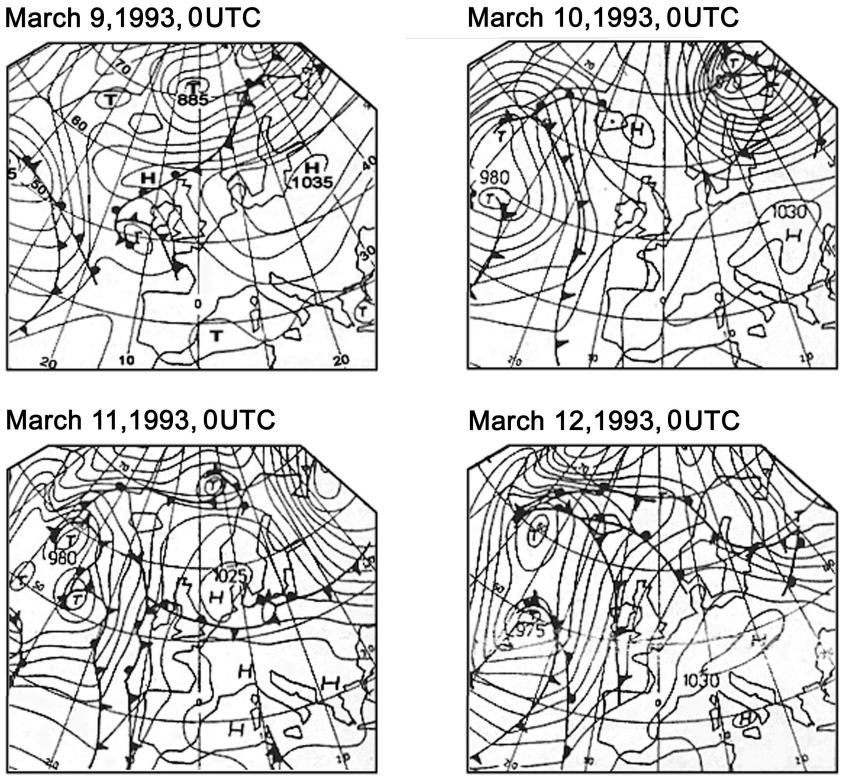

Figure 2.8: Manually drawn mean sea-level air pressure analyses from Berliner Wetterkarte, 9-12 March 1993.

b. Comparison with observational data

The two REMO runs (with standard boundary forcing and spectral nudging) and the NCEP re-analyses (only mean sea-level air pressure and temperature) were compared against observed time series of mean sea-level air pressure at a number of Central European stations. For the time period January - March 1993, also wind observations from the oil field Ekofisk in the Central North Sea were available; these are compared to the REMO simulations as well.

For air pressure at the 10 locations, REMO returns a bias of about 1 hPa for both formulations whereas NCEP has better mean values (Figure 2.10). However, the spread of errors is considerably smaller in the case of the spectral nudging simulation.

Figure 2.11 displays time series of the meridional and zonal components of the wind at 10 m height at Ekofisk in the Central North Sea. Actually, the observations are taken at a higher altitude, and the values are reduced to a standard height of 10 m through a standard calculation. All three curves coincide relatively well. A remarkable feature is that in many cases the maxima and minima of the wind components of the order of 20 m/s are reproduced. A closer inspection reveals intermittently significant deviations by the standard run and improvements in the spectral nudging run. The 9-12

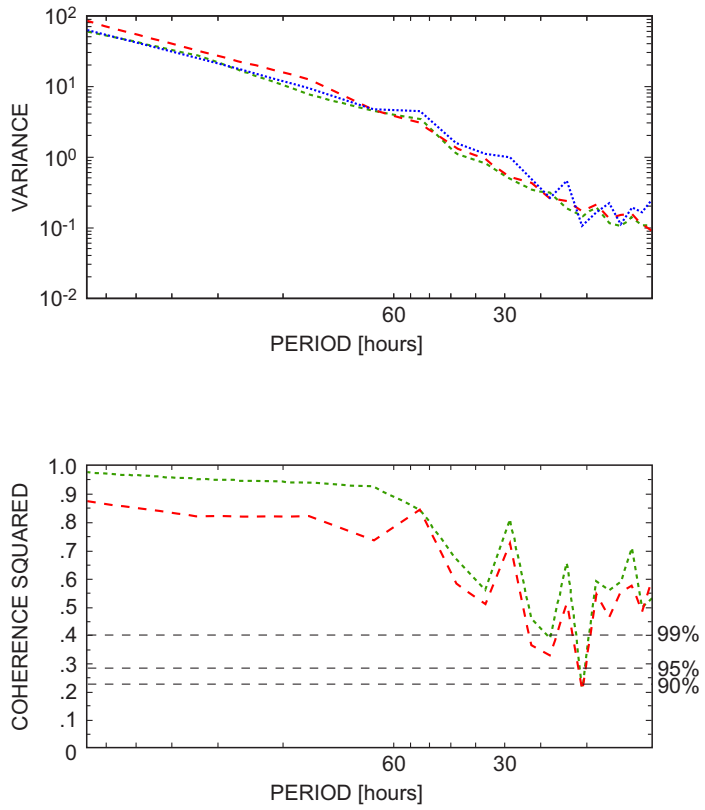

Figure 2.9: Spectra of analyzed and REMO simulated mean sea-level air pressure at the station De Bilt, The Netherlands.
Top: Auto-spectra: The blue line refers to the NCEP analyses, the red line to the standard REMO run, the green line to the spectral nudging REMO run.
Bottom: Squared coherency spectra; the red line refers to the coherence between the NCEP analyses and the standard run, whereas the green line represents the similarity of the spectral nudging run and the analyses.

March episode emerges clearly in the time series of the zonal wind.

c. Sensitivity experiments

Two additional simulations have been performed with different values of the nudging coefficient η^0. In one run, η^0 was doubled (i.e., $\alpha = 0.1$), in another simulations halved ($\alpha = 0.025$). In order to save computer time, the sensitivity experiments were done only for one month, starting with state of 1 March of the 3-month spectral nudging run considered so far.

We assess the sensitivity of the simulation to this choice by calculating the mea-

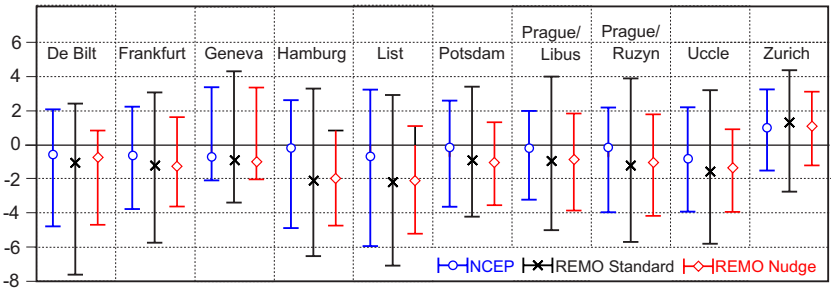

Figure 2.10: Differences "station data minus simulation" for a series of Central European stations and NCEP, REMO standard and REMO spectral nudging. The variable considered is mean sea-level air pressure. The center points represent the mean differences, and the bars indicate the range spanned by the 10% and 90% percentiles.

sures of similarity $\mathcal{P}_g$ and $\mathcal{P}_r$ as defined by (2.4) for scales well resolved by the NCEP reanalyses and by the REMO simulations only. The time mean measures of similarity, for the zonal and meridional wind components at 500 hPa, is listed in Table 2 for the different strengths of spectral nudging ($\alpha > 0$) as well as for the standard case ($\alpha = 0$).

Table 2: Time mean measures of similarity for zonal and meridional wind components at 500 hPa and for different strengths of spectral nudging.

	$\mathcal{P}_g$				$\mathcal{P}_r$			
wind	α				α			
at 500 hPa	0.1	0.05	0.025	0	0.1	0.05	0.025	0
zonal	0.996	0.994	0.991	0.931	0.344	0.325	0.304	0.216
meridional	0.984	0.976	0.964	0.855	0.205	0.239	0.205	0.076

The large-scale control seems to be exerted efficiently also by the other two choices of α, with markedly higher similarity measures. A more comprehensive study will be needed for designing an optimal configuration of the nudging technique, but this first sensitivity analysis indicates that the performance does not depend significantly on the choice of α.

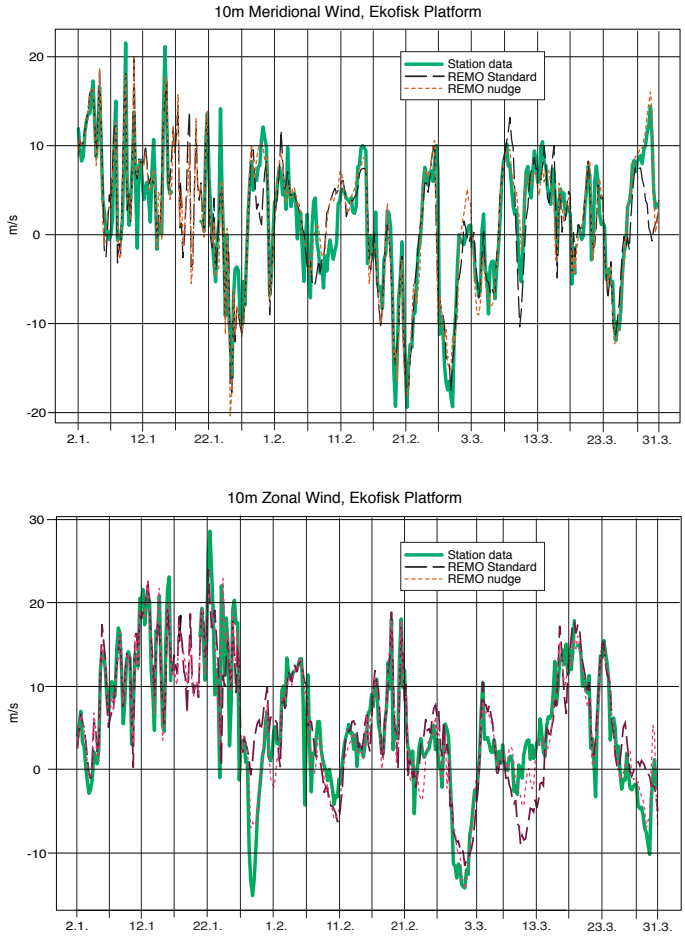

Figure 2.11: Time series of meridional and zonal wind components at Ekofisk in the Central North Sea from January to March 1993. The observed values are reduced to the standard height of 10m. Broad green line: observations; light dashed red continuous line: REMO spectral nudging, heavy dashed black line: REMO standard.

2.5. Conclusions

In the present paper we have tested the ”spectral nudging” technique, introduced by Waldron et al. (1996) into regional weather forecasting, in regional climate simulations. The ”spectral nudging” concept deviates from the classical approach as the problem is not considered to be a boundary value problem in the grid point domain, but a downscaling problem. That is, the information which is processed in the model is not so much the state specified at the areal boundaries but at the large-scales. In a generalized sense, this is again a boundary problem, but this time formulated in the spectral domain.

The purpose of the paper was not to delineate the optimal configuration of spectral nudging, but to demonstrate the concept, its feasibility and its potential. Our key argument for the success of the spectral nudging technique is the observation that the nudging technique prevents the regional model to go astray for limited times, generating internal states inconsistent with the driving fields. We have demonstrated that this uncontrolled wandering is not merely a theoretical problem of the regional model forced from the boundaries, but really takes place (see also Rinke and Dethloff (2000)). At the same time, the spectral nudging forcing does not impede the regional model's ability to develop regional and small scale features superimposed on the large-scale driving conditions.

Different purposes of models require different formulations. When dynamical aspects are to be addressed, such as the dynamics during the genesis of a storm, the spectral nudging should not be used, as it modifies the dynamics inasmuch as it introduces additional forcing terms into the momentum equation. Also, when a significant two-way-coupling is expected to take place, as in the case of the life cycle of a hurricane, the spectral nudging will not be adequate. When, however, specifications of regional climate statistics are needed, such as in paleoclimatic and historic reconstructions and climate change applications, our technique should be preferred as it generates weather streams consistent with the large-scale driving fields.

Acknowledgments

We are thankful to the reviewers for substantial suggestions, to Daniela Jacob and Ralf Podzun for their help with the model, to Arno Hellbach for helping us accessing the NCEP data, to Lennart Bengtsson for permission to use the model, to Mariza Costa-Cabral and Beate Müller for advice, and to Reiner Schnur for the observational data. Beate Gardeike professionally prepared many of the diagrams. Ralf Weisse made the spectral analysis (Figure 2.9) for us.

Bibliography

Cocke, S., and T.E. LaRow, 2000: Seasonal predictions using a regional spectral model embedded within a coupled ocean-atmosphere model. *Mon. Wea. Rev.*, **128**, 689–708.

Davies, H. C., 1976: A lateral boundary formulation for multi-level prediction models. *Quart. J. Roy. Meteor. Soc.*, **102**, 405–418.

Doms, G., W. Edelmann, M. Gertz, T. Hanisch, E. Heise, L. A., D. Majewski, P. Prohl, B. Ritter, and U. Schaettler, 1995: Dokumentation des EM/DM-Systems. Deutscher Wetterdienst Abteilung Forschung, Offenbach a.M., [Available from Deutscher Wetterdienst, Zentralamt, Abteilung Forschung, Postfach 10 04 65, 63004 Offenbach am Main, Germany.].

Frey-Buness, F., D. Heimann and R. Sausen, 1995: A statistical-dynamical downscaling procedure for global climate simulations. *Theor. Appl. Climatol.*, **50**, 117–131.

Fuentes, U. and D. Heimann, 1996: Verification of statistical-dynamical downscaling in the Alpine region. *Clim. Res.*,**7**, 151–186.

Giorgi, F., 1990: Simulations of regional climate using limited area models nested in a general circulation model. *J. Climate*,**3**, 941–963.

Giorgi, F., M.R. Marinucci and G.T Bates, 1993: Development of second-generation regional climate model (RegCM2). Part II: Convective processes and assimilation of lateral boundary conditions. *Mon. Wea. Rev.*,**121**, 2814–2832.

Jacob, D. and R. Podzun, 1997: Sensitivity Studies with the Regional Climate Model REMO. *Meteorol. Atmos. Phys.*, **63**, 119–129.

Jacob, D., R. Podzun and M. Claussen, 1995: REMO - A Model for Climate Research and Weather Prediction, Intl Workshop on Limited-Area and Variable Resolution Models, Beijing, China, pp. 273–278.

Juang, H.-M. H. and M. Kanamitsu, 1994: The NMC Regional Spectral Model. *Mon. Wea. Rev.*,**122**, 3–26.

Juang, H.-M. H., S.-Y. Hong and M. Kanamitsu, 1997: The NCEP Regional Spectral Model: An Update. *Bull. Amer. Met. Soc.*,**78**, 2125–2143.

Kalnay, E., M. Kanamitsu, R. Kistler, W. Collins, D. Deaven, L. Gandin, M. Iredell, S. Saha, G. White, J. Woollen, Y. Zhu, M. Chelliah, W. Ebisuzaki, W. Higgins, J. Janowiak, K. C. Mo, C. Ropelewski, J. Wang, A. Leetmaa, R. Reynolds, R. Jenne, and D. Joseph, 1996: The NCEP/NCAR reanalysis project. *Bull. Amer. Meteor. Soc.*, **77**, 437–471.

Kauker, F., 1998: Regionalization of climate model results for the North Sea. PhD thesis University of Hamburg, 109 pp.

Kida, H., T. Koide, H. Sasaki and M. Chiba, 1991: A new approach to coupling a limited area model with a GCM for regional climate simulation. *J. Meteor. Soc. Japan* ,**69**, 723–728.

Kidson, J.W. and C.S. Thompson, 1998: Comparison of statistical and model-based downscaling techniques for estimating local climate variations. *J. Climate* ,**11**, 735–753.

Kouker, W., D. Offermann, V. Küll, T. Reddemann, R. Ruhnke and A. Franzen, 1999: Streamers observed by the CRISTA experiment and simulated in the KASIMA model. *J. Geophys. Res.* ,**104**, D13, 16405–16418.

McGregor, J.L., J.J. Katzfey and K.C. Nguyen, 1998: Fine resolution simulations of climate change for southeast Asia. *Final Report for a Research Project Commissioned by the Southeast Asian Regional Committee for START (SARCS)* (CISRO Atmospheric Research, PMB 1, Aspendale VIC 3195, Australia), 51 pp.

Navarra, A., and K. Miyakoda, 1988: Anomaly General Circulation Models. *J. Atmos. Sci.* ,**45**, 1509–1530.

Podzun, R., A. Cress, D. Majewski, and V. Renner, 1995: Simulation of European climate with a Limited Area Model. Part II: AGCM boundary conditions. *Beitr. Phys. Atmos.* ,**68**, 205–225.

Rinke, A. and K. Dethloff, 2000: On the sensitivity of a regional Arctic climate model to initial and boundary conditions. *Clim. Res.*, **14**, 101–113.

Sasaki, H., J. Kida, T. Koide, and M. Chiba, 1995: The performance of long term integrations of a limited area model with the spectral boundary coupling method. *J. Meteor. Soc. Japan* ,**73**, 165–181.

von Storch, H., 1995: Inconsistencies at the interface of climate impact studies and global climate research. *Meteorol. Z.* ,**4**, NF, 72–80.

von Storch, H., 1999: The global and regional climate system. In: H. von Storch and G. Flöser (eds): *Anthropogenic Climate Change*, Springer Verlag, ISBN 3-540-65033-4, 3–36.

von Storch, H., M. Costa-Cabral, F. Feser and C. Hagner, 2000: Reconstruction of lead (Pb) fluxes in Europe during 1955-1995 and evaluation of gasoline lead-content regulations. *Conf. Proc. 11th Joint Conference on the Applications of Air Pollution Meteorology with the Air and Waste Management Association* pp. 55-56, 20-24 May 2002 in Norfolk, VA.

Waldron, K. M., J. Paegle and J.D. Horel, 1996: Sensitivity of a spectrally filtered and nudged limited area model to outer model options. *Mon. Wea. Rev.*, **124**, 529–547.

Chapter 3

Evaluation of a method to reduce uncertainty in wind hindcasts performed with regional atmosphere models

R. Weisse and F. Feser

Institute for Coastal Research, GKSS Research Centre
PO Box, 21502 Geesthacht, Germany

Published in:
Coastal Engineering, Vol. 48, No. 4, pp. 211-225, 2003.

Abstract

For more and more applications in coastal and offshore engineering numerical simulations of waves and surges are required. An important input parameter for such simulations are the wind fields. They represent one of the major sources for uncertainties in wave and surge simulations. Wind fields for such simulations are frequently obtained from numerical hindcasts with regional atmospheric models. The skill of these atmospheric hindcasts depends among others on the quality of the forcing at the boundaries. Furthermore, results may vary due to uncertainties in the initial conditions. By comparing different existing approaches for forcing a regional atmospheric model it is shown that the models sensitivity to uncertainties in the initial conditions may be reduced when a more sophisticated approach is used that has been suggested

recently. For a specific, although somewhat brief test period it is demonstrated that an improved hindcast skill for near surface wind fields is obtained when this approach is adopted. Consequences of the reduced uncertainty in the wield fields for the hindcast skill of subsequent wave modelling studies are demonstrated. Recently this new approach has been used together with a regional atmosphere model to produce a 40-year wind hindcast for the Northeast Atlantic, the North Sea and the Baltic Sea. The hindcast is presently extended to other areas and the wind fields are used to produce 40-year high-resolution hindcasts of waves and surges for various European coastal areas.

3.1. Introduction

Many applications in coastal and offshore engineering as well as in ocean modelling or for climate impact studies require detailed knowledge of the prevailing wind, wave and/or surge conditions at specific locations. Often such information is hardly available, either due to incomplete observational records or even due to a complete lack of observational data. In such cases hindcasts obtained from numerical models have become a frequently used tool as they may provide at least the best possible guess of the environmental conditions that may have been observed at given time and location. Therefore, hindcasts are often considered to be a substitute reality (Ewing et al. (1979), The WASA-Group (1998)).

In many cases hindcasts are performed with the objective to reproduce specific events; that is, limited time periods are modelled in order to obtain information on e.g., the wind, wave and surge conditions within a particular storm that, for instance, may have caused large damages in particular areas. Examples of such hindcasts are the simulation of the so-called Halloween storm in 1991 (Cardone et al. (1996)) or the simulation of the wave conditions that caused the abandonment of five yachts in the 1998 Sydney to Hobart yacht race and forced a further 66 boats to retire from the race (Greenslade (2001)).

More recently, however, hindcast simulations have also been performed for longer time periods covering many decades of years (Günther et al. (1998), Cox and Swail (2001), Soares et al. (2002)). The objective of these simulations is twofold: On the one hand they provide relatively homogeneous data records that are sufficiently long and that have sufficiently high spatial resolution in order to be used for design purposes or other statistical analyses. (For instance, the European project HIPOCAS [Hindcast of Dynamic Processes of the Coastal Areas of Europe] was set-up to provide a 40-year high-resolution data base of wind, waves and surges for European coastal areas (Weisse and Gayer (2000), Feser et al. (2001), Soares et al. (2002), Weisse et al. (2002))). Here the phrase *relatively homogeneous* refers to the fact that homogeneity has been improved by using a frozen state-of-the-art numerical model, but that there

are still remaining sources of inhomogeneity such as increasing density of observations that may be used for data assimilation (Swail et al. (1998), Swail and Cox (2000)). On the other hand such hindcast simulations are used as substitute reality in order to assess trends in storm, wave and surge conditions that may have occurred in the recent past (Günther et al. (1998), Wang and Swail (2001), Wang and Swail (2002), Debernhard et al. (2002)).

The conclusions that can be drawn from hindcast simulations depend to a large extent on the quality of the wave and surge hindcast which in turn depends critically on the quality of the driving wind fields. For instance, for a fully developed sea wave heights approximately scale with the square of the wind speed (Tolman (1998)) which implies that an error of about 10% in the driving wind speed will result in an error of at least 20% in the hindcast wave height. This is confirmed by other independent studies which showed that uncertainties in the wind field have a large impact on predicted waves (Teixeira et al. (1995), Holthuijsen et al. (1996)).

Wind fields to force numerical wave and surge hindcasts can be obtained in several ways and from different sources. For multi-decadal simulations, however, additional requirements regarding the quality of the wind fields have to be made. For instance, the wind fields should be free of any artificial trends. They should be homogeneous in time in order not to violate the statistics that may be obtained from the wave/surge model simulations. Furthermore, for coastal applications the spatial and the time resolution of the wind fields should be high enough to resolve the relevant topographic features of the coastline in order to obtain appropriate wave/surge model simulations.

So far, the number of wind data sets fulfilling these requirements is rather limited. Presently relatively homogeneous wind fields can be obtained, for instance, from the so-called re-analyses projects (Kalnay et al. (1996), Gibson et al. (1996)) for the past 15 to 40 years. In these projects global atmospheric circulation models (GCMs) have been used for re-analyzing observational data back in time for some decades using a frozen state-of-the-art data assimilation scheme together with an enhanced observational data base which additionally comprises observations which were not available in real time. In this way, global atmospheric data sets are generated that are considered to be much more homogeneous than any other global products available so far. Presently such global re-analyses have typical spatial resolutions of about 200 km and wind fields are provided every 6 hours.

While such global re-analyses provide a useful product for a variety of studies (e.g., climate studies), their spatial and temporal resolution remains too coarse for many environmental applications, such as ocean or wave modelling in coastal areas. Cox et al. (1995) have suggested an approach called *interactive objective kinematic analysis* (IOKA) to obtain high-quality and high-resolution wind fields from global or coarse resolution weather analyses or re-analyses. The approach is based on a manual interaction with an objective analysis system and has been proven to provide good

results for many wave modelling studies (Swail and Cox (2000), Caires et al. (2002)).

Due to the intensive manual part IOKA may become prohibitively expensive and time consuming. In addition, many applications such as surge modelling (Flather et al. (1998)) or the reconstruction of atmospheric transports (von Storch et al. (2002)) do require dynamically consistent fields of e.g., surface pressure, near-surface and upper level wind fields and/or temperature which are not provided by IOKA.

Therefore attempts have been made recently to use high-resolution regional atmospheric models (RAMs) driven by the re-analysis products at their lateral boundaries in order to obtain multi-decadal regional (wind) hindcasts that simulate the regional features in more detail (Feser et al. (2001)). While the simulation of Feser et al. (2001) focuses on the North and Baltic Sea, similar simulations are being performed now for other European coastal areas (Soares et al. (2002)).

A problem with such simulations is the internal model variability inherent in the RAMs (hereafter referred to as *inherent model uncertainty*); that is, small uncertainties in the initial conditions may sometimes accumulate to large differences during the integration. In other words, if two simulations are performed with only slightly different initial conditions the results of the two integrations may differ to a large extend after some time. While this behaviour is well-known for GCMs it has been acknowledged only recently for RAMs (Ji and Venrnekar (1997), Rinke and Dethloff (2000), Weisse et al. (2000), Weisse and Schneggenburger (2002)).

For forecasting purposes the uncertainty resulting from this behaviour is usually assessed using ensemble simulations (Molteni et al. (1996)). For hindcast simulations the assimilation of observed data may help to keep the model trajectory closer to the observations. For RAMs von Storch et al. (2000) suggested a method that could help to reduce the inherent model uncertainty in case that no further observational data are available for assimilation. They called this method *spectral nudging*. It is based on the idea that the trust or the *confidence* in the data derived from GCM simulations depends on the *spatial scale*; that is, features with horizontal scales smaller than a few hundred kilometres are usually not or at least less well resolved by the GCMs while large scale features such as the planetary scale circulation are well represented. In the spectral nudging approach suggested by von Storch et al. (2000) this additional information is fed into the RAM simulation. The spectral nudging approach may thus be considered as a simple approach to "assimilate" those scales of the global re-analysis in which one has the highest confidence. Details are given in von Storch et al. (2000).

The objective of this paper is twofold: Keeping in mind the importance of the quality of the wind fields for wave and surge model simulations we first investigate whether the spectral nudging approach is indeed capable of reducing the inherent model uncertainty in RAM hindcasts. This has not been addressed in von Storch et al. (2000). We then examine whether an improved hindcast skill can be obtained compared to hindcasts that use the conventional approach (that is, when spectral nudging is not used).

We focus primarily on the uncertainty for wind fields. Additionally, we investigate the consequences for wave hindcasts driven by RAM winds. The paper is structured as follows: In section 2 we briefly describe the RAM and the wave model used for our study. Additionally, the experiments that have been performed are described. Section 3 is dedicated to the analysis of the model results and to the comparison with observations. Our results are assessed and discussed in section 4.

3.2. Models and Experiments

3.2.1. *The Regional Atmosphere Model*

For the wind hindcasts the regional atmosphere model REMO was used. The model is described in detail in Jacob et al. (1995) and Jacob and Podzun (1997). The model and the model set-up are identical to that used by von Storch et al. (2000) for the implementation of spectral nudging. The model is based on the primitive equations and is formulated for a grid-point and terrain-following hybrid coordinate system. The prognostic variables are surface pressure, horizontal wind components, temperature, specific humidity and cloud water. Furthermore, a soil model is included to account for variations in soil temperature and water content.

For our experiments we use the same model domain as described by von Storch et al. (2000) (cf. their Figure 1). The integration area covers Europe and large parts of the Northeast North Atlantic. The model operates on rotated spherical coordinates in order to achieve a minimum distortion of the grid boxes. The horizontal resolution in all simulations is $0.5^\circ \times 0.5^\circ$ and a time step of 5 minutes was chosen.

3.2.2. *Experiments with the Regional Atmosphere Model*

Two sets of ensemble simulations for January 1993 were carried out. In the first set of integrations the boundary conditions were forced upon the REMO using the conventional approach (CTR). In the second set of integrations the spectral nudging technique was used (SPN). Within each set, the experiments differ slightly in their initial conditions to account for the internal variability of the RAM (Weisse et al. (2000), Rinke and Dethloff (2000), Weisse and Schneggenburger (2002)). For each set 6 experiments were performed starting successively on 26, 27, 28, 29, 30, and 31 December 1992 at 0:00 UTC. In the following the analysis is presented for the period 1 to 31 January 1993.

In all experiments REMO was driven by the NCEP re-analyses (Kalnay et al. (1996)). New boundary conditions were provided every 6 hours. The spatial resolution of the NCEP re-analyses is approximately 210 km ($1.875^\circ \times 1.875^\circ$). Since

Table 3.1: Wave model set-up.

	Coarse Grid	Fine Grid
Southernmost latitude	38.00°N	51.00°N
Northernmost latitude	77.00°N	56.00°N
Westernmost longitude	30.00°W	-3.00°W
Easternmost longitude	45.00°E	10.50°E
longitudinal resolution	0.75°	0.10°
latitudinal resolution	0.50°	0.05°
time step	900 s	180 s

REMO operates on rotated spherical coordinates the coverage of the REMO model domain with NCEP grid boxes is inhomogeneous. The highest improvement in spatial resolution is achieved in the southern part of the integration area. On average, the horizontal resolution is enhanced by a factor of 1:16 (von Storch et al. (2000)).

3.2.3. *The Wave Model and Experiments*

The wind fields obtained from the REMO experiments have been used to produce ensemble wave hindcasts using the third generation wave model WAM as described in The WAMDI-Group (1988). The model has been set-up as a nested system with a coarse grid covering the North Sea and large parts of the Northeast North Atlantic. The fine grid nested within the coarse grid covers the North Sea south of 56°N. For all wave model simulations the horizontal resolution is about 50 km for the coarse grid and 5.5 km for the fine grid. Details of the set-up can be obtained from Table 3.1. Further details are provided in Soares et al. (2002).

Using this set-up we have performed 12 experiments with the wave model WAM for the period 1 to 31 January 1993. For all simulations the wave model was initialized with a wind dependent spectrum as described in Günther et al. (1991). The simulations differ only in the wind fields applied. For the first 6 simulations we have used the 6 different wind fields that were obtained from the 6 REMO integrations that utilized the CTR approach. For the other 6 wave hindcasts the 6 different wind fields obtained from the REMO SPN simulations were applied. This way all differences in the wave model simulations may be interpreted as resulting from the variations in the driving wind fields only.

3.3. Results

3.3.1. *Inherent Model Uncertainty*

In this section we want to investigate the variability that emerges in the REMO and the wave model simulations as a result of only small differences in the initial conditions of the atmospheric simulations. This variability is hereafter referred to as *inherent model uncertainty* (IMU).

In order to assess the IMU, for each realization k within an ensemble (CTR, SPN) the root-mean-square distance r with respect to the ensemble mean obtained from all members of the same ensemble was computed as a function of time

$$r_k(t) = \sqrt{\frac{1}{M}\sum_{i=1}^{M}(x_{ik}(t) - < x_i(t) >)^2}. \tag{3.1}$$

Here t represents time, $i = 1 \ldots M$ are the grid points in the model domain, and $< \ldots >$ denotes ensemble averaging. For the RAM simulations x denotes sea level pressure (SLP) while for the wave model simulation x represents significant wave height (Hs).

The magnitude of the IMU as a function of time is illustrated in Figure 3.1. It can be inferred that both, periods with rather low (e.g., between 11 and 16 January) and periods with rather high IMU (e.g., between 5 and 8 January) do occur. Further it can be obtained that the internal variability is largest for the CTR ensemble while it appears to be strongly reduced for the SPN ensemble. We therefore conclude that the spectral nudging approach is in principle capable of reducing the IMU in hindcast simulations with regional models in case no further observational data are available for assimilation.

3.3.2. *Differences in Hindcast Skill*

The second question to address is whether the hindcast skill is in principle being improved for the SPN simulations. As a first step we investigated whether there are any systematic differences between the two ensembles. Therefore we computed the root-mean-square distance $\bar{r}$ between the ensemble means of the SPN and the CTR integrations

$$\bar{r}(t) = \sqrt{\frac{1}{M}\sum_{i=1}^{M}(< y_i(t) > - < x_i(t) >)^2}. \tag{3.2}$$

Here $< y_i(t) >$ represents the ensemble average of the SPN simulations (SLP or Hs), $< x_i(t) >$ denotes the ensemble mean of the CTR experiments (SLP or Hs, respectively) and $i = 1 \ldots M$ are the grid points in the model domain.

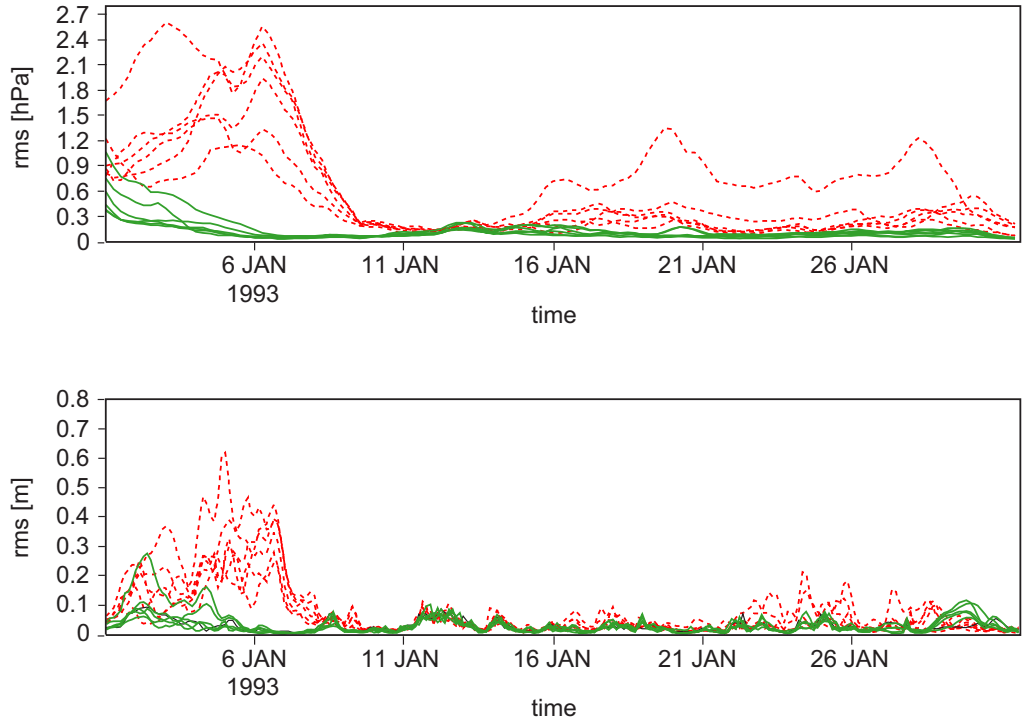

Figure 3.1: Root-mean-square (rms) distance for SLP in hPa (top) and Hs in m (bottom) between the individual realizations of the SPN ensemble and their ensemble mean (green solid curves) and between the individual realizations of the CTR ensemble and their ensemble mean (red dashed curves).

The result of this exercise is shown in Figure 3.2. It can be inferred that systematic differences between both ensembles do occur. Comparing the magnitude of these differences with the variations between the individual realizations of the CTR ensemble (Figure 3.1) reveals that most of the time the systematic differences between the ensemble means are larger than the IMU within the CTR ensemble. In addition, the temporary high internal variability within the CTR ensemble indicates that temporary large deviations between the model results and the observations must be expected since it is not a priori clear which model trajectory is going to be realized if only one integration is performed. This both suggests that systematic differences in the hindcast skill between both ensembles do occur.

For the SPN approach the IMU was remarkably reduced in our simulations (Figure 3.1). However, the question remains whether the hindcast skill in the SPN simulations was improved compared to the CTR experiments. To elaborate on this we compared our results with observed wind and wave data from two locations (Ekofisk, 56.5°N 3.2°E; Scharhörn, 54.0°N 8.4°E). For both locations hourly wind data for January 1993 were available. In addition, for Ekofisk also hourly wave data have been available.

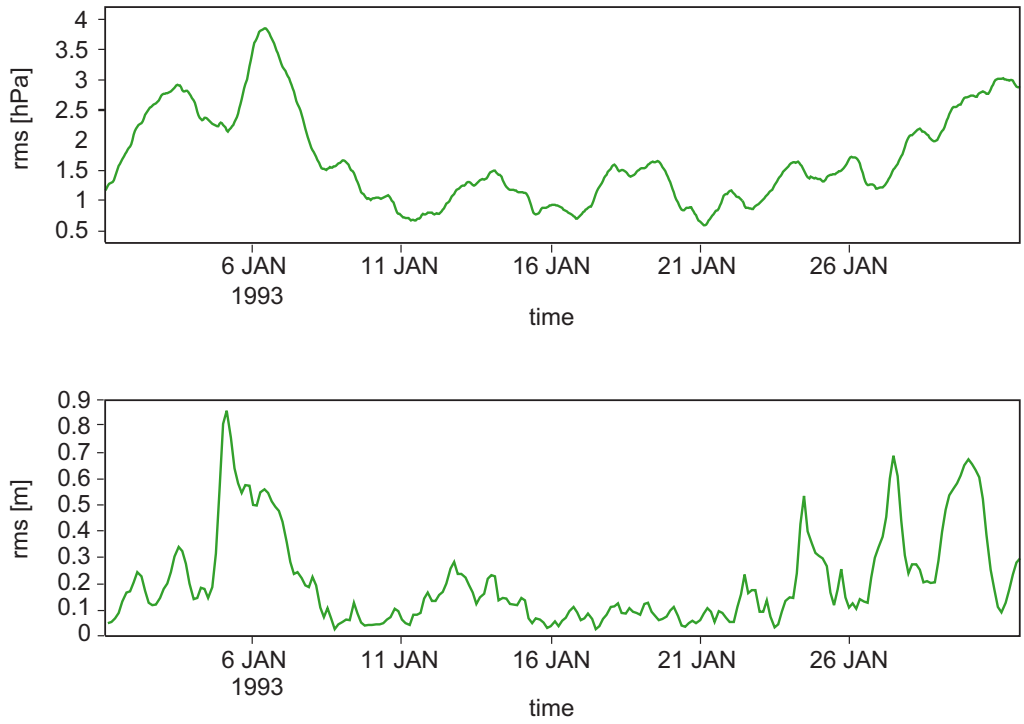

Figure 3.2: Root-mean-square (rms) distance for SLP in hPa (top) and Hs in m (bottom) between the ensemble means of the SPN and the CTR ensemble.

Figure 3.3 and 3.4 show the observed together with the simulated wind speed and wind direction for January 1993 at Ekofisk and Scharhörn. In general, a relatively good agreement between the observations and the simulations can be inferred for both, the conventional and the spectral nudging approach although some events, such as for example the wind speed of more than 30 ms^{-1} at 23:00 UTC on 13 January at Scharhörn, are neither reproduced by the SPN nor by the CTR simulations.

The increased IMU for the CTR simulations around 7 January (Figure 3.1) can also be recognized for the wind speed and wind direction at Ekofisk and Scharhörn. At Ekofisk most of the CTR simulations underestimate the observations by up to 9 ms^{-1}. The wind direction varies between about 150° and 230° and deviates from the observed direction by up to 100° (Figure 3.3a,b). At the same time the wind speed is overestimated by up to 10 ms^{-1} at Scharhörn (Figure 3.4a). Compared to that the simulations using the SPN approach perform remarkably better (Figure 3.3c,d and 3.4c,d). Additionally, the variability among the individual realizations is strongly reduced for the SPN experiments.

For wind speed the differences in hindcast skill between the CTR and the SPN simulations are elaborated in more detail in Table 3.2 in which several skill measures for the individual realizations are presented. It can be obtained that compared to the CTR

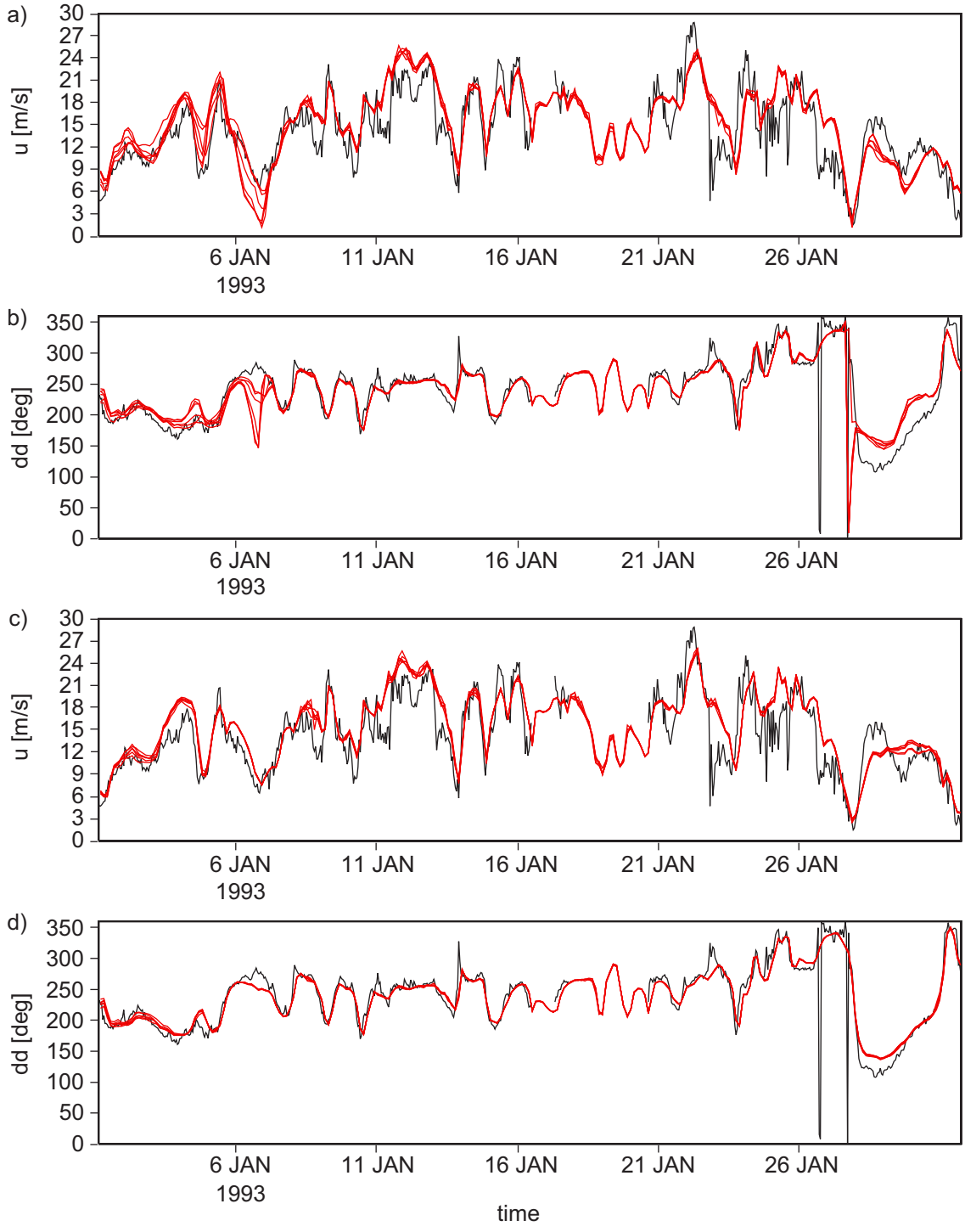

Figure 3.3: Observed (black) and simulated (red) wind speed (a, c) in ms^{-1} and wind direction in degrees (b, d) at Ekofisk. The upper two panels (a, b) show the CTR, the lower two panels (c, d) show the SPN simulations.

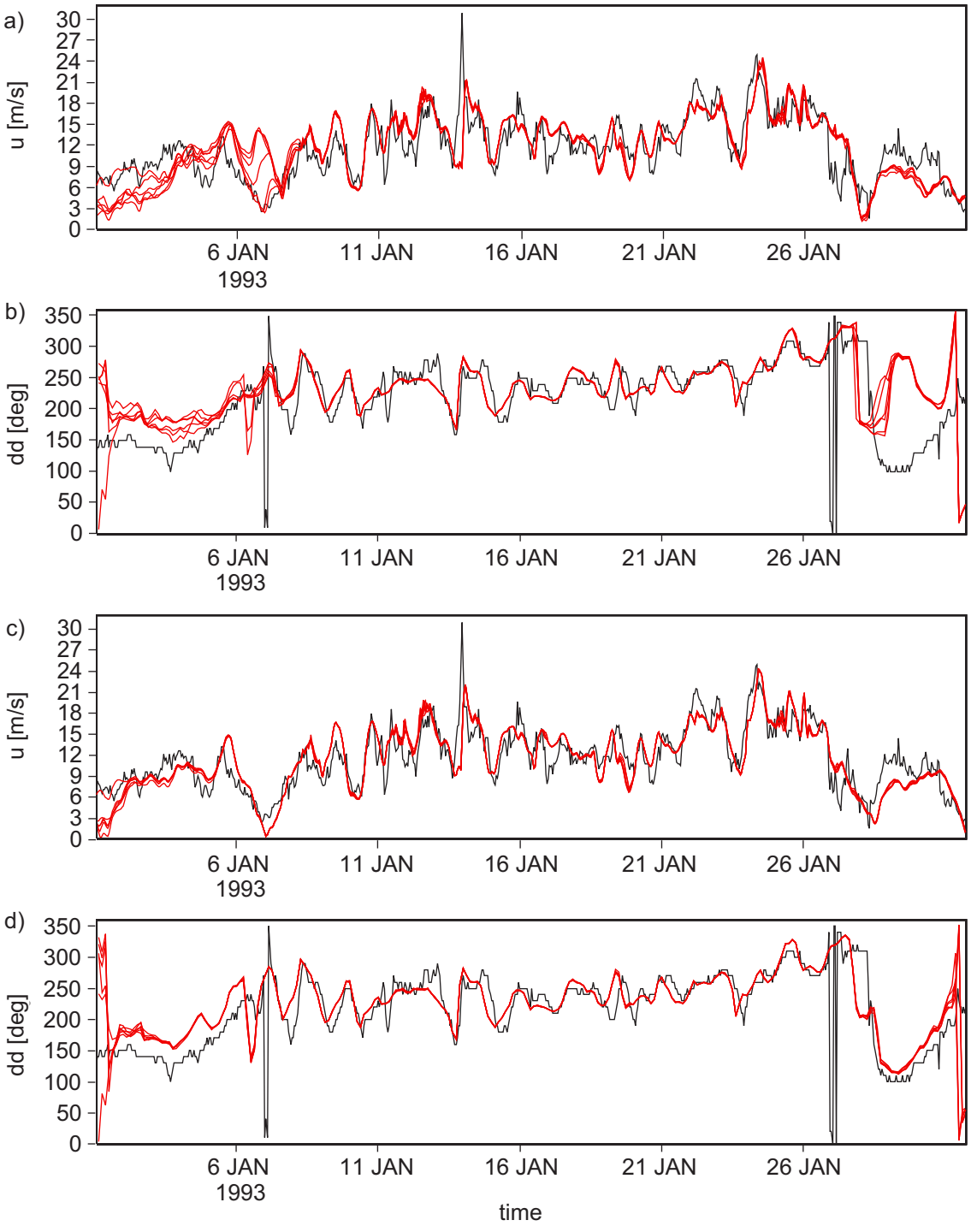

Figure 3.4: Observed (black) and simulated (red) wind speed (a, c) in ms^{-1} and wind direction in degrees (b, d) at Scharhörn. The upper two panels (a, b) show the CTR, the lower two panels (c, d) show the SPN simulations.

Table 3.2: Bias B in ms^{-1}, root-mean-square error R in ms^{-1}, and correlation C between the wind speed obtained from the $k = 1 \ldots 6$ simulations using the conventional (CTR) or the spectral nudging (SPN) approach and the observations at Scharhörn (54.0°N, 8.4°E) and Ekofisk (56.5°N, 3.2°E). In addition, the Brier Score $BS = 1 - R_{SPN}^2 R_{CTR}^{-2}$ is provided.

	CTR, Scharhörn			SPN, Scharhörn				CTR, Ekofisk			SPN, Ekofisk			
k	B	R	C	B	R	C	BS	B	R	C	B	R	C	BS
1	0.17	3.39	0.70	-0.12	2.56	0.83	0.43	0.69	3.59	0.81	1.00	3.18	0.85	0.22
2	0.21	3.40	0.70	-0.16	2.62	0.83	0.40	0.71	3.59	0.81	1.07	3.21	0.85	0.20
3	0.25	3.48	0.69	-0.12	2.53	0.84	0.47	0.70	3.54	0.81	1.07	3.18	0.85	0.19
4	-0.05	2.94	0.78	-0.09	2.53	0.84	0.26	0.85	3.41	0.82	1.01	3.19	0.85	0.13
5	0.04	3.19	0.75	-0.09	2.54	0.83	0.37	0.85	3.46	0.82	1.02	3.18	0.85	0.15
6	0.15	2.82	0.79	-0.01	2.46	0.84	0.24	0.85	3.33	0.83	0.97	3.17	0.85	0.09

integrations the root-mean-square error between the simulated and the observed wind speed was reduced significantly for all SPN simulations. Also the correlation between the observations and the simulations is higher for the SPN experiments. For the bias the picture is not that clear. However, the bias is rather sensitive on how the observations have been reduced to 10 m height. For Scharhörn the impact may not be that dramatic since the observations were taken at 11 m height above ground. At Ekofisk, however, the anemometer height was 85 m and the details of the algorithm used to reduce the wind speed to 10 m height may become important. We also computed the Brier-Score BS defined as

$$BS = 1 - R_{SPN}^2 R_{CTR}^{-2}, \tag{3.3}$$

where R denotes the root-mean-square error for the nudged and the control simulations respectively (Table 3.2). Any positive value of BS thus implies an improved hindcast skill for the SPN compared to the CTR simulations. For instance, a Brier-Score of 0.20 indicates that the mean-square error has been reduced by 20%. Thus, according to Table 3.2 at both stations each SPN realization is performing better than its CTR equivalent.

As the wave model results depend strongly on the driving wind fields the conclusions drawn from the atmospheric fields hold also for the wave fields. Figure 3.1 clearly shows the enhanced uncertainty in those wave model simulations that use wind fields from the REMO CTR simulations. This uncertainty is strongly reduced when wind fields from the SPN integrations are used. The differences in hindcast skill for the significant wave height at Ekofisk are shown in Table 3.3. For Scharhörn no wave height observations were available. As for the wind speed it can be obtained that for the

Table 3.3: Bias B in m, root-mean-square error R in m, and correlation C between the wave height obtained from the $k = 1 \ldots 6$ wave hindcasts using either the wind fields from the REMO CTR or the REMO SPN simulations and the observations at Ekofisk (56.5°N, 3.2°E). In addition, the Brier Score BS is provided.

	CTR			SPN			
	B	R	C	B	R	C	BS
1	0.60	1.23	0.87	0.60	1.03	0.91	0.30
2	0.62	1.25	0.87	0.63	1.05	0.91	0.28
3	0.61	1.24	0.87	0.63	1.04	0.81	0.29
4	0.61	1.21	0.88	0.61	1.05	0.91	0.25
5	0.62	1.22	0.88	0.61	1.03	0.91	0.29
6	0.62	1.19	0.88	0.59	1.04	0.91	0.23

SPN simulations the root-mean-square error is reduced and the correlation is increased compared to those obtained for the CTR experiments. Also for the wave heights, the Brier score indicates that an improvement in hindcast skill was obtained when winds from the SPN ensemble were used to drive the wave model.

3.3.3. *Differences at 7 January*

We found that in our simulations the highest IMU and the largest differences between the CTR and SPN simulations occurred around 7 January. We, therefore, would like to illustrate the synoptic conditions that are responsible for these differences.

The increased wind and wave height variability in the CTR integrations is associated with, and can be explained by, variations in the atmospheric conditions around 7 January. Figure 3.5 shows the SLP for 00:00 UTC 7 January 1993 for two CTR simulations which show a rather good (upper left) and a rather poor (upper right) agreement with observations together with the SLP for a SPN simulation (lower left) and the SLP obtained from the routine analysis performed by the German Weather Service (DWD) (lower right). In general there appears to be a reasonable agreement among all simulations and the DWD analysis. However, details differ and a closer inspection reveals pronounced differences in this overall agreement. For instance, the high pressure system over the Iberian peninsula has a core pressure of about 1035 hPa in the DWD analysis. While this is well represented in all SPN simulations the position and the strength of this high pressure system varies largely in the CTR simulations where core pressures of more than 1040 hPa are found. Furthermore, in the DWD analysis strong pressure gradients prevail over the Eastern Baltic Sea. While such strong pressure

gradients may be found in only some of the CTR experiments they are reasonably reproduced in all SPN simulations. For the North Sea the differences in pressure gradient and thus in wind speed at Scharhörn and Ekofisk may be inferred from the differences in position of the 1015 and the 1020 hPa contour line. Again the SPN simulations show on average a better agreement with the DWD analysis and the uncertainty between the individual realizations is strongly reduced.

In order to demonstrate this in more detail Figure 3.6 and 3.7 show again the IMU for the REMO and the wave model simulations for the North Sea area where Ekofisk and Scharhörn are located. For the CTR ensemble large differences in the position of the 1015 and the 1020 hPa contour line are obtained that are related to strong variations in the horizontal pressure gradients at Ekofisk and Scharhörn. These variations in the pressure gradient together with variations in the position of the pressure centers are finally responsible for the observed differences in the simulated wind speed described above. For the SPN ensemble these differences are hardly visible. The similar holds for the wave model hindcasts (Figure 3.7). The uncertainty in the wind speed and wind direction obtained from the REMO CTR experiments leads to strong variations in the observed wave height. These variations are remarkably reduced when the wind fields from the SPN simulations are used.

3.4. Summary and discussion

Many applications in offshore and coastal engineering require numerical simulations of waves or surges. Wind fields are an important input parameter for such simulations and they represent at the same time a major source of uncertainty. In this study we investigated whether this uncertainty may be reduced if a recently proposed approach by von Storch et al. (2000) is used for the production of the wind hindcasts and if the hindcast skill in these simulations could be improved. Further, the consequences of the improved wind hindcasts for wave model simulations were demonstrated.

The sensitivity of the simulated wind fields, and thus the uncertainty in the simulations depending on the initial conditions, was assessed using ensemble simulations for the period January 1993. In one ensemble the conventional approach was utilized in which the model is driven by boundary conditions at its lateral boundaries only. In the other ensemble the recently proposed spectral nudging approach (von Storch et al. (2000)) was used in which additional information regarding the large scale atmospheric circulation is fed into the RAM. It was shown that most of the time the ensemble variability appears to be small for both ensembles. However, for some periods the ensemble variability (uncertainty) was strongly increased in the control ensemble while it remained small in the spectral nudging integrations.

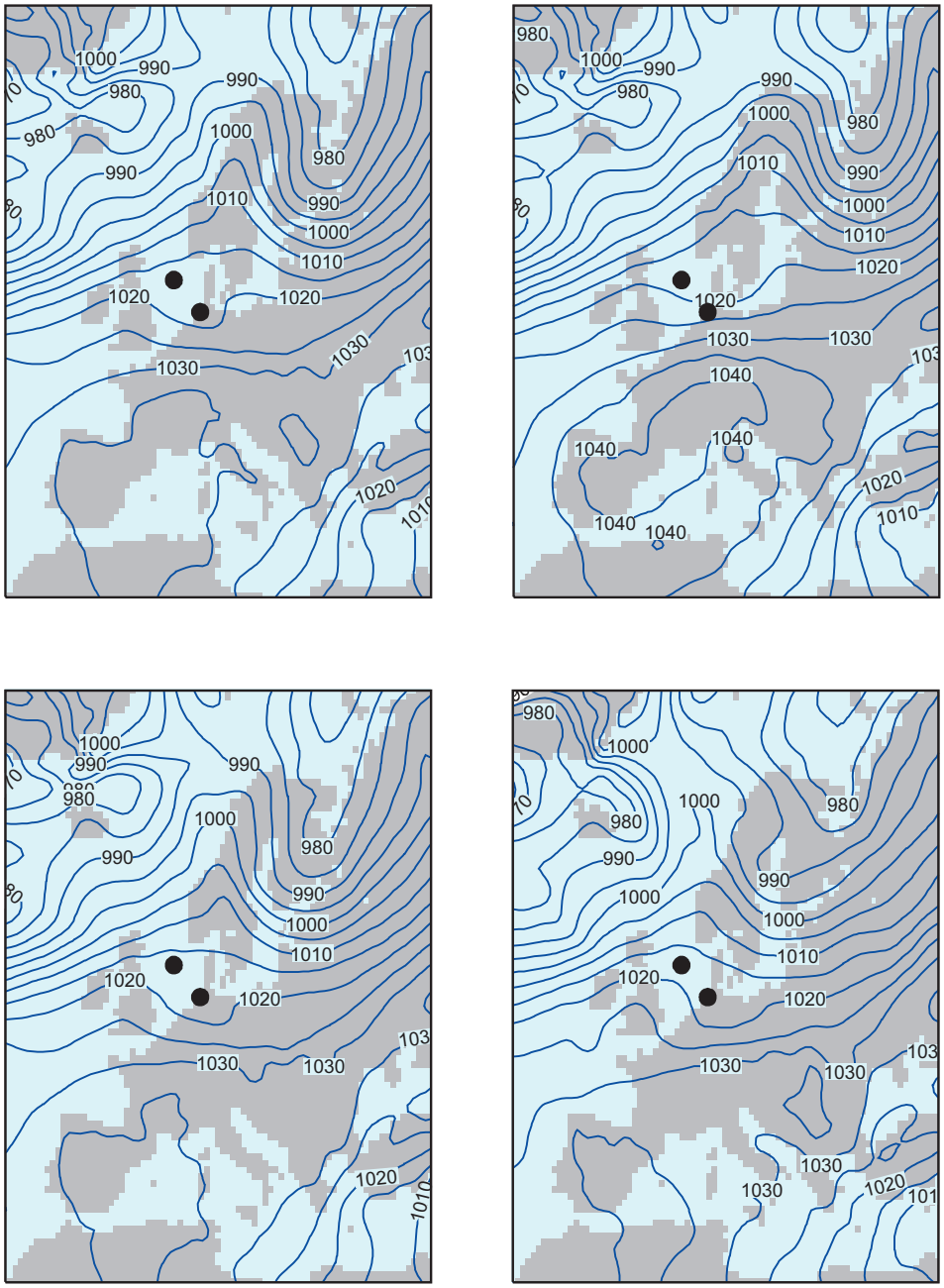

Figure 3.5: SLP in hPa for two REMO CTR (upper panel) and one REMO SPN (lower left panel) realizations at 00:00 UTC 7 January 1993 together with the SLP obtained from the routine analysis of the German Weather Service (lower right). The two solid black points in each panel indicate the positions of Ekofisk (northernmost point) and Scharhörn (southernmost point).

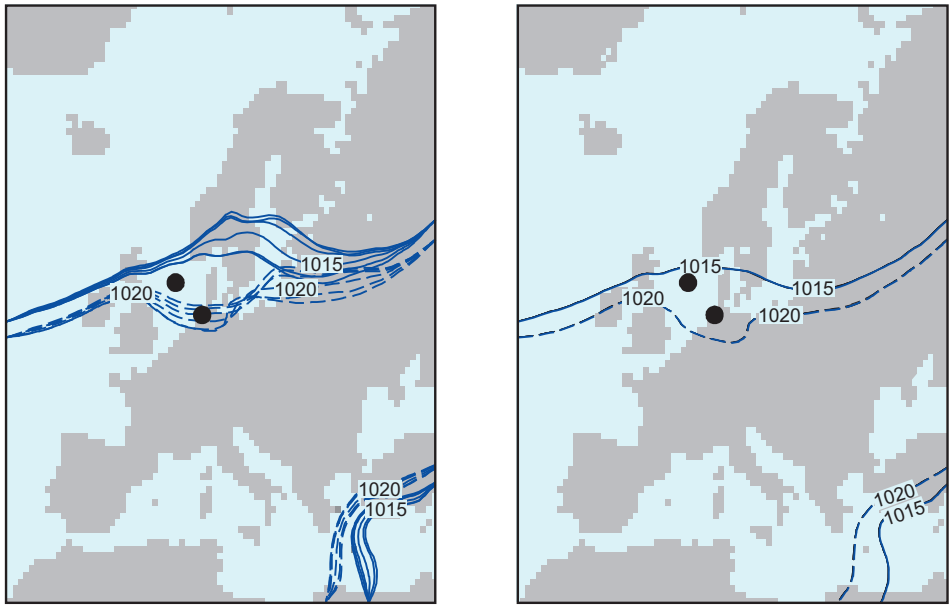

Figure 3.6: SLP in hPa obtained from the REMO CTR (left) and the REMO SPN (right) simulations at 00:00 UTC 7 January 1993. Shown are the 1015 hPa (solid) and the 1020 hPa (dashed) contour lines from all 6 REMO CTR (left) and all 6 REMO SPN (right) simulations. Note that the differences are hardly visible for the SPN simulations. The two solid black points indicate the positions of Ekofisk (northernmost) and Scharhörn (southernmost points).

In these situations there are several atmospheric states about equally likely to occur in the CTR integrations. Accordingly, the regional atmospheric model shows very different results for only slightly modified initial conditions. In the perspective of numerical multi-decadal hindcasts or historical reconstructions only the trajectory closest to the observed state is desired. For the CTR realizations, it is not clear whether this trajectory is going to be realized if only one integration can be performed. Using the SPN approach this uncertainty is strongly reduced.

For the examples shown in this paper it could be further demonstrated that for the SPN simulations the hindcast skill was improved for both, the winds and the wave model results. For multi-decadal hindcasts with regional atmospheric models ensemble simulations for the entire simulation period are not feasible. Our results suggest that for such hindcasts the SPN approach could provide an alternative to keep the models trajectory closer to the observed one in case no further data for data assimilation are available. Based on this experience the approach has recently been utilized by Feser et al. (2001) to produce a high-resolution wind hindcast for the North Sea, the Baltic Sea and the Northeast Atlantic covering roughly the past 40 years. Feser et al. (2001)

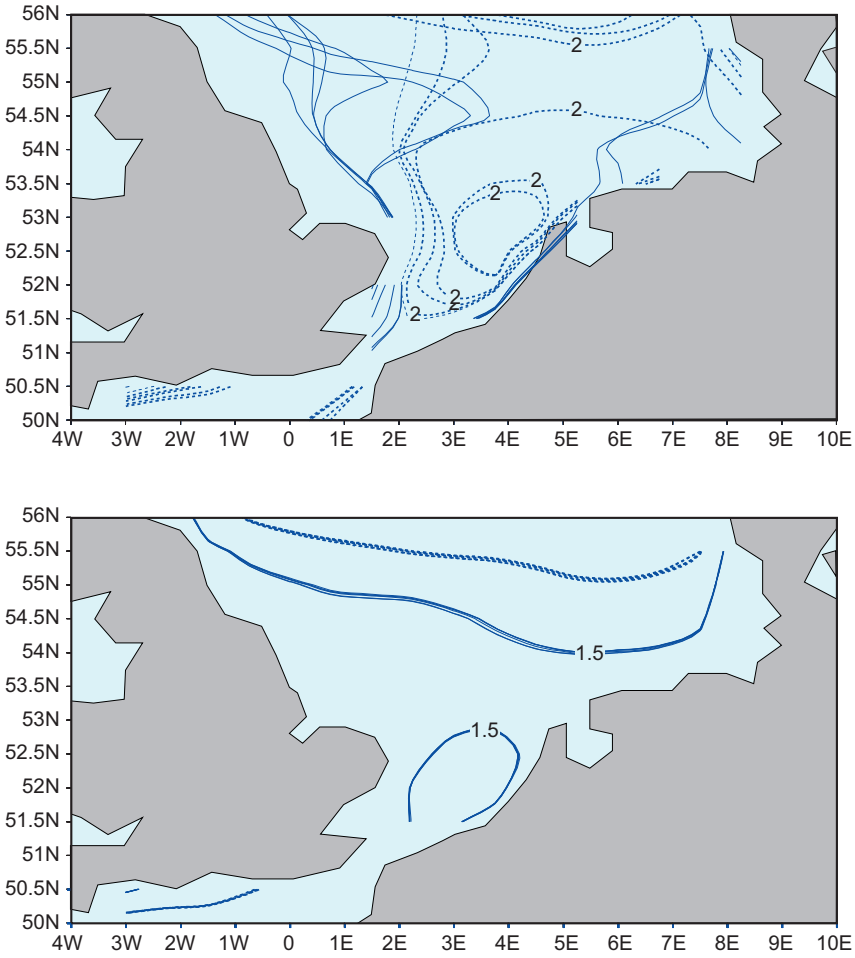

Figure 3.7: Total Hs in m for the WAM CTR (upper) and the WAM SPN (lower) simulations at 00:00 UTC 7 January 1993. Shown are the 1.5 m (solid) and the 2.0 m (dashed) contour lines for all 6 WAM CTR (upper) and all 6 WAM SPN (lower) simulations.

provided their wind fields hourly at a spatial resolution of about 50 $\times$ 50 km. Comparison of simulated and observed wind fields indicated that this way a reasonable and high resolution hourly wind data set covering many years could be produced (Weisse and Gayer (2000), Soares et al. (2002), Weisse et al. (2002)). Presently, the approach is used to produce further multi-decadal wind hindcasts for other areas. Furthermore, these wind fields are used to produce multi-decadal simulations of waves and surges for a number of European coastal areas (Soares et al. (2002)).

Although the additional computational resources required for the spectral nudging are minor compared with enhanced data assimilation schemes, data assimilation should be favoured in case additional observational data are available that have not been assimilated in the global analyses. In addition, our conclusions are based on the

analysis of a short time period only. Further tests over a larger data set are required to fully assess the improvements obtained from the SPN approach. Furthermore, the improvement in hindcast skill that can be obtained by using the SPN approach for multi-decadal hindcasts strongly depends on how often periods of enhanced IMU do occur and on the typical duration and spatial extend of such events. From the material presented here we may not conclude on the frequency and the typical spatial scale of such events. Further analysis of longer ensemble simulations is required to fully assess this topic. There are, however, a few recent studies which indicate that such events may occur a little more frequent: Rinke and Dethloff (2000) investigated the sensitivity of a regional arctic climate model to its initial conditions and found that due to the weaker lateral boundary control compared with mid-latitude RAMs a pronounced sensitivity of the Arctic simulations to uncertainties in initial conditions occurred. They concluded that changes in the monthly mean atmospheric structures caused by internal processes were in the same order as those induced by inaccurate physical parameterizations. Weisse et al. (2000) and Weisse and Schneggenburger (2002) investigated the sensitivity of a coupled regional atmosphere-wave-model to different sea state dependent roughnesses and initial conditions. They found that the sensitivity to modified momentum flux parameterizations was in the same order of magnitude as the internal variability caused by modified initial conditions. Further, they reported prolonged periods of enhanced internal model variability, some of which lasted several days up to almost a month. A similar result was found by De Zolt (pers. comm. 2000) who ran a regional atmospheric model for the Mediterranean for the year 1996.

Summarizing, the spectral nudging approach appears to be capable to reduce the IMU without squeezing the realistic small scale variability and to improve the hindcast skill for surface winds. Based on the analysis of wind speeds at Ekofisk and Scharhörn it is concluded that some indications do exist that the spectral nudging approach should be favoured instead of the conventional approach for such applications as multi-decadal hindcasts. Further studies are, however, needed to investigate the frequency of events with high internal model variability in integrations using the conventional approach. Spectral nudging may be seen as a sub-optimal and indirect data assimilation technique (von Storch et al. (2000)), depending on the quality of the global forcing fields. Here we have shown that it may represent a useful approach for regional multi-decadal hindcasts and climate reconstructions for which limited computational resources and no further observational data for assimilation are available.

3.5. Acknowledgments

We thank Daniela Jacob and Ralf Podzun for their help with REMO and Hans Luthardt for assistance with the NCEP data. Lennart Bengtsson provided the permission to use the REMO model. Eduardo Zorita, Hans von Storch, and Heinz Günther carefully read

the manuscript. We are grateful for their comments. The work was funded partly by the European Union under EVK2-CT-1999-00038
(HIPOCAS) and the Helmholtz Gemeinschaft Deutscher Forschungszentren via the Lead (Pb) Project.

Bibliography

Caires, S., Sterl, A., Bidlot, J., Graham, N., Swail, V., 2002. Climatological assessment of reanalysis ocean data. In: *7th International workshop on wave hindcasting and forecasting*. Banff, Alberta, Canada, pp. 1–12.

Cardone, V., Jensen, R., Resio, T., Swail, V., Cox, A., 1996. Evaluation of contemporary ocean wave models in rare extreme events: The "Halloween Storm" of October 1991 and the "Storm of the Century" of March 1993. *J. Atmos. Oceanic Technol.* **13**, 198–230.

Cox, A., Greenwood, J., Cardone, V., Swail, V., 1995. An interactive objective kinematic analysis system. In: *4th International workshop on wave hindcasting and forecasting*. Banff, Alberta, Canada, pp. 109–118.

Cox, A., Swail, V., 2001. A global wave hindcast over the period 1958-1997: Validation and climate assessment. *J. Geophys. Res.* **106** (C2), 2313–2329.

Debernhard, J., Sætra, Ø., Roed, L., 2002. Future wind, wave and storm surge climate in the Northern Seas. *Climate Res.* **23**, 39–49.

Ewing, J., Weare, T., Worthington, B., 1979. Hindcast study of extreme wave conditions in the North Sea. *J. Geophys. Res.* **84** (C9), 5739–5747.

Feser, F., Weisse, R., von Storch, H., 2001. Multi-decadal atmospheric modeling for Europe yields multi-purpose data. *Eos Transactions* **82** (28), 305, 310.

Flather, R., Smith, J., Richards, J., Bell, C., Blackman, D., 1998. Direct estimates of extreme storm surge elevations from a 40-year numerical model simulation and from observations. *Global Atmos. Oc. System* **6** (2), 165–176.

Gibson, R., Kålberg, P., Uppala, S., 1996. The ECMWF re-analysis (ERA) project. *ECMWF Newsl.* **73**, 7–17.

Greenslade, D., 2001. A wave modelling study of the 1998 Sydney to Hobart yacht race. *Aust. Met. Mag.* **50**, 53–63.

Günther, H., Hasselmann, S., Janssen, P., 1991. Wamodel Cycle 4. *Tech. Rep. 4*, Deutsches Klimarechenzentrum, Available from Deutsches Klimarechenzentrum, Bundesstr. 55, D-20146 Hamburg, Germany, 102pp.

Günther, H., Rosenthal, W., Stawarz, M., Carretero, J., Gomez, M., Lozano, I., Serrano, O., Reistad, M., 1998. The wave climate of the Northeast Atlantic over the period 1955-1994: The WASA wave hindcast. *Global Atmos. Oc. System* **6** (2), 121–164.

Holthuijsen, L., Booji, N., Bertotti, L., 1996. The propagation of wind errors through ocean wave hindcasts. *J. Offshore Mech. and Arctic Eng.* **118**, 184–189.

Jacob, D., Podzun, R., 1997. Sensitivity studies with the regional climate model REMO. *Meteorol. Atmos. Phys.* **63**, 119–129.

Jacob, D., Podzun, R., Claussen, M., 1995. REMO - a model for climate research and weather prediction. In: *Proc. Internat. Workshop on Limited-Area and Variable Resolution Models*. Beijing, China, pp. 273–278.

Ji, Y., Venrnekar, A., 1997. Simulation of the Asian Summer Monsoon of 1987 and 1988 with a regional model nested in a global GCM. *J. Climate* **10**, 1965–1979.

Kalnay, E., M. Kanamitsu, R. Kistler, W. Collins, D. Deaven, L. Gandin, M. Iredell, S. Saha, G. White, J. Woollen, Y. Zhu, M. Chelliah, W. Ebisuzaki, W. Higgins, J. Janowiak, K. C. Mo, C. Ropelewski, J. Wang, A. Leetmaa, R. Reynolds, R. Jenne, and D. Joseph, 1996: The NCEP/NCAR reanalysis project. *Bull. Amer. Meteor. Soc.*, **77**, 437–471.

Molteni, F., Buizza, R., Palmer, T., Petroliagis, T., 1996. The ECMWF ensemble prediction system. *Quart. J. Roy. Meteor. Soc.* **122** (529), 73–119.

Rinke, A., Dethloff, K., 2000. On the sensitivity of a regional Arctic climate model to initial and boundary conditions. *Climate Res.* **14** (2), 101–113.

Soares, C., Weisse, R., Carretero, J., Alvarez, E., 2002. A 40 years hindcast of wind, sea level and waves in European waters. In: *Proceedings of OMAE 2002: 21st International Conference on Offshore Mechanics and Arctic Engineering 23-28 June 2002*. Norway, Oslo.

Swail, V., Cardone, V., Cox, A., 1998. A long term North Atlantic wave hindcast. In: *5th International workshop on wave hindcasting and forecasting*. Melbourne, Florida, USA, pp. 1–16.

Swail, V., Cox, A., 2000. On the use of NCEP/NCAR reanalysis surface marine wind field s for a long term North Atlantic wave hindcast. *J. Atmos. Oceanic Technol.* **17**, 532–545.

Teixeira, J., Abreu, M., Soares, C., 1995. Uncertainty of ocean wave hindcasts due to wind modelling. *J. Offshore Mech. and Arctic Eng.***117**, 294–297.

The WAMDI-Group, 1988. The WAM model - a third generation ocean wave prediction model. *J. Phys. Oceanogr.* **18**, 1776–1810.

The WASA-Group, 1998. Changing waves and storms in the Northeast Atlantic? *Bull. Amer. Meteor. Soc.* **79** (5), 741–760.

Tolman, H., 1998. Validation of NCEP's ocean winds for the use in wind wave models. *Global Atmos. Oc. System* **6** (3), 243–268.

von Storch, H., Hagner, C., Costa-Cabral, M., Feser, F., Pacyna, J., Pacyna, E., Kolb, S., 2002. Reassessing past European gasoline lead policies. *Eos Transactions* **83** (36), 393,399.

von Storch, H., Langenberg, H., Feser, F., 2000. A spectral nudging technique for dynamical downscaling purposes. *Mon. Wea. Rev.* **128** (10), 3664–3673.

Wang, X., Swail, V., 2001. Changes of extreme wave heights in the Northern Hemisphere Oceans and related atmospheric circulation regimes. *J. Climate* **14**, 2204–2221.

Wang, X., Swail, V., 2002. Trends of atlantic wave extremes as simulated in a 40-yr wave hindcast using kinematically reanalyzed wind fields. *J. Climate* **15** (9), 1020–1035.

Weisse, R., Feser, F., Günther, H., 2002. A 40-year high-resolution wind and wave hindcast for the Southern North Sea. In: *7th International workshop on wave hindcasting and forecasting*. Banff, Alberta, Canada, pp. 97–104.

Weisse, R., Gayer, G., 2000. An approach towards a 40-year high-resolution wave hindcast for the Southern North Sea. In: *Proceedings, 6th International Workshop on Wave Hindcasting and Forecasting*. Monterey, California, USA, pp. 204–210.

Weisse, R., Heyen, H., von Storch, H., 2000. Sensitivity of a regional atmospheric model to a sea state dependent roughness and the need of ensemble calculations. *Mon. Wea. Rev.* **128** (10), 3631–3642.

Weisse, R., Schneggenburger, C., 2002. The effect of different sea state dependent roughness parameterizations on the sensitivity of the atmospheric circulation in a regional model. *Mon. Wea. Rev.* **130** (6), 1595–1602.

Chapter 4

A spatial two-dimensional discrete filter for limited area model evaluation purposes

Frauke Feser and Hans von Storch

Institute for Coastal Research, GKSS Research Centre
PO Box, 21502 Geesthacht, Germany

Published in:
Monthly Weather Review, Vol. 133, No. 6, pp. 1774-1786, 2005.

Abstract

A two-dimensional discrete spatial filter was developed. It serves as a means to classify meteorological fields on a limited area grid according to their spatial dimensions by filtering certain wave number ranges. Thereby it performs an isotropic spatial scale separation of the atmospheric fields. A general algorithm was developed, which allows the construction of a filter that closely approximates a specific isotropic response function. The filter is simple in the construction and easy to apply while giving reasonable results. The method allows for considerable flexibility in choosing this specific response. This way, low-, band- and high-pass filters are obtained. Examples show an effective scale separation of atmospheric fields on limited area grids which can be used for process studies, model evaluation or comparisons.

4.1. Introduction

Limited area models (LAMs) for the atmosphere are used for simulating the regional climate (Giorgi et al. (2001)). The spatial gridding of these regional climate models (RCMs) currently ranges from about 50 to 10 kilometers and time periods of up to several decades have been simulated. However, the question if RCMs provide added value compared to global analyses (such as the NCEP re-analysis; Kalnay et al. (1996)) or global models of lower resolution is still only partly answered. We believe this is mainly due to the lack of a convenient tool to properly describe the added value - namely a filter procedure that compares the performance of the global analysis or model with that of the regional model on large and medium-to-small spatial scales. In this paper, we suggest to use digital filters for the separation of components of a limited spatial field with different spatial scales. The spatially filtered fields may then be used for model validation, diagnostic purposes, or comparisons between the global coarse-grid data and the regional model refinement.

When identifying the added value of RCM simulations, we suggest the application of the downscaling paradigm which states that smaller scale dynamics may be understood as being conditioned by large scale variability and physiographic regional detail (von Storch (1995)). In doing so, we consider the large scales described properly by the global analyses or global climate models. On the other hand, the global models and analyses have little skill at scales smaller than a few grid points, e.g., a few hundred kilometers. On these scales, we expect the added value of RCMs. In the present paper, we deal with the problem how to achieve conveniently and efficiently this scale separation.

Spatial filters are rarely used for the evaluation of RCM output, in particular not in the context of regional climate simulations with a RCM. One approach, used in LAM forecasting and evaluation, is to expand a limited field in a 2-d Fourier series, and to rebuild a filtered field by recombining only Fourier components with relevant scales (Errico (1985), Stamus et al. (1992)). This Fourier concept was also incorporated into the spectral nudging or large-scale forcing concept by Waldron et al. (1996), von Storch et al. (2000) and Miguez-Macho et al. (2004), which keeps the large-scale part of a regional model solution close to the forcing global field in the model interior. Bettge and Baumhefner (1980) introduced digital filters using classical ideas proposed by Shuman (1957) and Shapiro (1970).

In the present paper, we provide an algorithm to construct two-dimensional digital filters for the spatial scale separation of limited area fields (Sections 4.5 and 4.6). Examples of such filters are presented and their utility is demonstrated (Section 4.7). Before doing so, we want to discuss alternatives to our approach.

The most straightforward approach is Errico's approach to decompose the two-dimensional field into a series of sinusoidal harmonics in x- and y-directions, as men-

tioned above. This approach has the distinctive advantage that the scale separation is very accurate. However, the harmonic analysis suffers from the erroneous description of spatial ”trends” (non-sinusoidal components of the spatial fields, such as linear or higher polynomials) as being composed of ”waves”. The harmonic analysis works fine if the considered field is periodic. However, LAM output is almost never periodic and often exhibits a trend; for instance, in winter, air pressure is often lower over the ocean and higher over land. We demonstrate the problem of subjecting a ”trend” to harmonic analysis by a synthetic example of a pure spatial trend without any wave components (Figure 4.1a). This linear trend (shown as dots) can be decomposed into sine and cosine waves as shown in Figure 4.1a. If this spatial trend is filtered with a Fourier low-pass filter (lowest four wave contributions of Figure 4.1a were retained in this example), the resulting curve (blue dashed curve in Figure 4.1b) replicates the overall trend but adds significant large-scale wave components - in particular at the margins. One might argue that in LAM applications the overshooting in the marginal zone would not matter, since it would affect only the sponge zone which is normally not considered. However, there is also a false identification of short wave contributions by the high-pass spatial filter (red dashed curve in Figure 4.1b; shortest four wave contributions of Figure 4.1a were retained) which is not limited to the sponge zone but which occurs also in the interior. The discrete cosine-filter method suggested by Denis et al. (2002) is better in describing spatial trends, but it also maps all variability on wavy components, so that any recombination of a subset of these components, which is needed for formulating a filter, may generate artificial wavy contributions.

Errico (1985) had noticed the problem of spatial trends and has suggested to subtract linear functions; in the following we extend his approach by considering not only linear but also quadratic polynomials (Section 4.2).

Digital filters (e.g. Shuman (1957), Shapiro (1970), Shapiro (1975)) have the advantage that they operate with a finite ”support base”, e.g. the filtered value at some location is a function of the values in a neighbourhood of that location and not, as in case of harmonic analysis, of all locations. The disadvantage is that the scale separation is less effective than with a Fourier filter, since the response function of a digital filter is smooth and not a step-function as in the case of a Fourier filter. That is, for a low-pass filter, the long waves will not exactly be retained but only approximately; similarly, a high-pass filter will not completely remove all contributions of long waves - which is a problem, when the intensity of short waves is much smaller than those of long waves. Digital filters usually lead to a loss of data at the margins of the domain, as the determination of a filtered value needs data in a symmetric neighbourhood of that point. However, with RCMs this is not a problem, as such models are run with a sponge zone within which little added value is expected. Thus, if the filtering neighbourhood is not wider than the sponge zone, a scale separation for the entire relevant interior domain can be achieved.

Usually, digital filters are one-dimensional, and are applied to two-dimensional fields by first applying it in one direction and then in the other. Bettge and Baumhefner (1980) used such a one-dimensional digital band-pass filter for obtaining a scale-separation of limited area atmospheric fields. They applied the 1-2-1 low-pass filter operator presented by Shuman (1957) and created band-pass filters by repetition and differences. Another one-dimensional digital filter, a high-order, high-pass implicit filter, was used by Raymond (1989). Such filters are, unfortunately, not isotropic and their filter characteristics are not really flexible. Therefore a method for the flexible construction of two-dimensional isotropic discrete filter was required. The filter weights are obtained by solving an approximation problem.

2-d-wavelets (e.g. Yano et al. (2001), Desrochers and Yee (1999), Jameson et al. (2002)) may be a promising, alternative approach. However, so far their application in scale separation used in regional climate modelling is very limited. For our limited area model application with terabytes of data a fast filtering approach is essential. In general the image decomposition in fast wavelet algorithms is made with a dyadic resolution factor (Daubechies (1992), Starck et al. (1998)). If, as in our case, special wave numbers are of interest as cut-off frequencies they usually are not matched directly by the dyadic resolution approach. To achieve the separation into certain wave-number bands a post-processing of the wavelet with the multi-resolution analysis (Mallat (1989), Mallat (1998)) is necessary, which costs extra computing time, both in terms of determining the wavelet transform and the back transformation. We suggest that wavelets are not a viable alternative to our digital filters which are computationally simple and adapted to the specific wave-number band.

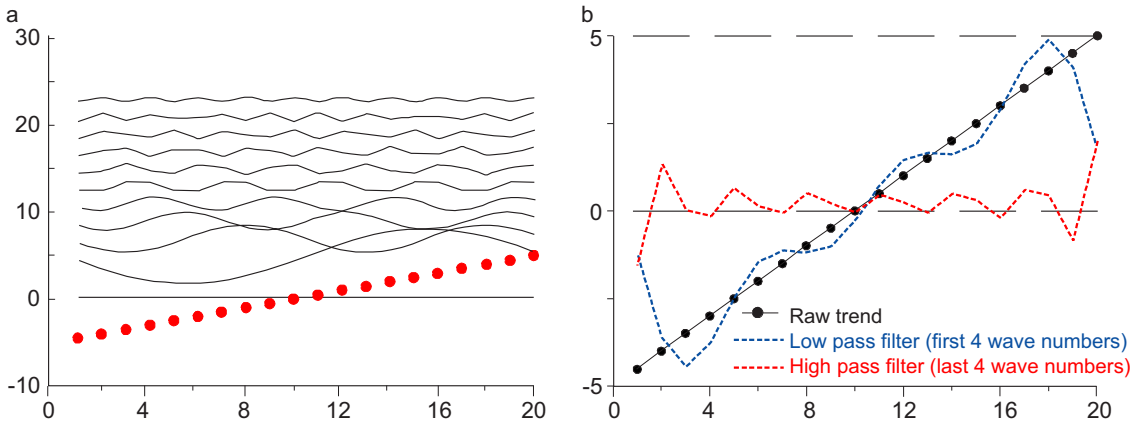

Figure 4.1: Fourier decomposition of a spatial trend (a) and low- and high-pass Fourier-filtered spatial trend (b). The x-axis denotes the grid points of the LAM.

4.2. Pre-processing: Subtraction of two-dimensional polynomials

Before filtering, the meteorological fields in our study were 'pre-processed', whereby two-dimensional polynomials were subtracted. This serves two purposes:

- Fourier expansions of fields on regionally limited grids suffer from the fact that the non-periodic components are falsely represented by "waves". By identifying the dominant non-periodic components P, we may conceptually express the 2-d LAM fields as

  $$f(x,y) = P_f^K(x,y) + L_f(x,y) + M_f(x,y) + S_f(x,y) \tag{4.1}$$

  Here, P_f^K represents the polynomial of k-th order of the two-dimensional field f, L_f its large-scale wave component, M_f the medium-scale wave component and S_f the short-scale wave component of f.
  When the P_f-component is disregarded, the non-periodic contribution falsely compounds the wavy components on all scales. Thus, the inclusion of P_f^K leads to a better separation and description of components.

- Practically, the separation into the three wave components L, M and S is obtained by a digital filter. Such filters operate fine if the variance of the wave numbers to be suppressed is not much larger than the variance which is supposed to be retained. This is always the case with low-pass filters, when high wave number variance is eliminated - high wave numbers have always smaller variance than low wave numbers. There is usually also not a problem for medium-pass filters. However, high-pass filters are usually negatively impacted, as the elimination of low-pass components is not perfect and minor remnants of low-wave number variability remain - and minor remnants are comparable to high wave number contributions in terms of variance. An example for this is given in Errico (1987). The subtraction of polynomials can help to ease this problem, as this operation reduces the variance of the large-scale.

Equations for the polynomial subtraction are given in appendix 4.10. Figure 4.2 shows the K=1 and K=2 polynomials fitted to the wind speed on December 3rd, 1999, 6 p.m., and the total wind speed field as well as after subtraction of the K=1,2 polynomials. In contrast to the linear K=1 polynomial, the fitted quadratic polynomial exhibits a marked non-linear pattern, describing higher wind speeds over the North Atlantic and a gradual increase towards southern latitudes and continental areas. The wind speed field in the bottom of Figure 4.2 is rather noisy. Thus the subtraction of the polynomials is not changing the overall character of the spatial wind speed distribution, but the NW-SE asymmetry is eliminated. We suggest to subtract the quadratic polynomials for data to be band- or high-pass filtered. The polynomial subtraction was applied to all band- and high-pass filtered fields shown in section 4.7.

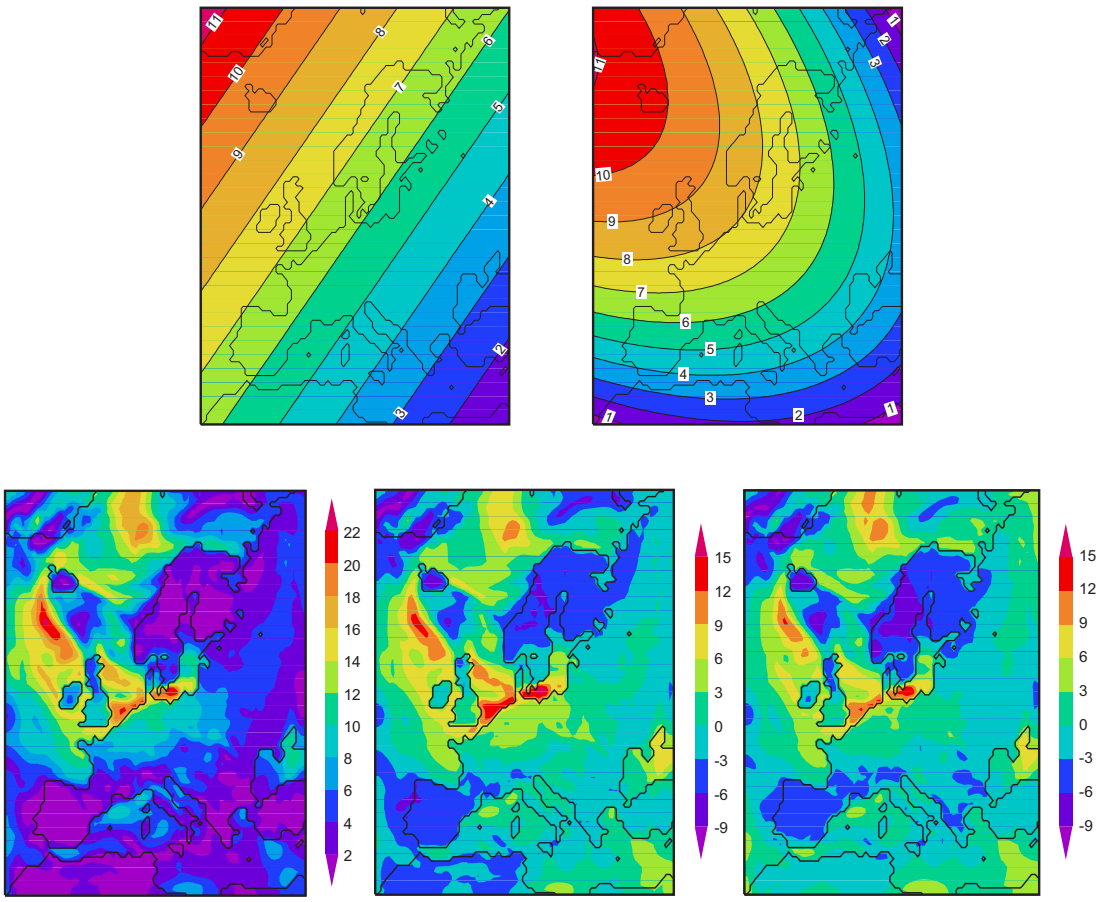

Figure 4.2: Top: $K = 1, 2$-polynomials P_u^1 and P_u^2 fitted to the wind speed field (m/s) at a height of 10 m on December 3rd, 1999, 6 p.m. (storm 'Anatol').
Bottom: Full wind speed field for the same date, and after subtraction of the $K = 1, 2$-polynomials i.e., $u - P_u^1$ and $u - P_u^2$.

4.3. Selection of pre-specified wave numbers

The idea was to construct an almost isotropic filter. Thus, it is meaningful to select all wave numbers with the same or similar two-dimensional wave number $k^* = \sqrt{k^2 + l^2}$ and to assign the same response $\kappa(k^*)$.

A low pass filter is generated by requesting $\kappa(k^*) = 1$ for all k^* below a small wave number, for instance 5, and $\kappa(k^*) = 0$ for all wave numbers k^* larger than a large number, say 20. In the intermediate range, the response is expected to smoothly transform from 1 to 0. It is advisable that the two regions with specified responses are not covering the entire domain; instead a band of unspecified responses should be used in an in-between region.

Similarly high-pass and band-pass filters can be constructed. For a band-pass filter three parameters have to be selected, a region with zero responses for small and large wave numbers, and a response of one for medium wave numbers.

4.4. Filter weights

The filter array must be quadratic and symmetrical with respect to the zonal and meridional directions, and also with respect to both diagonals. Thus, only a few filter weights are to be determined - in the sketch marked by "x" while those determined by symmetry are given by "o", for instance in a filter with 9 and with 25 weights:

```
                o  o  o  o  o
o  o  o         o  o  o  o  o
o  x  o         o  o  x  o  o
o  x  x         o  o  x  x  o
                o  o  x  x  x
```

Apart from the central point, which is weighted by the central filter weight $a_{0,0}$, N points to the left (top) and N points to the right (bottom) are used, such that $2N + 1$ points are considered in either direction. For a LAM domain of 81 x 91 grid points we chose filters with $N = 8$ points, so that their spatial extension is $(2N + 1)$x$(2N + 1)$ = 17x17 points.

The symmetric conditions are $a_{m,n} = a_{-m,n} = a_{m,-n} = a_{-m,-n} = a_{n,m}$; whereby $_{n,m}$ denote rows and columns, respectively. Thus, the filter weights a_{nm} look like the following in case of a filter with 25 weights:

$$\begin{pmatrix} a_{-2,-2} & a_{-2,-1} & a_{-2,0} & a_{-2,1} & a_{-2,2} \\ a_{-1,-2} & a_{-1,-1} & a_{-1,0} & a_{-1,1} & a_{-1,2} \\ a_{0,-2} & a_{0,-1} & a_{0,0} & a_{0,1} & a_{0,2} \\ a_{1,-2} & a_{1,-1} & a_{1,0} & a_{1,1} & a_{1,2} \\ a_{2,-2} & a_{2,-1} & a_{2,0} & a_{2,1} & a_{2,2} \end{pmatrix} = \begin{pmatrix} a_{2,2} & a_{2,1} & a_{2,0} & a_{2,1} & a_{2,2} \\ a_{2,1} & a_{1,1} & a_{1,0} & a_{1,1} & a_{2,1} \\ a_{2,0} & a_{1,0} & a_{0,0} & a_{1,0} & a_{2,0} \\ a_{2,1} & a_{1,1} & a_{1,0} & a_{1,1} & a_{2,1} \\ a_{2,2} & a_{2,1} & a_{2,0} & a_{2,1} & a_{2,2} \end{pmatrix} \tag{4.2}$$

The resulting filter weights for a low-, band- and high-pass filter are shown in Figure 4.3. The low-pass filter weights (Figure 4.3 a) show a homogenous structure with highest values in the middle of the weighting area and decreasing values further away from the filter base point. This will result in a large mean value and therefore a low-pass filtered field. The band-pass filter weights (Figure 4.3 b) include several transitions between positive and negative values and thereby the mean value will be filtered and

only the smaller structures will remain. This is even stronger enforced for the high-pass filter weights (Figure 4.3 c) which comprise a yet higher number of changes in sign. Thus, only the smallest structures will pass this filter.

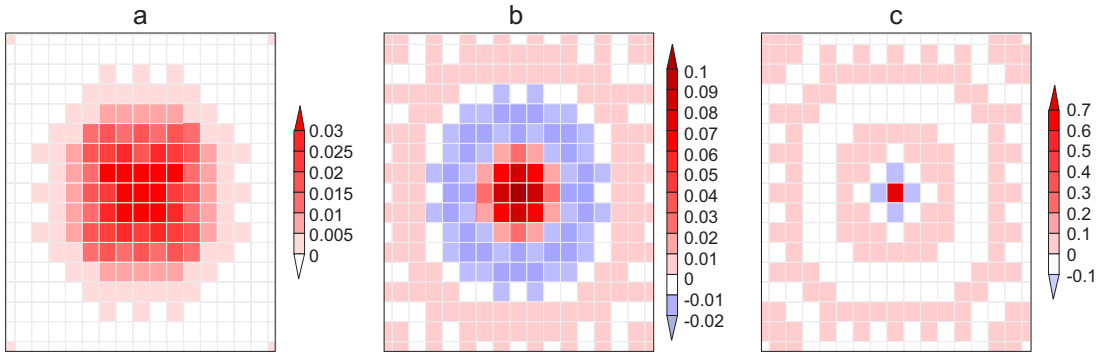

Figure 4.3: Filter weights for a low-pass (a), band-pass (b), and high-pass (c) filter. a_{00} is in the centre; representation as in equation (4.2). The axes denote grid points of the LAM. Filters were chosen with $N = 8$ points, so that their spatial extension is $(2N + 1)$x$(2N + 1)$ = 17x17 points.

4.5. Response function

We assume a 2-d periodical function f which can be expanded into Fourier components:

$$f(x, y) = \sum_{k,l=-K}^{K} \alpha_{kl} e^{i(kx+ly)} \tag{4.3}$$

with the Fourier coefficients $\alpha_{k,l} = \alpha^*_{-k,-l}$ because $f(x, y)$ is a real function. k and l are the zonal and meridional wave numbers, respectively. The arguments x and y vary between 0 and 2π. The filtered function $\tilde{f}$ is given by:

$$\tilde{f}(x, y) = a_{00} f(x, y) + A + B + C \tag{4.4}$$

with

$$\begin{aligned} A &= \sum_{n=1}^{N} a_{n0} \left[f(x, y + \hat{n}) + f(x, y - \hat{n}) \right. \\ &\qquad \left. + f(x + \hat{n}, y) + f(x - \hat{n}, y) \right] \\ B &= \sum_{n=1}^{N} a_{nn} \left[f(x + \hat{n}, y + \hat{n}) + f(x + \hat{n}, y - \hat{n}) \right. \\ &\qquad \left. + f(x - \hat{n}, y + \hat{n}) + f(x - \hat{n}, y - \hat{n}) \right] \end{aligned} \tag{4.5}$$

$$
\begin{aligned}
C &= \sum_{n=2}^{N} \sum_{m=1}^{n-1} a_{nm} \left[f(x+\hat{n}, y+\hat{m}) + f(x+\hat{n}, y-\hat{m}) \right. \\
&\quad + f(x-\hat{n}, y+\hat{m}) + f(x-\hat{n}, y-\hat{m}) \\
&\quad + f(x+\hat{m}, y+\hat{n}) + f(x+\hat{m}, y-\hat{n}) \\
&\quad \left. + f(x-\hat{m}, y+\hat{n}) + f(x-\hat{m}, y-\hat{n}) \right]
\end{aligned}
$$

with the convention $\hat{n} = n \cdot 2\pi/L$ and $\hat{m} = m \cdot 2\pi/L$. L is the number of grid points, which are counted by the integers n and m. The transformation from n to $\hat{n}$ is required as we have written (4.3) for functions defined on the interval $[0, 2\pi]$. The filter weights are denoted by a_{nm}. A represents the central row and column of matrix (4.2), B the diagonals and C the remaining elements. Further detailed calculation steps are given in appendix 4.11.

The filtered function may also be expanded into a Fourier decomposition

$$
\tilde{f}(x, y) = \sum_{k,l=-L}^{K} \tilde{\alpha}_{kl} e^{i(kx+ly)} \tag{4.6}
$$

with $\tilde{\alpha}_{k,l} = \tilde{\alpha}^*_{-k,l} = \tilde{\alpha}^*_{k,-l} = \tilde{\alpha}_{-k,-l}$. The response function is given by

$$
\kappa(k, l) = \tilde{\alpha}_{kl} / \alpha_{kl} \tag{4.7}
$$

By concatenating the various contributions in (4.4), the response function κ can be written as in the following for wave numbers $k, l = -K, -K+1 \ldots -1, 0, 1 \ldots K-1, K$:

$$
\begin{aligned}
\kappa(k, l) &= a_{0,0} + \sum_{n=1}^{N} \left[2a_{n,0} (cos(k\hat{n}) + cos(l\hat{n})) + 4a_{n,n} cos(k\hat{n}) cos(l\hat{n}) \right] \\
&\quad + 4 \sum_{n=2}^{N} \sum_{m=1}^{n-1} a_{n,m} \left[cos(k\hat{n}) cos(l\hat{m}) + cos(l\hat{n}) cos(k\hat{m}) \right]
\end{aligned} \tag{4.8}
$$

The constants 2 and 4 in (4.8) account for the multiple use of the filter weights in one filtering step. The response functions are shown in Figure 4.4 for the low-pass (a), band-pass (b), and high-pass (c) filters with the filter weights of Figure 4.3. The wave number ranges were chosen as in the following for the low-pass filter:
$\kappa(k^*)$ = 1 for all $k^* \leq 6$ and $\kappa(k^*)$ = 0 for all $k^* \geq 11$;
for the band-pass filter:
$\kappa(k^*)$ = 0 for all $k^* \leq 6$, $\kappa(k^*)$ = 1 for all $k^* \geq 8$ and ≤ 16, and $\kappa(k^*)$ = 0 for all $k^* \geq 18$;
and for the high-pass filter:
$\kappa(k^*)$ = 0 for all $k^* \leq 21$ and $\kappa(k^*)$ = 1 for all $k^* \geq 26$
for a filter of 17 x 17 grid points used for a LAM domain of 81 x 91 grid points. The response functions show a well-defined wave number range where the response is

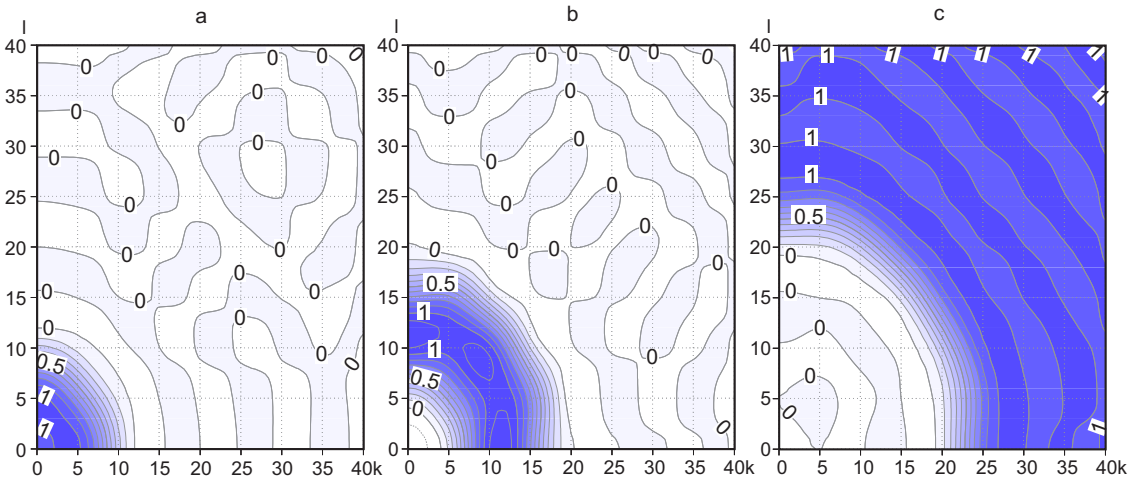

Figure 4.4: Response functions for the low-pass (a), band-pass (b), and high-pass (c) filters with the filter weights of Figure 4.3. The axes show the zonal wave numbers k (x-axis) and the meridional wave numbers l (y-axis).

close to 1 and a smooth transition to response values of about 0. The transition area can be selected quite narrow as can be seen for the band-pass filter (b) which results in a rather sharply defined filter.

Some cases of overshooting of the response function occurred when the areas of response values of 1 and 0 were chosen in a way that the transition area in between was too narrow, so that only a small number of unspecified responses resulted. Overshooting can be identified by locating large positive or negative values in the response function which are far beyond the value of 0 or 1. In that case the response function showed very irregular patterns compared to the smooth patterns shown in Figure 4.4. To prevent overshooting it is advisable that the regions with specified responses are not covering the entire domain and that they are well separated so that there is enough space for unspecified responses.

4.6. Optimal discrete filters

Equation (4.8) is linear in the coefficients $a_{0,0}, a_{1,0}, a_{2,0}, a_{2,1} \ldots a_{N,1}$. If the filter has the width $2N+1$, then $(N+1)\cdot(N+2)/2$ coefficients need to be determined. This can be done by specifying responses $\kappa(k,l)$ at a variety of wave numbers, so that a set of linear equations is obtained

$$\begin{aligned}\kappa(k,l) &= a_{0,0} + 2a_{1,0}(cos(k\hat{1}) + cos(l\hat{1})) + 4a_{1,1}cos(k\hat{1})cos(l\hat{1}) \\ &\quad +4\sum_{n=1}^{N}\left[2a_{n,0}(cos(k\hat{n}) + cos(l\hat{n})) + \sum_{m=1}^{n-1} a_{n,m}4\left\{cos(k\hat{n})cos(l\hat{m})\right.\right.\end{aligned}$$

$$+cos(l\hat{n})cos(k\hat{m})\} + 4a_{n,n}cos(k\hat{n})cos(l\hat{n})] \tag{4.9}$$

When we introduce the notation $A_1 = a_{0,0}$, $A_2 = a_{1,0}$, $A_3 = a_{1,1}$, and

$$A_{n\cdot(n+1)/2+1+m} = a_{n,m} \quad \text{for } n \geq 2 \text{ and } m = 0 \ldots n \tag{4.10}$$

and

$$\begin{array}{rcll} M_{K,1} & = & 1 & \\ M_{K,n\cdot(n+1)/2+1} & = & 2\left\{cos(k\hat{n}) + cos(l\hat{n})\right\} & \text{for } n \geq 1 \\ M_{K,n\cdot(n+1)/2+1+m} & = & 4\left\{cos(k\hat{n})cos(l\hat{m}) + cos(l\hat{n})cos(k\hat{m})\right\} & \\ & & \text{for } m = 1 \ldots n-1 & \text{and } n \geq 2 \\ M_{K,n\cdot(n+1)/2+1+n} & = & 4cos(k\hat{n})cos(l\hat{n}) & \text{for } n \geq 1 \end{array} \tag{4.11}$$

equation (4.9) may be rewritten with $K = (k, l)$:

$$\kappa(K) = \sum_{j=1}^{(N+1)\cdot(N+2)/2} M_{K,j}A_j \tag{4.12}$$

One option is to select as many wave numbers with specified responses as the number of weights $(N+1)\cdot(N+2)/2$. In that case, a linear set of equations with an invertible matrix emerges. We have tried this out, but unsatisfactory results emerged - the solution for the two-dimensional response function κ is a superposition of waves, and fixing κ at a number of selected wave numbers creates a two-dimensional κ which fits exactly the specified responses at a few locations, but between these locations unacceptable overshooting phenomena emerged, in particular when band- and high-pass filters were constructed.

Therefore, the response is specified at more wave numbers than there are filter weights. Then, the set of linear equations is over-determined. An approximate solution is obtained by minimising

$$\sum_K \left(\kappa(K) - \sum_{j=1}^{(N+1)\cdot(N+2)/2} M_{K,j}A_j \right)^2 \tag{4.13}$$

The filter weights solution for this problem is given by

$$\mathbf{A} = \left(\mathcal{M}^T\mathcal{M}\right)^{-1}\mathcal{M}^T\vec{\kappa} \tag{4.14}$$

with the matrix $\mathcal{M}$ with $(N+1)\cdot(N+2)/2$ columns (dimension of $\mathbf{A}$) and as many rows as wave numbers have been selected with given responses (dimension of $\vec{\kappa}$).

Please note that the sum of the filtered plus the polynomial pieces does not equal the total. The individual filtered pieces are not orthogonal to each other. That is, the variances of the different contributions do not add exactly to the total variance. This would be a nice property to have, but for the specific purpose in mind, namely the characterization of phenomena on different scales, this is not really needed.

4.7. Applications

The results of a regional model run (Feser et al. (2001)) for Western Europe forced with the NCEP reanalyses (Kalnay et al. (1996)) were filtered with the presented filter for 3 wave number ranges. The quadratic polynomials (section 4.2) were subtracted before applying the band- and high-pass filters. A first example for the storm 'Anatol' can be seen in Figure 4.5. It shows the unfiltered (a), low-pass (b), band-pass (c), and high-pass filtered (d) wind speed fields at a height of 10 m for the 3rd of December 1999, 6 p.m., for Western Europe when the storm was centred over the north-eastern tip of Denmark with a low pressure core of 956 hPa. The low-pass filtered field (b) shows the smoothed field and displays only the very large scales. The band-pass filtered data (c) lacks the large-scale information and shows land-sea interactions on the regional scale but also regional wind speed structures over the North Sea connected with the intense low-pressure system. The high-pass filtered part (d) displays the smallest scales with largest values almost exclusively in the coastal zones for this wind speed example. An effective scale separation was achieved.

The band-pass and high-pass filtered fields show anomalies from the large-scale field, therefore the values are positive and negative around the zero-point. The white 'frames' around the filtered fields are a result of the digital filter's weighted average operation around a base point, which can not be calculated in the direct vicinity of the LAM's boundaries due to a lack of grid points. Therefore the points close to the lateral boundaries (in our example 8 rows and columns of grid points which is equal to the sponge zone width of the LAM we used) have a value of zero.

Another example of the filter application is given in Figure 4.6. It shows precipitation fields for the storm Anatol, accumulated for December 3rd, 1999. Again, the unfiltered (a), low-pass (b), band-pass (c), and high-pass (d) filtered fields are shown. The low-pass and the band-pass filtered data display the frontal precipitation related to the intense low-pressure system on their respective scale. Also the high-pass filtered precipitation is most intense in the vicinity of the storm's cloud systems.

Figure 4.7 shows the mean sea level pressure field for the storm 'Anatol'. The storm centre over the north-eastern tip of Denmark can be seen both in the unfiltered and low-pass filtered fields (a and b). The band-pass filtered data (c) depicts anomalies around the low-pressure core and over the North Atlantic. For calculating the high-pass filtered field (d) not only the polynomials were subtracted, but also the low-pass filtered field (whereby the polynomials were subtracted as well). This was necessary because the spectrum of the mean sea level field drops off rather sharply so that the remnants of large-scale features in the high-pass filtered field S_f are comparable to the small-scale features. Therefore, the large-scale contribution is suppressed explicitly before high-pass filtering by calculating $f - P_f^K - L_{f-P_f^K}$. Then, this reduced field is filtered. Because of the double filter application the spatial extension of the data is

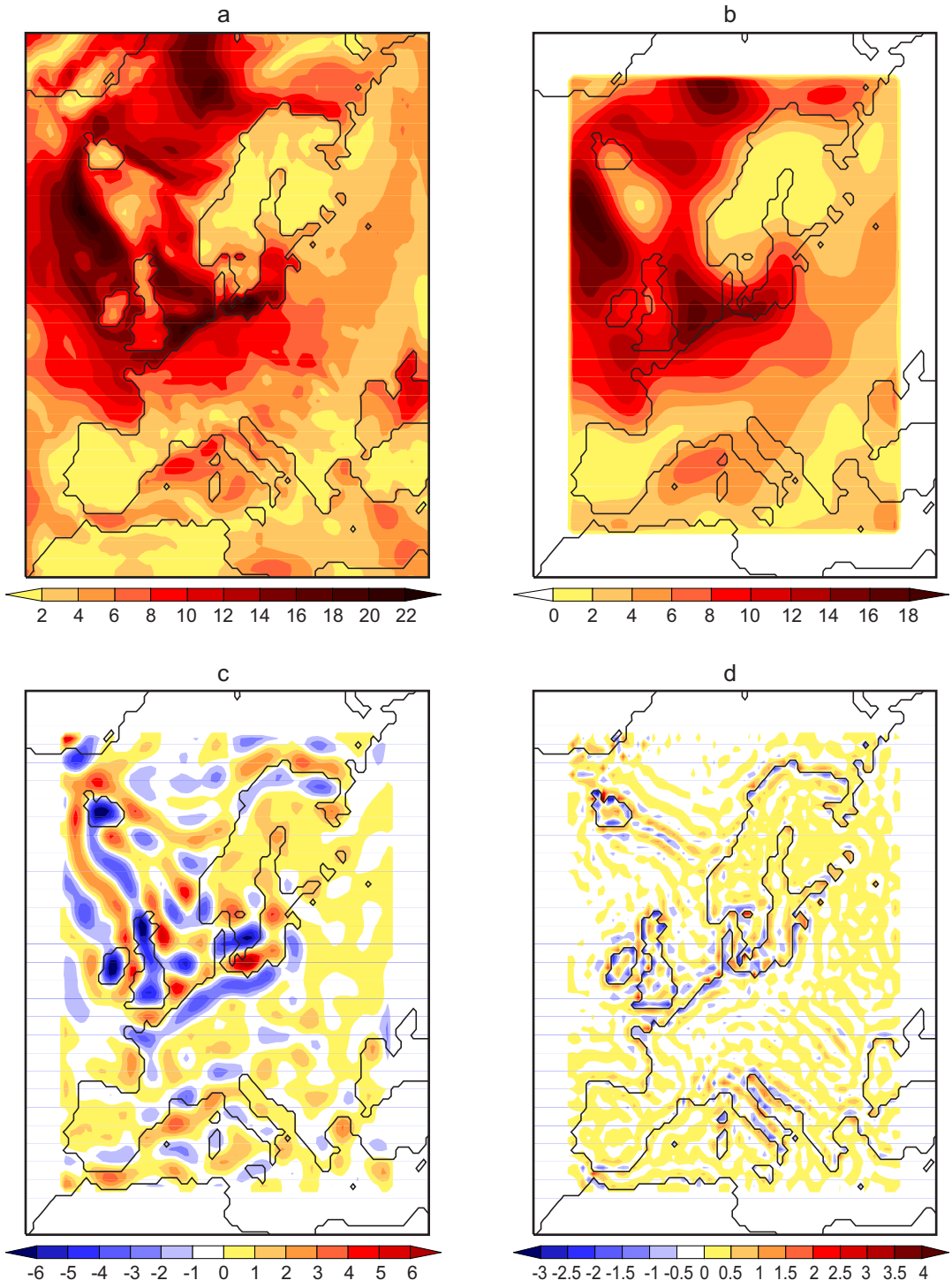

Figure 4.5: 10m wind speed fields (m/s) for the storm 'Anatol' on December 3rd, 1999, 6 p.m., of a LAM simulation: (a) Unfiltered, (b) low-pass filtered, (c) band-pass filtered, and (d) high-pass filtered data.

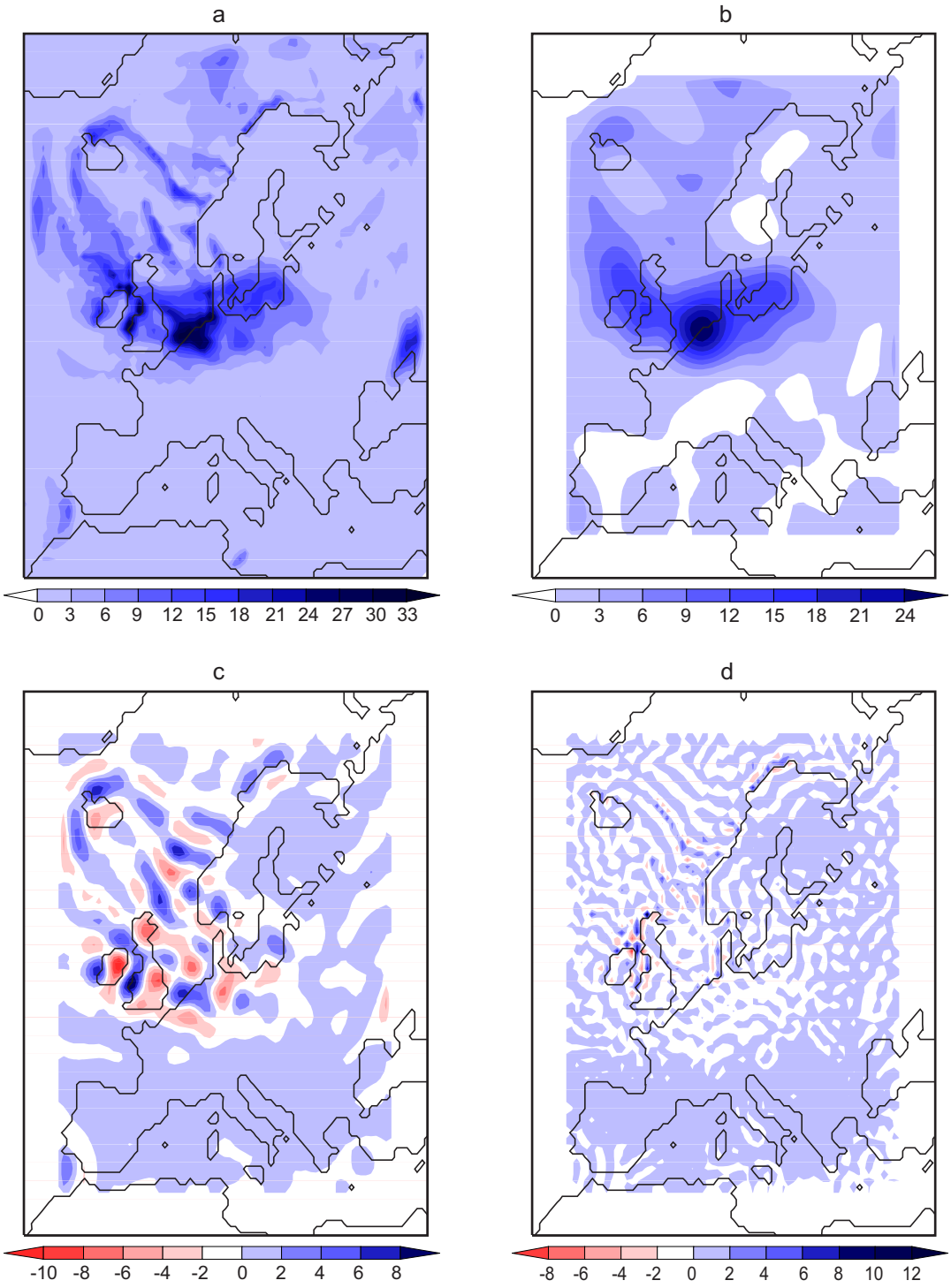

Figure 4.6: Precipitation fields (mm) for the storm 'Anatol' accumulated for December 3rd, 1999, of a LAM simulation: (a) Unfiltered, (b) low-pass filtered, (c) band-pass filtered, and (d) high-pass filtered data.

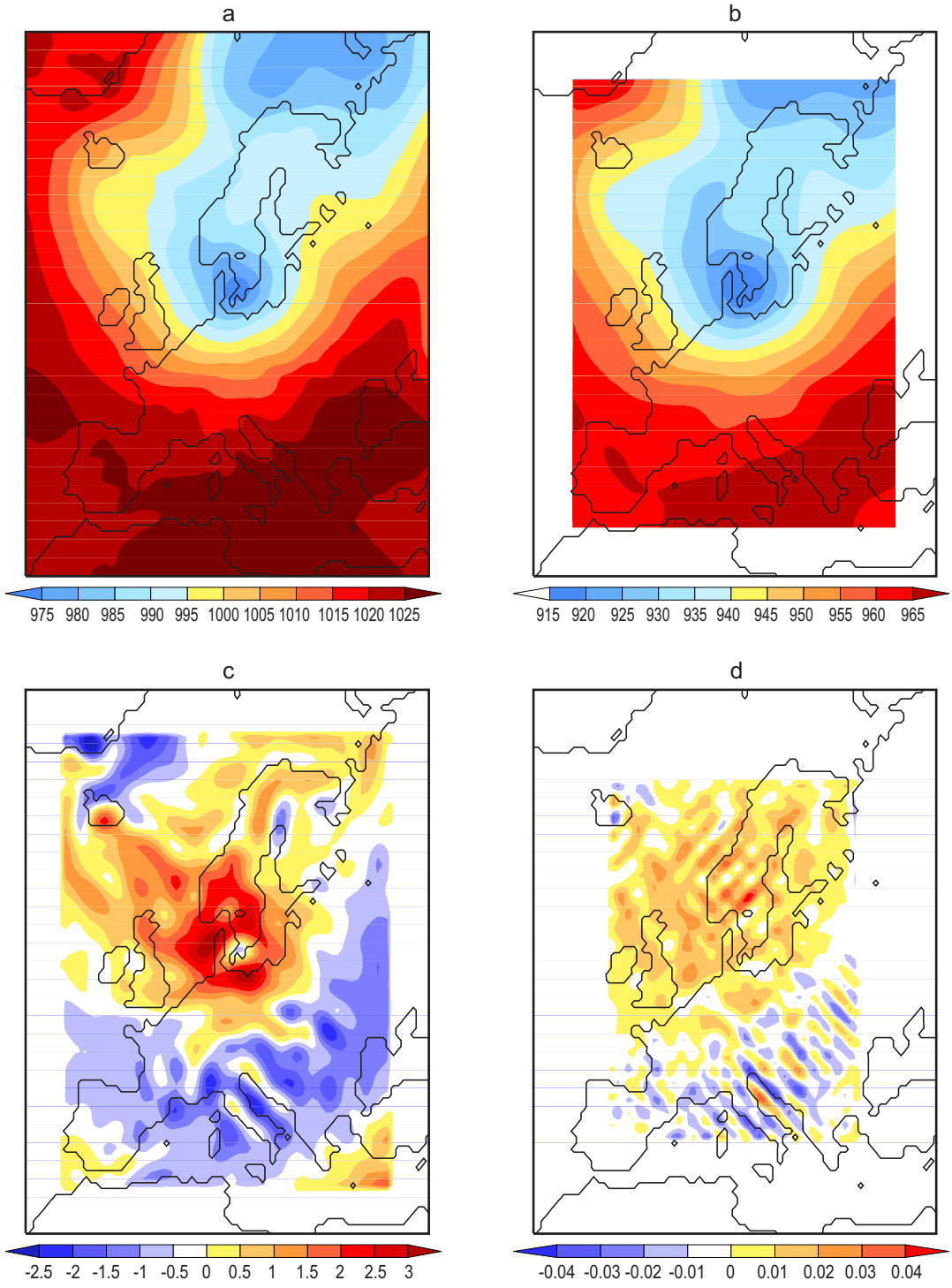

Figure 4.7: Mean sea level pressure (hPa) for the storm 'Anatol' for December 3rd, 1999, 6 p.m. of a LAM simulation: (a) Unfiltered, (b) low-pass filtered, (c) band-pass filtered, and (d) high-pass filtered data.

decreased, now there are 16 instead of 8 rows and columns of zero value around the filtered data. The largest anomalies can be seen North of the low pressure core and over the North Sea.

Since the main purpose of this paper is to present the method of spatial two-dimensional discrete filtering and not the application of it we will not go into further detail here. For further studies the filter may be used as a tool to compare such fields for model evaluation, for process studies on different spatial scales or to show the resolvable scales of the LAM.

4.8. Summary and Conclusions

In this paper we have presented a method to construct isotropic digital filters suited for scale separations of atmospheric fields on limited area grids. There are several methods to do scale separations, like Fourier filtering, the discrete Cosine transform or digital filters. We suggest to use near-isotropic two-dimensional digital filters because these filters operate with a finite basis, can be constructed flexibly and are easily implemented and run with little computation cost. Our method allows the construction of filters for a broad range of applications and for data on homogeneous, limited area grids. A wave number range of interest has to be selected and the according response values can then be calculated automatically using an approximation method. The filter weights are then calculated by a matrix inversion.

In our example, we constructed several isotropic discrete filters for differing wave number ranges, to isolate the large, medium, and small scales of limited area atmospheric fields. Applications of the filters produced reasonable results.

As a next step we will apply these filters for model evaluation purposes, to study processes on a limited area domain or to advance with the question of added value of regional models.

4.9. Acknowledgments

We are grateful to R. Laprise for valuable discussions regarding this work. He proposed the idea of a full two-dimensional filter. We thank M. Quante for the discussion on wavelet analyses, and M. Widmann and R. Weisse for reading the manuscript and for their constructive modification proposals. We thank B. Gardeike who prepared some of the Figures for us.

4.10. Appendix: Polynomial fit

4.10.1. *Formal presentation of problem*

We want to expand a discrete set of numbers x_{ij} on a rectangular grid of points (i, j) with $i = 1 \ldots n_x$ and $j = 1 \ldots n_y$ into a polynomial of order K, i.e.,

$$x_{ij} = \sum_{r,q=0}^{r+q \leq K} a_{rq} i^r j^q + \epsilon_{i,j} \tag{4.15}$$

a are the polynomial coefficients which are to be determined and r and q are the indices which number serially the polynomial terms. ϵ represents a remainder, the square of sums $\sum_{i,j} \epsilon_{ij}^2$ is assumed to be minimum. The sum is made up of $(K+1)(K+2)/2$ terms.

This expression (4.15) means for

$$\begin{aligned}
K = 0: \quad x_{ij} &= a_{00} + \epsilon_{ij} \\
K = 1: \quad &= a_{00} + a_{10} i + a_{01} j + \epsilon_{ij} \\
K = 2: \quad &= a_{00} + a_{10} i + a_{20} i^2 + a_{01} j + a_{02} j^2 + a_{11} ij + \epsilon_{ij} \\
\text{etc.}
\end{aligned}$$

The expansion (4.15) may be rewritten as

$$x_{ij} = \sum_{k=0}^{K} T_k + \epsilon_{ij} \tag{4.16}$$

with

$$T_k = \sum_{q=0}^{K-k} a_{kq} i^k j^q \tag{4.17}$$

For example:

$$\begin{aligned}
K = 1: \quad T_0 &= a_{00} + a_{01} j \\
T_1 &= a_{10} i \\
K = 2: \quad T_0 &= a_{00} + a_{01} j + a_{02} j^2 \\
T_1 &= a_{10} i + a_{11} ij \\
T_2 &= a_{20} i^2
\end{aligned}$$

For a given field x_{ij}, we want to determine optimal coefficients a_{rq} so that

$$\hat{\epsilon} = \sum_{ij} \left[x_{ij} - \sum_{k=0}^{K} T_k \right]^2 = min \tag{4.18}$$

4.10.2. *Solution of minimum problem*

The minimum of (4.18) is derived by first calculating derivatives with respect to the quantity to be determined, and then finding zeros of these derivatives, i.e.,

$$\frac{\partial \hat{\epsilon}}{\partial a_{rq}} = 0 \tag{4.19}$$

It is $\frac{\partial \sum T_k}{\partial a_{rq}} = \frac{\partial T_r}{\partial a_{rq}} = i^r j^q$, and thus

$$\begin{aligned}
\frac{\partial \hat{\epsilon}}{\partial a_{rq}} &= \sum_{ij} \left[\frac{\partial}{\partial a_{rq}} \left(x_{ij} - \sum_{k=0}^{K} T_k \right)^2 \right] \\
&= \sum_{ij} \left[2 \left(x_{ij} - \sum_{k=0}^{K} T_k \right) \left(-\frac{\partial T_r}{\partial a_{rq}} \right) \right] \\
&= 2 \sum_{ij} \sum_{k=0}^{K} T_k i^r j^q - 2 \sum_{ij} x_{ij} i^r j^q
\end{aligned}$$

or for all pairs (r, q):

$$\sum_{k=0}^{K} \sum_{s=0}^{K-k} a_{ks} \sum_{ij} (i^k j^s)(i^r j^q) = \sum_{ij} x_{ij} i^r j^q \tag{4.20}$$

Setting this derivative to zero results in a set of linear equations for all $(K+1)(K+2)/2$ coefficients a_{rq}. Thus, the problem is reduced to a conventional matrix inversion problem. A minor technical challenge is to properly map the two-dimensional index (r, s) on a 1-dimensional index.

4.11. Appendix: Response function of 2-d digital filter

To determine the response function κ of the filter, (4.3) is inserted in (4.4). Because of $e^{ix} + e^{-ix} = 2cos(x)$, the terms A, B and C can be rewritten as:

$$\begin{aligned} A &= \sum_{n=1}^{N} a_{n,0} \left(\sum_{k,l=-K}^{K} \alpha_{k,l} e^{i(kx+ly)} \left[e^{ik\hat{n}} + e^{-ik\hat{n}} + e^{il\hat{n}} + e^{-il\hat{n}} \right] \right) \\ &= 2 \sum_{n=1}^{N} a_{n,0} \left(\sum_{k,l=-K}^{K} \alpha_{k,l} e^{i(kx+ly)} (cos(k\hat{n}) + cos(l\hat{n})) \right) \\ &= \sum_{k,l=-K}^{K} \left(2 \sum_{n=1}^{N} a_{n,0} (cos(k\hat{n}) + cos(l\hat{n})) \right) \alpha_{k,l} e^{i(kx+ly)} \end{aligned}$$

$$\begin{aligned} B &= \sum_{n=1}^{N} a_{nn} \left(\sum_{k,l=-K}^{K} \alpha_{k,l} e^{i(kx+ly)} \left[e^{ik\hat{n}+il\hat{n}} + e^{-ik\hat{n}-il\hat{n}} + e^{ik\hat{n}-il\hat{n}} + e^{-ik\hat{n}+il\hat{n}} \right] \right) \\ &= \sum_{n=1}^{N} a_{nm} \left(\sum_{k,l=-K}^{K} \alpha_{k,l} e^{i(kx+ly)} 2 \left[e^{ik\hat{n}} cos(l\hat{n}) + e^{-ik\hat{n}} cos(ln) \right] \right) \\ &= \sum_{k,l=-K}^{K} \left(4 \sum_{n=1}^{N} a_{nn} cos(kn) cos(ln) \right) \alpha_{k,l} e^{i(kx+ly)} \end{aligned}$$

and

$$\begin{aligned} C &= \sum_{n=2}^{N} \sum_{m=1}^{n-1} a_{nm} \sum_{k,l=-K}^{K} \alpha_{k,l} e^{i(kx+ly)} \left[e^{ik\hat{n}+il\hat{m}} + e^{ik\hat{n}-il\hat{m}} \right. \\ &\quad + e^{-ik\hat{n}+il\hat{m}} + e^{-ik\hat{n}-il\hat{m}} + e^{ik\hat{m}+il\hat{n}} + e^{ik\hat{m}-il\hat{n}} \\ &\quad \left. + e^{-ik\hat{m}+il\hat{n}} + e^{-ik\hat{m}-il\hat{n}} \right] \\ &= \sum_{n=2}^{N} \sum_{m=1}^{n-1} a_{nm} \sum_{k,l=-K}^{K} \alpha_{k,l} e^{i(kx+ly)} 2 \left[e^{ik\hat{n}} cos(l\hat{m}) \right. \\ &\quad \left. + e^{-ik\hat{n}} cos(l\hat{m}) + e^{ik\hat{m}} cos(l\hat{n}) + e^{-ik\hat{m}} cos(l\hat{n}) \right] \\ &= \sum_{k,l=-k}^{K} \left(4 \sum_{n=2}^{N} \sum_{m=1}^{n-1} a_{nm} [cos(k\hat{n}) cos(l\hat{m}) + cos(l\hat{n}) cos(k\hat{m})] \right) \alpha_{k,l} e^{i(kx+ly)} \end{aligned}$$

Bibliography

Bettge, T. W. and D. P. Baumhefner, 1980: A Method to Decompose the Spatial Characteristics of Meteorological Variables within a Limited Domain. *Mon. Wea. Rev.*, **108**, 843–854.

Daubechies, I., 1992: *Ten Lectures on wavelets*. SIAM CBMS 61, Philadelphia, PA, 357 pp.

Denis, B., J. Côté, and R. Laprise, 2002: Spectral Decomposition of Two-Dimensional Atmospheric Fields on Limited-Area Domains Using the Discrete Cosine Transform (DCT). *Mon. Wea. Rev.*, **130**, 1812–1829.

Desrochers, P. R. and S. Y. K. Yee, 1999: Wavelet Applications for Mesocyclone Identification in Doppler Radar Observations. *J. Appl. Meteor.*, **38**, 965–980.

Errico, R., 1985: Spectra Computed from a Limited Area Grid. *Mon. Wea. Rev.*, **113**, 1554–1562.

— 1987: A Comparison between Two Limited-Area Spectral Analysis Schemes. *Mon. Wea. Rev.*, **115**, 2856–2861.

Feser, F., R. Weisse, and H. von Storch, 2001: Multi-decadal Atmospheric Modeling for Europe Yields Multi-purpose Data. *EOS Transactions*, **82**, 305,310.

Giorgi, F., B. Hewitson, J. Christensen, M. Hulme, H. von Storch, P. Whetton, R. Jones, L. Mearns, and C. Fu: 2001, *Climate Change 2001. The Scientific Basis*, Cambridge University Press, chapter Regional climate information - evaluation and projections. 583–638.

Jameson, L., T. Waseda, and H. Mitsudera, 2002: Scale Utilization and Optimization from Wavelet Analysis for Data Assimilation: SUgOiWADAi. *Journal of Atmospheric and Oceanic Technology*, **19**, 747–758.

Kalnay, E., M. Kanamitsu, R. Kistler, W. Collins, D. Deaven, L. Gandin, M. Iredell, S. Saha, G. White, J. Woollen, Y. Zhu, M. Chelliah, W. Ebisuzaki, W. Higgins, J. Janowiak, K. C. Mo, C. Ropelewski, J. Wang, A. Leetmaa, R. Reynolds, R. Jenne, and D. Joseph, 1996: The NCEP/NCAR reanalysis project. *Bull. Amer. Meteor. Soc.*, **77**, 437–471.

Mallat, S., 1989: A theory for multiresolution signal decomposition: the wavelet representation. *IEEE Trans. Patt. Recog., and Mach. Intell.*, **11**, 674–693.

— 1998: *A wavelet tour of signal processing*. Academic Press, San Diego, 577 pp.

Miguez-Macho, G., G. L. Stenchikov, and A. Robock, 2004: Spectral nudging to eliminate the effects of domain position and geometry in regional climate model simulations. *J. Geophys. Res.*, **109**, D13104, 10.1029/2003JD004495.

Raymond, W. H., 1989: High-Order, High-Pass Implicit Filters for Evaluating Information within Finite Areas. *Mon. Wea. Rev.*, **117**, 2772–2781.

Shapiro, R., 1970: Smoothing, Filtering, and Boundary Effects. *Reviews of Geophysics and Space Physics*, **8**, 359–387.

— 1975: Linear Filtering. *Mathematics of Computation*, **29**, 1094–1097.

Shuman, F. G., 1957: Numerical methods in weather prediction: II. Smoothing and filtering. *Mon. Wea. Rev.*, **85**, 357–361.

Stamus, P., F. Carr, and D. Baumhefner, 1992: Application of a Scale-Separation Verification Technique to Regional Forecast Models. *Mon. Wea. Rev.*, **120**, 149–163.

Starck, J.-L., F. Murtagh, and A. Bijaoui, 1998: *Image processing and data analysis: the multiscale approach*. Cambridge University Press, 287 pp.

von Storch, H., 1995: Inconsistencies at the interface of climate impact studies and global climate research. *Meteorolog. Z.*, **4**, 72–80.

von Storch, H., H. Langenberg, and F. Feser, 2000: A Spectral Nudging Technique for Dynamical Downscaling Purposes. *Mon. Wea. Rev.*, **128**, 3664–3673.

Waldron, K. M., J. Paegle, and J. D. Horel, 1996: Sensitivity of a Spectrally Filtered and Nudged Limited-Area Model to Outer Model Options. *Mon. Wea. Rev.*, **124**, 529–547.

Yano, J.-I., M. W. Moncrieff, and X. Wu, 2001: Wavelet Analysis of Simulated Tropical Convective Cloud Systems. Part II: Decomposition of Convective-Scale and Mesoscale Structure. *J. Atmos. Sci.*, **58**, 868–876.

Chapter 5

Enhanced detectability of added value in limited area model results separated into different spatial scales

Frauke Feser

Institute for Coastal Research, GKSS Research Centre
21502 Geesthacht, Germany

Submitted to:
Monthly Weather Review, 2005.

Abstract

Regional climate models (RCMs) are a widely used tool to describe regional scale climate variability and change. However, the added value provided by such models is not well-explored so far, and claims have been made that RCMs have little utility (Butler (2003)). Here, it is demonstrated that RCMs are indeed returning significant added value. Employing appropriate spatial filters, the scale-dependent skill is examined of a state-of-the-art RCM (with and without nudging of large scales) by comparing its skill with that of the global reanalyses driving the RCM. This skill is measured by pattern correlation coefficients of the global reanalyses or the RCM simulation and, as a reference, of an operational regional weather analysis. For the spatially smooth variable air pressure the RCM improves this aspect of the simulation for the medium scales if

the RCM is driven with large scale constraints, but not for the large scales. For the regionally more structured quantity near-surface temperature the added value is more obvious. The simulation of medium-scale 2m temperature anomaly fields amounts to an increase of the mean pattern correlation coefficient of up to 30%.

5.1. Introduction

Regional climate models are a widely used tool to derive regionally specific information about the statistics of weather (i.e., climate), trends and possible future changes. Such models feature an atmospheric limited area model combined with a description of the thermodynamics of the upper soil levels (e.g., Giorgi et al. (2001)) plus, possibly, other components of the Earth System (e.g., marginal seas, lakes). They are forced by time variable conditions along the lateral atmospheric boundary, sometimes also with large-scale constraints in the interior. These constraints are taken from either global model scenarios (e.g., Christensen and Christensen (2003)) or from global reanalyses (e.g. Feser et al. (2001)). Simulations lengths are several decades of years.

The purpose of regional climate modelling is to provide additional detail beyond the resolution of global reanalyses or global climate simulations. The enhanced spatial resolution of a RCM is thought to allow for a better description of the atmospheric dynamical processes, which lead to the formation of meso-scale features (such as fronts or meso-scale disturbances (e.g., Denis et al. (2002)). The dependency of the smaller scales on the larger scales is considered to be better described ("downscaling" von Storch (1995)). Another benefit is that the influences of the physiographic detail, such as surface vegetation characteristics, coastlines, or complex topography, are better captured (e.g., Jacob and Podzun (1997)). Thus, the theatre of regional weather is considered to be made up from two main influences, namely the large-scale atmospheric state and the regional physiographic detail.

The global analysis or simulation is assumed to reliably describe the dynamics of the large scales. The RCM should be better than the global analysis or simulation on medium spatial scales (600 km and less). Thus, the expected added value of regional climate modelling is mainly on these medium scales (e.g. Laprise (2003)).

The concept of scale-separation is used to analyse limited area model (LAM) results on different scales. It can serve as a tool for model evaluation or to explain the connection between weather phenomena with varying size. The concept was also incorporated into the spectral nudging or large-scale forcing concept by Waldron et al. (1996) and von Storch et al. (2000), which keeps the large-scale part of a regional model solution close to the forcing global field in the model interior. In the past, LAM fields were mainly looked upon as a whole not separated into different spatial scales to study processes, to predict the regional climate or to resolve regional weather details

at a high resolution. Whenever filters were applied, this was generally done to filter in time. In this work the use of a spatial filter is proposed in order to separate the LAM results into several independent spatial scale bands. The individual fraction of the regional model in adding value to the global model solution can thus be estimated. An explicit comparison with the forcing global model and observational reference data can assess the regional models simulation quality.

5.2. Models used for comparisons

In the following the hypothesis will be tested that the regional models describe the phenomena on both, large and medium, scale bands better than the driving large-scale state. To do so, the case of an extended simulation is considered with the regional climate model REMO (REgional MOdel, Jacob and Podzun (1997)) forced with global 6-hourly NCEP (National Centers for Environmental Prediction) reanalyses (Kalnay et al. (1996)) from 1958-2002, which are given on a horizontal grid of about 2°.

REMO is a grid point model featuring the discretized primitive equations in a terrain-following hybrid coordinates system. The prognostic variables are surface air pressure, temperature, horizontal wind components, specific humidity and cloud water. The physics scheme applied is a version of the global model ECHAM4 physics of the Max-Planck-Institute for meteorology adapted for the regional model. The integration area has a horizontal spherical grid spacing of 0.5^{o} ($\sim$ 47 - 55 km in zonal direction, $\sim$ 55 km in meridional direction) and 81 $\times$ 91 grid points. The region considered is western Europe, extending about 4300 km longitudinally and 5000 km latitudinally. In the vertical 20 hybrid model levels are adapted to the orography close to the surface. The time step of the calculation is 5 minutes. A more detailed description of the multi-decadal simulation is given in Feser et al. (2001).

The LAM was forced with 6-hourly NCEP reanalyses over the whole integration period from 1958 to 2002. The horizontal grid size of the reanalyses is about 1.875^{o} longitudinally and latitudinally (T62 Gaussian grid). Because of the rotated spherical grid used by the LAM, its coverage with NCEP grid-boxes is inhomogeneous with maximum resolution improvement in the southern part of the integration area. One LAM simulation was done in the conventional set-up with lateral and surface forcing only, another one with additional "nudging of large scales" (von Storch et al. (2000)). Nudging of large scales keeps the simulated state close to the driving state at larger scales, while allowing the model to freely generate medium-scale features consistent with the large-scale state. This is achieved by adding nudging terms in the spectral domain for the horizontal wind components above 850 hPa with maximum strengths for low wave numbers at the top model level.

The LAM results were compared to the NCEP reanalyses at different spatial scales. To transfer the coarse grid reanalyses to the 50 km grid used by the RCM, the reanalyses atmospheric fields were horizontally interpolated according to a 16 point formula as explained in Doms et al. (1995). The sea level pressure (SLP) is computed following Doms et al. (1995) by first calculating an extrapolation of the temperature T^* at the height of the LAMs orography using the temperature T_{KE} of the lowest model level:

$$T^* = T_{KE} + 0.0065\frac{R}{g}T_{KE}(\frac{p_s}{p_{KE}} - 1) \tag{5.1}$$

whereby p_s is the unreduced surface pressure and p_{KE} is the pressure at the lowest model level.
Then, the temperature T_{SL} at sea level and the mean temperature gradient γ are computed.

$$T_{SL} = T^* + \gamma\frac{\Phi_s}{R} \tag{5.2}$$

with the orography $\Phi_s = g * z_s$ and $\gamma = 0.0065\frac{R}{g}$.
SLP is then computed as:

$$p_{SL} = p_s \exp\{\frac{\Phi_s}{RT^*}[1 - 0.5\frac{\gamma\Phi_s}{RT^*} + 0.333(\frac{\gamma\Phi_s}{RT^*})^2]\} \tag{5.3}$$

Accordingly, the 2m temperature was calculated using the horizontally interpolated reanalyses temperature fields.

As a reference data set analyses of Germany's National Meteorological Service (DWD) are used. They were calculated with the "Europe Model" of the DWD on a rotated spherical grid with hybrid model levels and were available every 6 hours. The same rotated North pole and model grid was used as in the LAM simulation so that a straightforward comparison was possible.

5.3. Filter application

To analyse the above described simulation data an isotropic digital filter was used (Feser and von Storch (2005)). It is able to separate the LAM's model results into different spatial scales by filtering certain wave number ranges. The digital 2-dimensional filter uses a footprint of 17×17 grid points to determine large-scale, medium-scale and small-scale features from a field of 81×91 grid points. The filter weights are determined so that the 2-d-response function is approximately isotropic and for predetermined wave number ranges close to one or close to zero. In this context only the low pass and the medium pass filters are used.

The filter parameters were chosen as explained in Feser and von Storch (2005), see their Figure 4 of the filter response function. For the low-pass filter a wave number

range of 0 to 6 was chosen, which means that weather phenomena larger than about 700 km can pass this filter. The medium-pass filter was set to only let pass wave numbers 8 to 16 which corresponds to scales of about 550 km to 250 km. These wave number ranges were selected to describe the scales that should be best resolved in the global model (low-pass filter), and the scales that are assumed to be best resolved in the LAM (medium-pass filter).

5.4. Temperature and sea level pressure comparisons

Both the RCM simulations and the NCEP reanalyses are compared to operational high-resolution regional analyses, which have been constructed for routine regional weather forecasts by the DWD. The DWD analyses are considered as a "true" reference. It is expected that the RCM compares to the reference about as well as the driving NCEP reanalyses for large scales; on the medium scales, however, a significantly improved performance of the RCM is assumed.

Two variables are considered, namely the spatially smooth air pressure and the spatially heterogeneous air temperature at or near the surface. The DWD temperature data are available from 1992 to 1999, for SLP only in 1994, 1995, 1998 and 1999. The data of the LAM, the NCEP reanalyses and the DWD analyses were filtered and compared at the two spatial scale ranges described before.

The percentage ratio of standard deviations of low-pass filtered 2m temperature DWD analyses to NCEP reanalyses for summers 1992 to 1999 is shown in Figure 5.1 (a) and the percentage ratio of standard deviations of low-pass filtered 2m temperature DWD analyses to the regional model run for the same period in (b). The ratio between the analyses and NCEP is mostly above 100 percent, indicating higher near-surface temperature variability in the DWD analyses, especially over the North Atlantic with a factor of up to 1.5. The ratio between DWD and LAM shows smaller values, they range from 80 to 120 percent apart from a small area at the south-eastern tip of Greenland. Even though a slightly higher agreement can be seen between the low-pass filtered LAM and the reference data than between NCEP and the reference data, this is not the scale which should be the best resolved one of the LAM, the one where most added value could be assumed. Therefore the following Figures will focus on medium-scale filtered data.

Figure 5.2 shows the ratio of standard deviations of medium-pass filtered 2m temperature DWD analyses to NCEP reanalyses in percent for summers 1992 to 1999 (a) and the ratio of standard deviations of medium-pass filtered 2m temperature DWD analyses to the regional model run, again in percent, for summers 1992 to 1999 (b). Obviously the more highly resolved analyses show a much higher variability in the near-surface temperature than NCEP, up to a factor of 4.4. All values are above 100

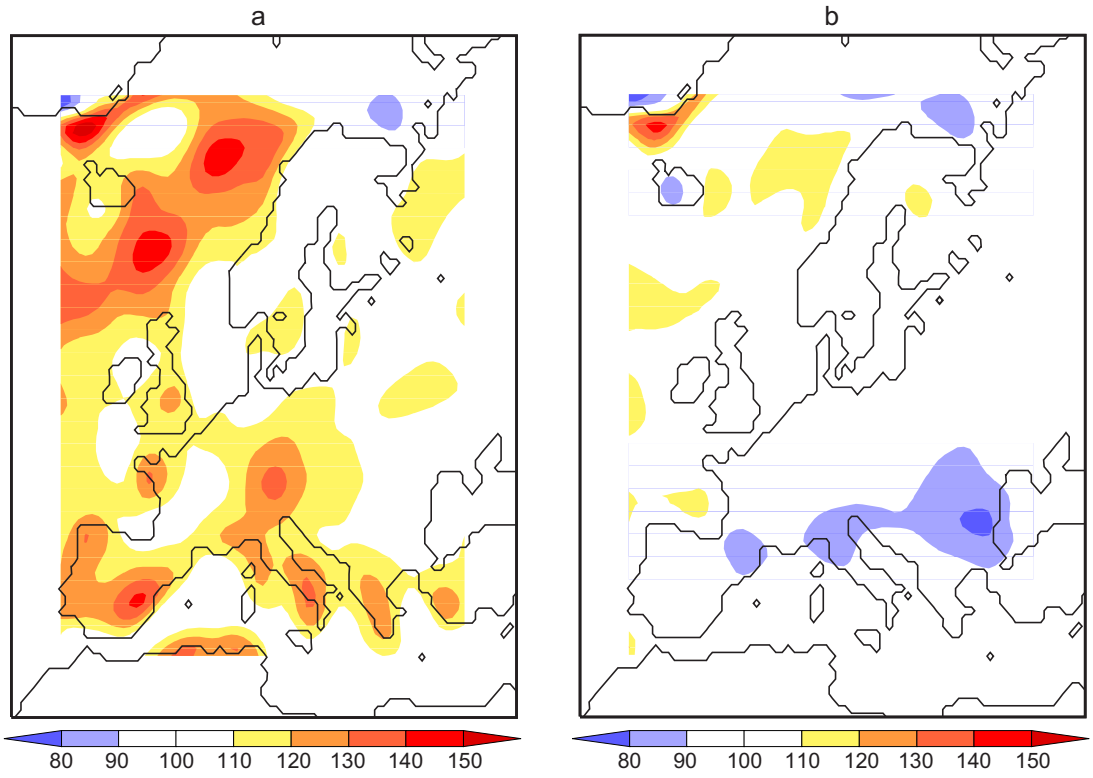

Figure 5.1: Ratio of standard deviations of low-pass filtered 2m temperature DWD analyses / NCEP reanalyses in percent for JJA 1992 to 1999 (a) and ratio of standard deviations of 2m temperature DWD analyses / LAM simulation in percent for JJA 1992 to 1999 (b).

percent and hence the variability of the DWD analyses is higher at every grid point than the NCEP variability. The comparison of the LAM and the DWD results shows high agreement. The variability in the near-surface temperature is about the same in both simulations with only few areas of slight discrepancies. Figure 5.3 shows the same as Figure 5.2, but now for winter. A similar pattern can be seen, with high variability for the analyses and much smaller values for the coarser NCEP reanalyses. The variability is up to a factor of 3 higher in the analyses than in the reanalyses. Again, the LAM simulation is much closer to the reference data set than the global forcing data.

Figure 5.4 shows the ratio of standard deviations of medium-pass filtered SLP DWD analyses to NCEP reanalyses in percent (a) and the ratio of standard deviations of medium-pass filtered SLP DWD analyses to the LAM simulation in percent (b) for winter 1998/1999. The low pass filtered field was subtracted from the data prior to applying the medium-pass filter as explained in Feser and von Storch (2005) for achieving a better scale separation. An irregular pattern can be seen with many values above 100 percent. Large regions especially in southern Europe have larger

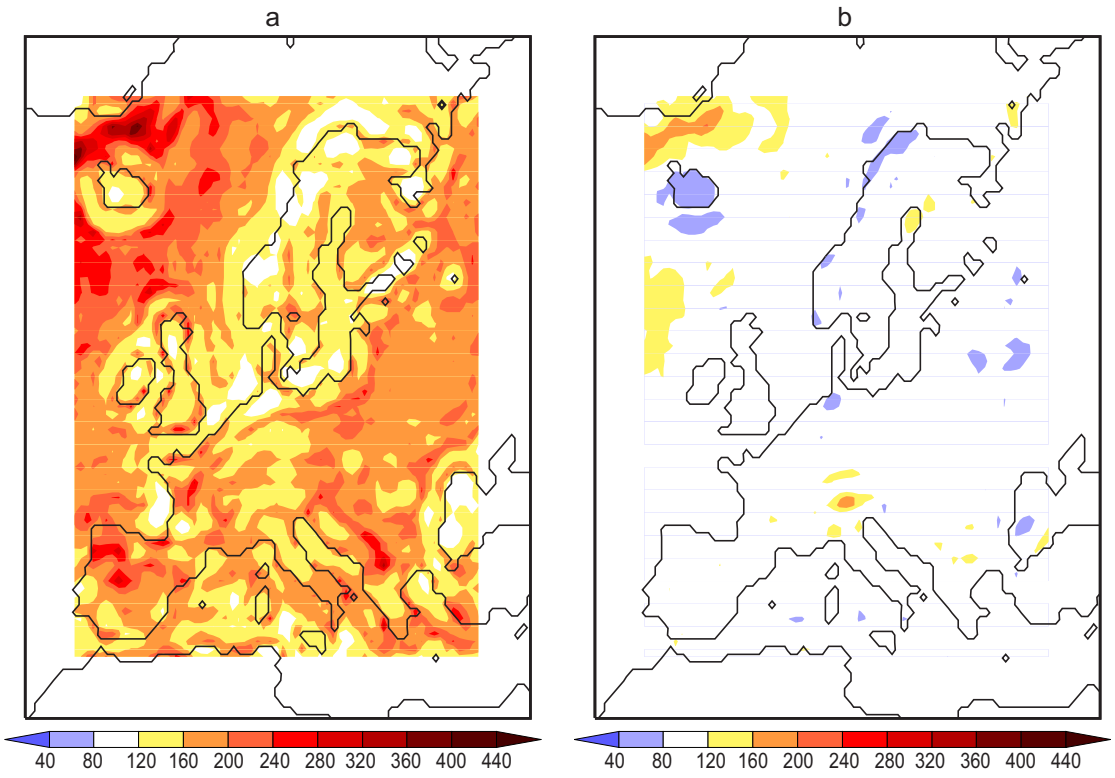

Figure 5.2: Ratio of standard deviations of medium-pass filtered 2m temperature DWD analyses / NCEP reanalyses in percent for JJA 1992 to 1999 (a) and ratio of standard deviations of 2m temperature DWD analyses / LAM simulation in percent for JJA 1992 to 1999 (b).

SLP variability in the NCEP reanalyses than in the reference data whereby adjacent regions show the opposite combination. The reason for this effect is unknown. The comparison of DWD analyses and the LAM run shows mostly values around 100 percent. The ratio for the summer months (not shown) depicts the same sort of pattern, but the values are slightly larger.

5.5. Regional details

The modelled fields, unfiltered, low pass or medium pass filtered are compared to the DWD reference with the "pattern correlation coefficient" (pcc, it is to be interpreted as a conventional correlation coefficient but this time across space) $P_{DWD}(x)$ with $x =$ NCEP, sn and nn. "NCEP" represents the NCEP reanalyses, "sn" the RCM simulation with nudging of large scales and "nn" the same without nudging of large scales. The results shown so far all dealt with "sn". The RCM simulation x is considered to be

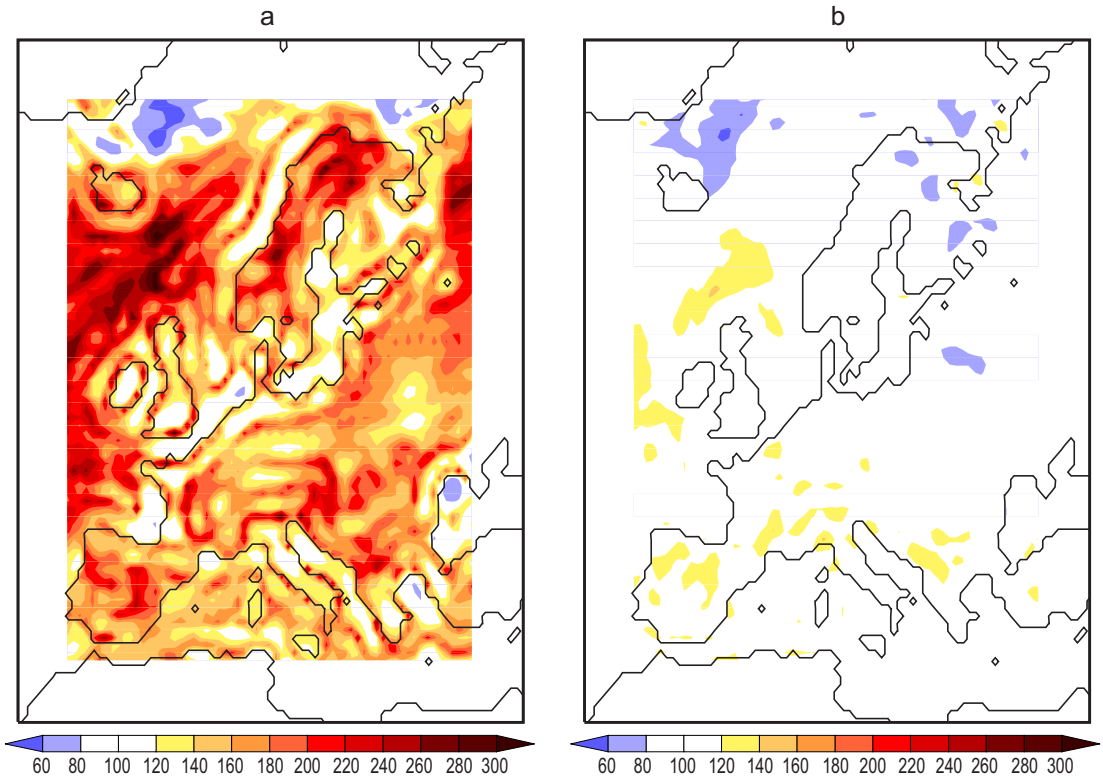

Figure 5.3: Ratio of standard deviations of medium-pass filtered 2m temperature DWD analyses / NCEP reanalyses in percent for DJF 1992 to 1999 (a) and ratio of standard deviations of 2m temperature DWD analyses / LAM simulation in percent for DJF 1992 to 1999 (b).

an improvement over NCEP if $\Delta_{x,NCEP} = P_{DWD}(x) - P_{DWD}(NCEP) > 0$. The pattern correlation coefficient of two spatial fields **a** and **b** with grid values a_i and b_i is formally the same as the sample correlation coefficient of a pair of time series:

$$P_{\mathbf{a}}(\mathbf{b}) = \frac{\sum_i (a_i - \bar{a})(b_i - \bar{b})}{\sqrt{(\sum_i (a_i - \bar{a})^2 \cdot \sum_i (b_i - \bar{b})^2)}} \tag{5.4}$$

Here, $\bar{a}$ and $\bar{b}$ are the spatial means of **a** and **b**. The denominator features the spatial standard deviations of **a** and **b**.

In this article, the reference **a** is given by the DWD analyses, while the role of the second field **b** is taken over by the NCEP reanalyses, and the RCM simulations with (sn) and without (nn) nudging of large scales. Unfiltered fields and filtered fields are compared with each other.

Figure 5.5 shows time series of pcc's for two sample seasons. The dependency of the RCM results on the large-scale forcing is apparent in the pressure pcc's; large

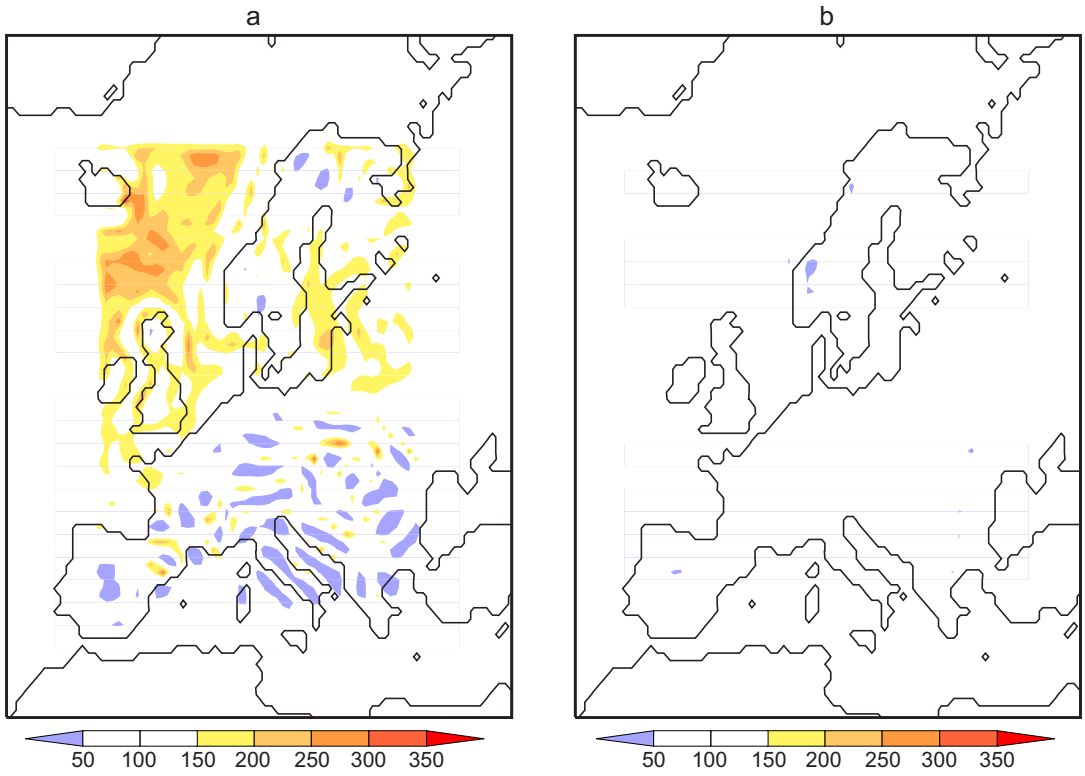

Figure 5.4: Ratio of standard deviations of medium-pass filtered SLP DWD analyses / NCEP reanalyses in percent for DJF 1998/1999 (a) and ratio of standard deviations of medium-pass filtered SLP DWD analyses / LAM simulation in percent for DJF 1998/1999 (b).

differences between NCEP and the DWD analyses coincide with even greater differences between the RCM simulations and the DWD analyses for the unfiltered and the low-pass filtered fields. This effect is reduced by applying the nudging technique.

For the spatially smooth *pressure fields* the added value of the RCM simulations is limited to the medium scales and to the simulation with nudging of large scales. For *air temperature* anomalies, the pcc's of the medium-pass filtered and unfiltered fields are for the RCM simulations always higher than for the global reanalyses. Because of high fluctuation in pcc especially for the NCEP reanalyses, a running average with a length of 4 was applied for better readability of the figure. The largest added values are apparent again for the medium scales where the regional models were expected to give the best results. For the pcc of the low-pass filtered fields the conventional RCM simulation shows a deterioration compared to the NCEP reanalyses. By contrast, when applying nudging of large scales a small added value is achieved (note that the nudging is towards the NCEP reanalyses, not towards the DWD analyses).

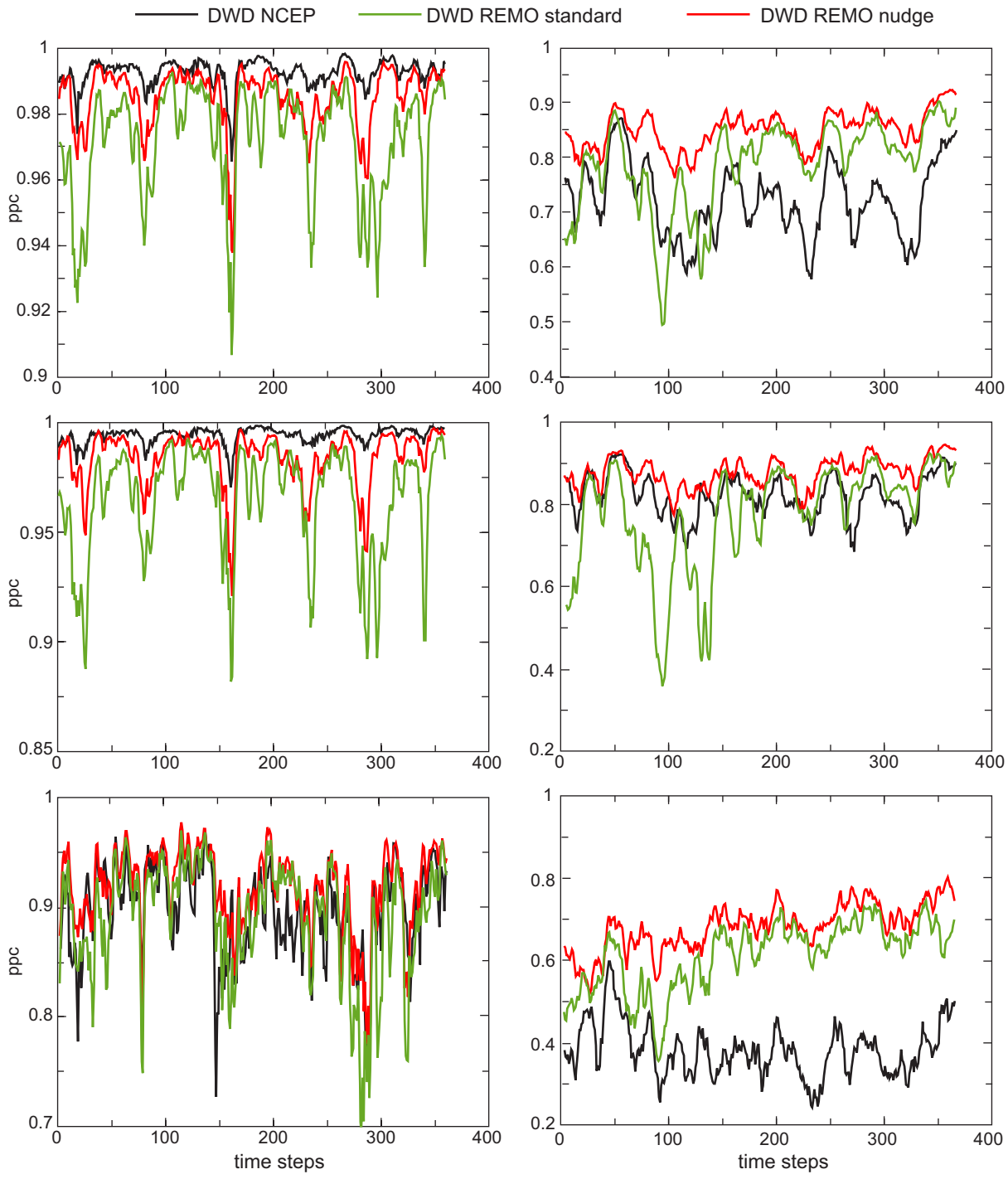

Figure 5.5: Left column: 6-hourly time series of SLP pattern correlation coefficients (PCC) for winter 1998/1999; and right column: Time series of 2m temperature anomalies PCC for summer 1998. Top: for full fields, middle: for low pass filtered fields, bottom: for medium pass filtered fields.

These findings are substantiated by Table 5.1, which is listing the mean pcc $P_{DWD}(NCEP)$ for full and anomaly fields (i.e., deviations from the time mean fields). Also, the differences $\Delta_{sn,NCEP}$ and $\Delta_{nn,NCEP}$ are listed. Positive differences are given in bold; statistically significant differences are marked with an asterisk.

The mean improvement in *SLP* for the regional model is 1.4% for winter and 4.1% for summer in case of nudging of large scales. No added value is provided for the standard RCM simulation. A similar result is obtained for the SLP anomalies, i.e., for deviations from the long term mean.

The result is much more encouraging for *air temperature*. Simulations with nudging of large scales return significant added value in both seasons for all spatial scales. When anomalies are considered, large-scale pcc increases by 5.5% and 6.3% in DJF and JJA, and the medium-scale pcc by 21.5% and even 30.4%. Without nudging of large scales, no added value is obtained for large scales, but there is a significant increase in terms of medium-scale pcc.

It is emphasised that this analysis describes only one measure of added value. There may be other useful such measures, and it may be that also in case of the conventional set-up a more pronounced added value emerges from such a measure.

5.5.1. *Case studies for selected weather situations*

To get an idea of the different patterns that are associated with high and low pcc values some examples were calculated for near-surface temperature and SLP. Figure 5.6 shows an example of high similarity between the LAM results and the DWD analyses. Shown are anomalies of medium-pass filtered 2m temperature fields for August 30, 1998, 6 a.m.. The upper left panel shows the DWD reference data, the upper right panel the NCEP reanalyses, the lower left panel the LAM results with nudging of large scales and the lower right panel the LAM temperatures for the conventional run. Also plotted are contour lines of unfiltered SLP. This example is a case of better performance of the LAMs than NCEP. The medium-scale temperature anomalies pcc's are 88.1% for the LAM with nudging of large scales and 80.9% without nudging. NCEP has a pcc of 9.6% for this date. NCEP shows deviations in the temperature pattern for the Mediterranean area as well as for Scandinavia, England, and Ireland in comparison with the analyses. The LAM results are closer to the DWD temperature pattern for these regions. The pressure fields do not show large deviations between the different simulations.

Figure 5.7 is an example for higher SLP pcc values for the NCEP reanalyses than for the LAM results. Again, anomalies of medium-pass filtered 2m temperature are plotted, this time for June 22, 1998, 6 p.m.. The pressure field of the reanalyses is closer to the DWD data than the regional simulations. The LAM results show deviations compared to the operational analyses, especially the one without nudging of

Table 5.1: Time mean pattern correlation coefficients $P_{DWD}(NCEP)$ (in %) of pairs of DWD and NCEP analysed regional fields (middle column), and mean differences when NCEP is replaced by REMO simulation with ($\Delta_{sn,NCEP}$) and without ($\Delta_{nn,NCEP}$) nudging of large scales (two right columns). Positive numbers, given in bold, indicate an improvement over the NCEP reanalyses, negative values a deterioration. 95%-significant deviations are marked by a *.
"Unfiltered" refers to unfiltered fields, "low pass", and "medium pass" to filtered fields.

Full fields

var	season	field	$P_{DWD}(NCEP)$	$\Delta_{sn,NCEP}$	$\Delta_{nn,NCEP}$
SLP	DJF	unfiltered	99.4	-0.7*	-2.2*
		low pass	99.6	-1.0*	-3.4*
		medium pass	91.3	**1.4***	-1.1*
SLP	JJA	unfiltered	98.0	-2.0*	-8.0*
		low pass	98.5	-2.6*	-11.6*
		medium pass	84.2	**4.1***	-0.6
T	DJF	unfiltered	96.0	**1.0***	**0.5***
		low pass	95.8	**0.8***	-0.8*
		medium pass	76.9	**3.6***	**1.5***
T	JJA	unfiltered	95.8	**1.4***	**0.5***
		low pass	96.3	**0.8***	-1.0*
		medium pass	65.4	**10.4***	**6.1***

Anomaly fields

var	season	field	$P_{DWD}(NCEP)$	$\Delta_{sn,NCEP}$	$\Delta_{nn,NCEP}$
SLP	DJF	unfiltered	99.1	-0.9 *	-2.9*
		low pass	99.3	-1.3*	-4.2*
		medium pass	89.6	**1.0***	-2.0*
SLP	JJA	unfiltered	98.3	-1.9*	-8.9*
		low pass	98.6	-2.7*	-12.9*
		medium pass	84.9	**2.6***	-3.0*
T	DJF	unfiltered	70.7	**9.8***	**6.2***
		low pass	79.2	**5.5***	-0.5*
		medium pass	27.0	**21.5***	**15.5***
T	JJA	unfiltered	70.2	**13.2***	**7.8***
		low pass	80.2	**6.3***	-2.5*
		medium pass	36.0	**30.4***	**24.3***

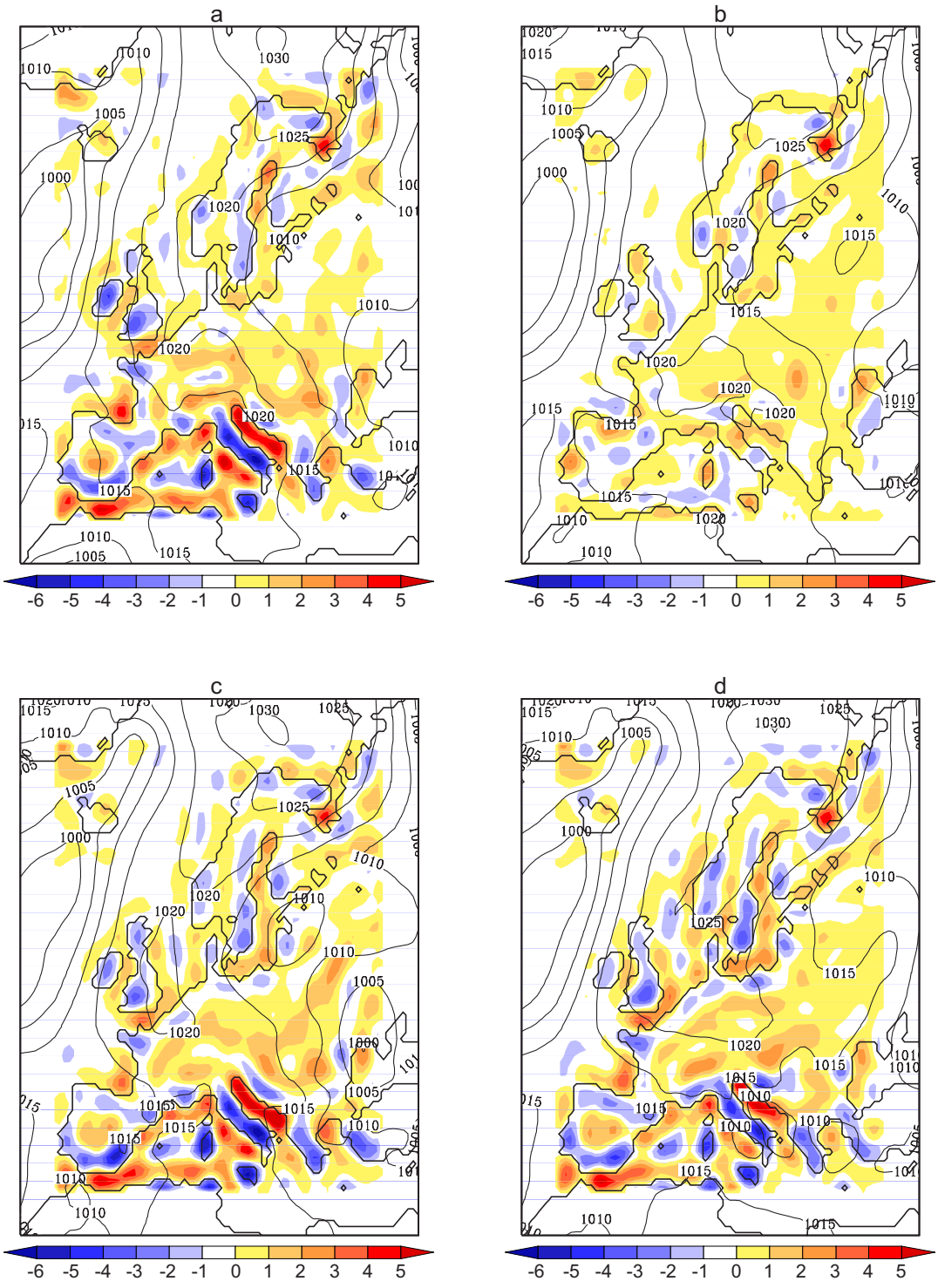

Figure 5.6: Anomalies of medium-pass filtered 2m temperature (K) fields (shaded) and unfiltered SLP isobars (hPa): a) DWD, b) NCEP, c) LAM_{sn}, d) LAM_{nn} for August 30, 1998, 6 a.m..

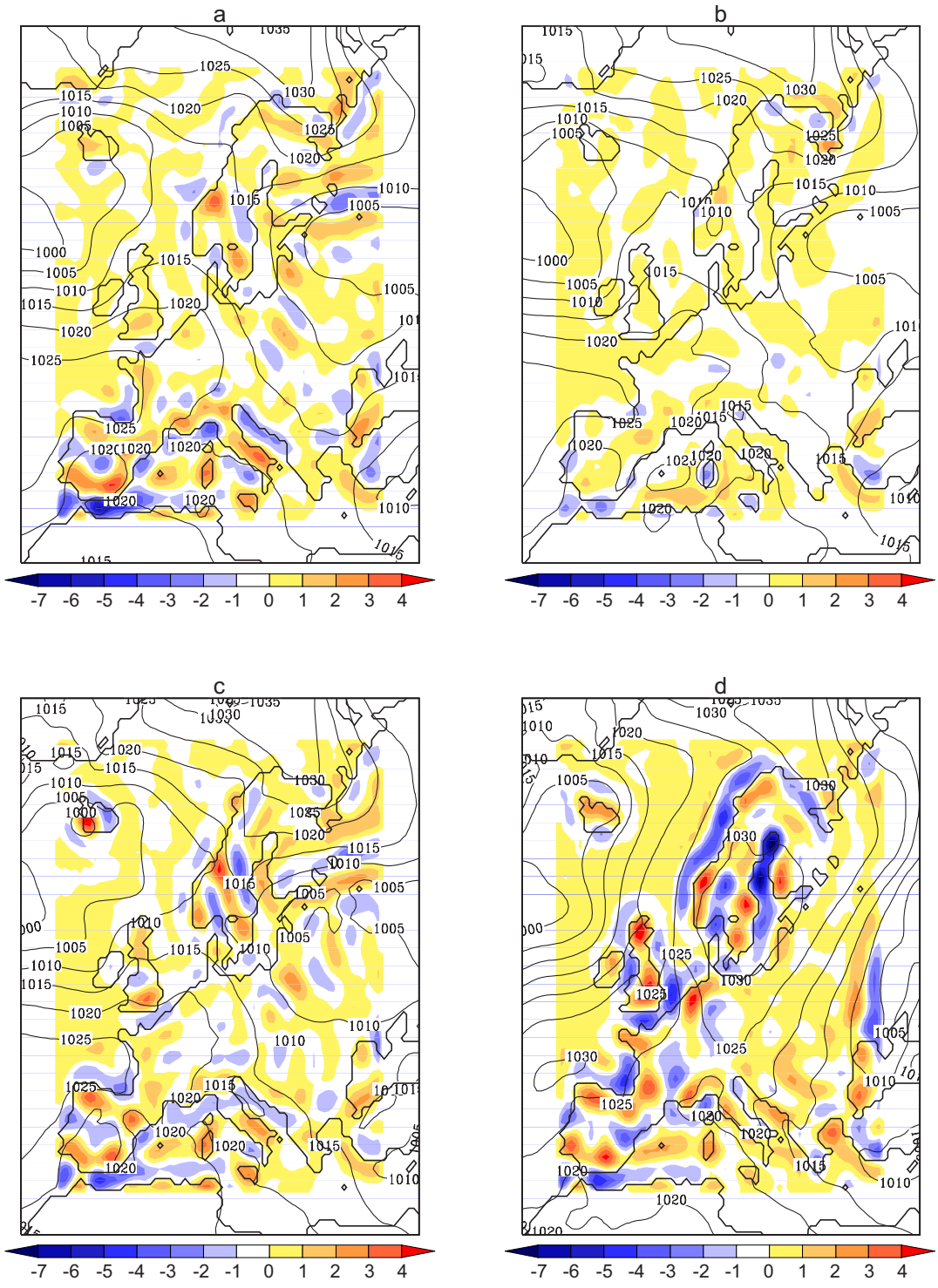

Figure 5.7: Anomalies of medium-pass filtered 2m temperature (K) fields (shaded) and unfiltered SLP isobars (hPa): a) DWD, b) NCEP, c) LAM$_{sn}$, d) LAM$_{nn}$ for June 22, 1998, 6 p.m..

large scales. The pcc values for the unfiltered SLP fields are 98.2% for the NCEP reanalyses, 97.2% for the LAM with and 60.7% for the LAM without nudging of large scales. For the LAM simulation without nudging of large scales the influence of the pressure field on the temperature pattern can be seen for Sweden and the northern Baltic Sea area as well as for the eastern boundary of the integration domain. A high pressure system of 1030 hPa was simulated by the regional model that was nonexistent in the operational analyses. The medium-scale temperature anomalies pattern hence looks quite different from the DWD data in this area. For the southern part of the integration domain both LAM simulations are much closer to the operational analyses than NCEP. The medium-scale temperature anomalies pcc is 29.2% for the NCEP reanalyses, 57.7% for the LAM with and 36.8% for the LAM without nudging of large scales. Even though the SLP pattern was best described by the reanalyses, the high-resolution temperature field was not well interpreted by them. It is reasoned that these are dynamically induced regional temperature details that could not be resolved by the coarse-resolution global reanalyses and that additional information could be added by the RCMs on the spatial scale that was considered.

5.6. Summary and Conclusions

An isotropic digital spatial filter was applied to evaluate and analyse LAM results separately at different spatial scales. The idea is that regional models mainly add detail at the specific scale they were constructed for, which means that for detection of an added value a scale separation of the model results is reasonable. Ratios of standard deviations of filtered near-surface temperature and SLP fields between regional model simulations or global reanalyses and an operational analysis were calculated. Hereby, the LAM showed larger variability than the global reanalyses and its values were comparable to those of the reference data set. The result was more distinct for the more regional quantity near-surface temperature than for the larger scale SLP. As a means for the skill of the individual simulations, pattern correlation coefficients were computed between the models and the reference analyses. For SLP, an added value can be found for the regional model simulation in case of nudging of large scales for the medium-pass filtered results. For the standard RCM simulation this is not possible with the presented method. Since SLP is a rather large-scale quantity the focus is put on near-surface temperature in order to detect an added value on the medium scales. The pattern correlation coefficients between the regional model results and the reference data are higher than the global reanalyses pattern correlation coefficients for the unfiltered and the medium-pass filtered temperature fields. With nudging of large scales an improvement also for the large scales could be achieved. Consistent with the concept of downscaling, an improvement in the representation of large scales is associated with an improvement of the simulation at the medium scales. When the role of the physiographic detail is less important, as in case of *air pressure*, the overall added

value is small; in that case, the RCM has hardly a chance to improve the large-scale field, as the only relevant factor available is the driving reanalyses. The situation is different in terms of *air temperature*, because the regional dynamics of this variable depends strongly on the physiographic detail. Therefore, the RCM is capable of improving the simulation not only of the medium-scale temperature fields but also of the large-scale field. By comparing the results for full fields and for anomaly fields, it is found that the added value is not mainly related to an improvement of time mean fields but is apparent in the anomalies as well. A maximum improvement is given for temperature anomalies at the medium scales; the regional model run with nudging of large scales gives a pattern correlation coefficient that is on average more than 30% higher than the pattern correlation coefficient of the global reanalyses. The results show that the main achievements of a RCM can be seen at smaller spatial scales while only little added value is given at the larger scales which are already well resolved in the global forcing model. Therefore it is proposed to use spatial filters to look at the regional model results separated into different spatial scales in order to detect additional information given by the high-resolution model. The analysis of RCM results separated into different spatial domains presented in this work revealed significant added value on the regional scale.

5.7. Acknowledgments

The author thanks R. Laprise and H. von Storch for valuable discussions regarding this work. B. Gardeike prepared some of the Figures for this paper. The author also thanks the German Climate Computing Center (DKRZ) which provided the computer hardware for the multi-decadal LAM simulation in the project 'Anthropogenic and natural regional environmental change'. The NCEP-NCAR reanalyses data was provided by the National Center for Atmospheric Research (NCAR). The author also thanks Germany's National Meteorological Service for providing the operational analyses.

Bibliography

Butler, D., 2003: Heatwave underlines climate-model failures. *Nature*, **424**, doi:10.1038/424867a.

Christensen, J. and O. Christensen, 2003: Severe summertime flooding in Europe. *Nature*, **421**, 805–806.

Denis, B., R. Laprise, D. Caya, and J. Côté, 2002: Downscaling ability of one-way nested regional climate models: The Big brother experiment. *Clim. Dyn.*, **18**, 627–646.

Doms, G., W. Edelmann, M. Gertz, T. Hanisch, E. Heise, L. A., D. Majewski, P. Prohl, B. Ritter, and U. Schaettler, 1995: Dokumentation des EM/DM-Systems. Deutscher Wetterdienst Abteilung Forschung, Offenbach a.M., [Available from Deutscher Wetterdienst, Zentralamt, Abteilung Forschung, Postfach 10 04 65, 63004 Offenbach am Main, Germany.].

Feser, F. and H. von Storch, 2005: A spatial two-dimensional discrete filter for limited area model evaluation purposes. *Mon. Wea. Rev.*, **133**, 1774–1786.

Feser, F., R. Weisse, and H. von Storch, 2001: Multi-decadal Atmospheric Modeling for Europe Yields Multi-purpose Data. *EOS Transactions*, **82**, 305,310.

Giorgi, F., B. Hewitson, J. Christensen, M. Hulme, H. von Storch, P. Whetton, R. Jones, L. Mearns, and C. Fu: 2001, *Climate Change 2001. The Scientific Basis*, Cambridge University Press, chapter Regional climate information - evaluation and projections. 583–638.

Jacob, D. and R. Podzun, 1997: Sensitivity Studies with the Regional Climate Model REMO. *Meteorol. Atmos. Phys.*, **63**, 119–129.

Kalnay, E., M. Kanamitsu, R. Kistler, W. Collins, D. Deaven, L. Gandin, M. Iredell, S. Saha, G. White, J. Woollen, Y. Zhu, M. Chelliah, W. Ebisuzaki, W. Higgins, J. Janowiak, K. C. Mo, C. Ropelewski, J. Wang, A. Leetmaa, R. Reynolds, R. Jenne, and D. Joseph, 1996: The NCEP/NCAR reanalysis project. *Bull. Amer. Meteor. Soc.*, **77**, 437–471.

Laprise, R., 2003: Resolved scales and nonlinear interactions in limited-area models. *J. Atmos. Sci.*, **60**, 768–779.

von Storch, H., 1995: Inconsistencies at the interface of climate impact studies and global climate research. *Meteorolog. Z.*, **4**, 72–80.

von Storch, H., H. Langenberg, and F. Feser, 2000: A Spectral Nudging Technique for Dynamical Downscaling Purposes. *Mon. Wea. Rev.*, **128**, 3664–3673.

Waldron, K. M., J. Paegle, and J. D. Horel, 1996: Sensitivity of a Spectrally Filtered and Nudged Limited-Area Model to Outer Model Options. *Mon. Wea. Rev.*, **124**, 529–547.

Chapter 6

Summary and Conclusions

The first, fundamental advancement in regional climate modelling was the development of the sponge zone by Davies (1976). It was developed to overcome the noise and instabilities which were produced by the inconsistencies between the regional model's solution and the driving boundary conditions. The installation of the sponge zone effectively solved this deficiency. Subsequently, another, sometimes serious, issue concerning regional modelling arose. For certain weather conditions or model regions with a low exchange rate with the surrounding model boundaries, the regional model tends to develop several, equally probable solutions. This is noteable in ensemble studies that show intermittently large deviations between the ensemble members for these periods. For hindcasts this is problematic, as only the solution closest to reality is desireable. A new regional modelling refinement approach to solve this problem is presented in this work, namely the nudging of large scales. The large-scale solution of the regional model is kept close to the driving large scales of the global model. This way, hindcast deviations not provoked by regional features, but by differing large-scale weather conditions, are reduced.

Following the idea of looking at model results at certain spatial scales to improve the model's performance, a new way of scale-separated model results analysis for detection of added value emerged. Both methods are based on the concept of spatial scale separation, stating that each climate model has an area of well-resolved spatial scales and an area of smaller spatial scales that can not be resolved by the model. The overlapping areas between the driving global model or reanalysis and the regional model are the ones of interest. First, the model results at the well-resolved large scales overlapping area of both the global and regional model should be similar, at least for climate hindcasts and possibly also for scenarios and regional forecasts. Second, the overlapping area of insufficiently-resolved global model scales and well-resolved regional model scales is the area where the regional model is superior to the global model and added value should be located on these scales. The technique of spatial scale separation introduced in this thesis allows for advanced application and analy-

sis of regional climate modelling. It combines the nudging of large scales and the spatial filtering technique for analysis of limited-area model results, and improves the detection possibilities of added value in regional modelling.

To assure that both regional and global simulations are alike on the large scales, the spectral nudging method was developed. It performs a scale separation and adds nudging terms to the regional model solution for low wave numbers that have to be specified according to the confidence level that is put in the global model. So far, mainly horizontal wind components were nudged starting at a height of 850 hPa to avoid disturbance of regional surface processes. Nudging of temperature or moisture would be promising if the quality of the driving model can be assured for these variables. The nudging coefficient increases in strength with height up to the highest model level. The nudging terms then pull the regional model solution in the direction of the global model results for the selected large scales only. The regional scales are left unchanged.

Ensembles of regional model simulations were computed, five with and five without using spectral nudging. It was demonstrated that nudging of large scales led to improved wind and wave fields in the regional climate hindcast. In most cases the ensemble variability was small for both forcing approaches. However, for certain periods the variability increased dramatically for the ensemble using the standard boundary forcing while remaining small for the spectral nudging ensemble. Comparisons with station data confirm that the hindcast skill was improved by using nudging of large scales. The model's trajectories were in this case, on average, closer to the data gathered at the analysed locations than the standard boundary-only forced ensemble.

The design of nudging of large scales and the concept of scale separation led to the idea of analysing climate model results at the scales they were designed for in order to enhance the detectability of valuable information added by the model. The assumption is that regional models mainly add detail at the specific scale they were constructed for, which means that for an added value detection a scale separation would lead to more explicit results. Spatial discrete, and isotropic filters were developed to work with a general algorithm with considerable flexibility in the choice of the appropriate filter response function. When a wave number range of interest has been selected, an approximation method leads to automatically computed response values. Effectively scale-separated atmospheric model fields can be used for model evaluation, comparisons or process studies, as well as for locating added value.

The added value provided by regional models has not been well-explored and further studies are needed. By applying isotropic spatial filters, the scale-dependent skill of a limited-area atmospheric climate simulation was examined. A comparison of ratios of standard deviations between regional model simulations or global reanalyses and a reference regional operational analysis of filtered near-surface temperature and sea level pressure was calculated. The computations revealed larger variability as well

as better agreement with the operational analyses for the regional model simulations than for the global model. Pattern correlation coefficients (pccs) between the reference analysis and the model simulations were calculated to test the skills of the individual model. For the rather large-scale quantity sea level pressure, an added value on the smaller scales could be detected for the regional simulation using spectral nudging. For near-surface temperature the pccs between analysis and regional model simulations were higher than for the global model, especially on the smaller scales. Nudging of large scales also increased the large-scale similarity between analysis and regional model to a higher value than that of the pccs between analysis and global model. The added value was not only related to an improvement in the time mean fields, it was also found in the anomalies.

This thesis addressed the topic of scale separation in regional modelling. The intention was to encourage further applications and research on both improved model performance by advancing the spectral nudging approach and on progress with the relatively unexplored detection of added value in regional modelling. The work was intended to give new thought-provoking insights for further analysis, validation, and use of regional climate models.

For future applications an interesting approach would be to use spectral nudging for the Big Brother Experiment (Denis et al. (2002), BBE). For the BBE, a large domain (Big Brother) is computed with a regional model, then low-pass filtered and then used as input for a smaller domain (Little Brother) to compute another simulation with the same regional model. Both high-resolution simulations can then be compared and sensitivity studies can be calculated. The advantage is that both simulations use the same model's physics and differences can then be mainly attributed to errors associated with the nesting and downscaling technique. However, the large simulation domain needed for the Big Brother can lead to great differences between the driving global model and the regional model at the large scales. This may also happen for weather conditions with low exchange rates between the model boundaries and the interior. Spectral nudging might help to reduce the deviations between Little and Big Brother that were caused by these effects.

While the nudging of large scales has been well established in a number of studies (Miguez-Macho et al. (2004), Kang et al. (2005), Kanamaru and Kanamitsu (2005)), new applications should be explored. Additionally, for example, for regional weather forecasts, spectral nudging might lead to improvements. For weather forecasts, usually ensembles are computed repeatedly, differing only slightly in their initial conditions. When the ensemble members converge, a reliable forecast can be given. The nudging of large scales might reduce the variability that is caused solely by deviations between driving analyses and regional forecast model at the large scale. Thereby the convergence of ensemble simulations may happen at an earlier stage. But this remains to be proven by applying spectral nudging to numerical regional weather forecast models.

For detecting the added value of regional modelling, spatial scale separation of model results is expected to give clearer results than the analysis of total, unfiltered model fields. The first encouraging findings were presented in this thesis. For sea level pressure an added value was extracted at the medium scales for a regional model simulation with nudging of large scales. A maximum improvement was found for near-surface temperature anomalies at the medium scales. The pattern correlation coefficient between a spectrally nudged regional model simulation and observational analyses was on average more than 30% higher than the pattern correlation coefficient between the driving global reanalyses and the reference analyses. More model variables and simulations should be analysed in detail to advance with the research on added value of regional modelling.

Acknowledgments

This thesis was written at the Institute for Coastal Research of the GKSS Research Centre in Geesthacht, Germany.

I thank Prof. Dr. Hans von Storch for his support throughout the last years, for numerous discussions and his scientific advice. I also thank Prof. Dr. Klaus Dethloff for reviewing the thesis. I am grateful to Dr. Burkhardt Rockel, Prof. Dr. K. Heinke Schlünzen and Prof. Dr. Jürgen Sündermann for their participation in my examination board.

I thank Dr. René Laprise for valuable discussions and ideas regarding the isotropic spatial filter design.

My colleagues provided stimulating ideas and discussions concerning this work, especially Dr. Ralf Weiße, Dr. Arnt Pfizenmayer, Katja Woth, Dr. Beate Geyer, Dr. Julie Jones, Dr. Martin Widmann, and Dr. Eduardo Zorita.

Beate Gardeike helped greatly with the preparation of the figures for this paper. Dr. Hermann Kuhn did a great job on administrating the computer network during the years at GKSS. I would like to thank Dr. Dennis Bray for proof-reading parts of this work.

I also thank the German Climate Computing Center (DKRZ) which provided the computer hardware for the multi-decadal RCM simulation in the project 'Anthropogenic and natural regional environmental change'. The NCEP-NCAR reanalyses data was supplied by the National Center for Atmospheric Research (NCAR). I also thank Germany's National Meteorological Service for providing the operational analyses.

I thank my parents for making my studies of meteorology possible.

Finally, I want to thank Jan for supporting me in every way.